



**AN INVESTIGATION OF THE HALF-MODEL
REFLECTION-PLANE TECHNIQUE FOR DYNAMIC
STABILITY TESTING AT TRANSONIC MACH NUMBERS**

**PROPULSION WIND TUNNEL FACILITY
ARNOLD ENGINEERING DEVELOPMENT CENTER
AIR FORCE SYSTEMS COMMAND
ARNOLD AIR FORCE STATION, TENNESSEE 37389**

January 1977

Final Report for Period January 16, 1973 — March 31, 1976

Approved for public release; distribution unlimited.

Prepared for

**DIRECTORATE OF TECHNOLOGY (DY)
ARNOLD ENGINEERING DEVELOPMENT CENTER
ARNOLD AIR FORCE STATION, TENNESSEE 37389**

NOTICES

When U. S. Government drawings specifications, or other data are used for any purpose other than a definitely related Government procurement operation, the Government thereby incurs no responsibility nor any obligation whatsoever, and the fact that the Government may have formulated, furnished, or in any way supplied the said drawings, specifications, or other data, is not to be regarded by implication or otherwise, or in any manner licensing the holder or any other person or corporation, or conveying any rights or permission to manufacture, use, or sell any patented invention that may in any way be related thereto.

Qualified users may obtain copies of this report from the Defense Documentation Center.

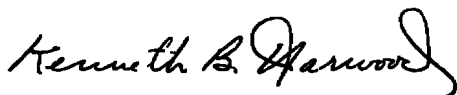
References to named commercial products in this report are not to be considered in any sense as an endorsement of the product by the United States Air Force or the Government.

This report has been reviewed by the Information Office (OI) and is releasable to the National Technical Information Service (NTIS). At NTIS, it will be available to the general public, including foreign nations.

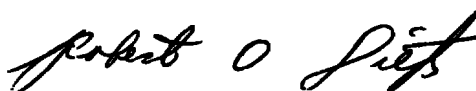
APPROVAL STATEMENT

This technical report has been reviewed and is approved for publication.

FOR THE COMMANDER



KENNETH B. HARWOOD
Major, CF
Research & Development
Division
Directorate of Technology



ROBERT O. DIETZ
Director of Technology

UNCLASSIFIED

REPORT DOCUMENTATION PAGE		READ INSTRUCTIONS BEFORE COMPLETING FORM
1. REPORT NUMBER AEDC-TR-76-165	2. GOVT ACCESSION NO.	3. RECIPIENT'S CATALOG NUMBER
4. TITLE (and Subtitle) AN INVESTIGATION OF THE HALF-MODEL REFLECTION-PLANE TECHNIQUE FOR DYNAMIC STABILITY TESTING AT TRANSONIC MACH NUMBERS		5. TYPE OF REPORT & PERIOD COVERED Final Report - January 16, 1973 - March 31, 1976
7. AUTHOR(s) T. O. Shadow - ARO, Inc.		6. PERFORMING ORG. REPORT NUMBER
9. PERFORMING ORGANIZATION NAME AND ADDRESS Arnold Engineering Development Center (DY) Air Force Systems Command Arnold Air Force Station, Tennessee 37389		8. CONTRACT OR GRANT NUMBER(s)
11. CONTROLLING OFFICE NAME AND ADDRESS Arnold Engineering Development Center (DYFS) Arnold Air Force Station Tennessee 37389		10. PROGRAM ELEMENT, PROJECT, TASK AREA & WORK UNIT NUMBERS Program Element 65807F.
14. MONITORING AGENCY NAME & ADDRESS (if different from Controlling Office)		12. REPORT DATE January 1977
		13. NUMBER OF PAGES 93
		15. SECURITY CLASS. (of this report) UNCLASSIFIED
		15a. DECLASSIFICATION/DOWNGRADING SCHEDULE N/A
16. DISTRIBUTION STATEMENT (of this Report) Approved for public release; distribution unlimited.		
17. DISTRIBUTION STATEMENT (of the abstract entered in Block 20, if different from Report)		
18. SUPPLEMENTARY NOTES Available in DDC		
19. KEY WORDS (Continue on reverse side if necessary and identify by block number) half-model pressure testing transonic flow reflection scale models dynamics angle of attack stability		
20. ABSTRACT (Continue on reverse side if necessary and identify by block number) An experimental investigation was made to determine the feasibility of the half-model reflection-plane technique for measuring dynamic stability derivatives in the transonic speed range. Three model configurations simulating an aircraft, a missile, and a bluff body were investigated both full and half span at Mach numbers from 0.6 to 1.2 and angles of attack from -2 to 90 deg. The half-model reflection-plane technique fully		

UNCLASSIFIED

UNCLASSIFIED

20. ABSTRACT (Continued)

duplicated the full-span results only at subsonic subcritical speeds and angles of attack up to 20 deg. In tests at higher Mach numbers in the transonic range and higher angles of attack up to 90 deg, it was not demonstrated that the half-model technique can provide better than qualitative, order of magnitude results.

PREFACE

The work reported herein was conducted by the Arnold Engineering Development Center (AEDC), Air Force Systems Command (AFSC), under Program Element 65807F. The monitor of the project was Maj. Kenneth B. Harwood (CF) (AEDC, DYR). The results presented were obtained by ARO, Inc. (a subsidiary of The Sverdrup Corporation), contract operator of AEDC, AFSC, Arnold Air Force Station, Tennessee. The tests were conducted from January 16, 1973, through March 31, 1976, under ARO Project Numbers PF215, PF415, and P32A-C9A. The author of this report was T. O. Shadow, ARO, Inc. Analysis of the data was completed in July 1976, and the manuscript (ARO Control No. ARO-PWT-TR-76-127) was submitted for publication on October 27, 1976.

CONTENTS

	<u>Page</u>
1.0 INTRODUCTION	7
2.0 APPARATUS	
2.1 Test Facilities	9
2.2 Test Articles	10
2.3 Test Mechanism	11
2.4 Instrumentation	13
3.0 PROCEDURE	
3.1 Test Conditions and Procedures	14
3.2 Precision of Measurements	14
3.3 Data Reduction	16
4.0 RESULTS	
4.1 Reflection-Plane Pressure Surveys	17
4.2 Pitch Damping Tests	19
5.0 CONCLUDING REMARKS	26
REFERENCES	26

ILLUSTRATIONS

Figure

1. Rod Model Test Mechanism	31
2. Sting Model with External Excitation	32
3. Ribbon-Mounted Model Test Mechanism	33
4. Magnetic Suspension System	34
5. Half-Model Test Mechanism	35
6. General Arrangement of Tunnel 1T	36
7. Test Models	37
8. Reflection-Plane Geometry	40
9. Pressure Survey Test Mechanism	41
10. Sting-Mounted Free-Oscillation Balance	43
11. Tunnel 1T Sting Support Equipment	44
12. Tunnel 4T Support Equipment	46

<u>Figure</u>	<u>Page</u>
13. Low-Alpha Wall-Mounted Balance	49
14. High-Alpha Wall-Mounted Balance	51
15. Rod-Mounted Model	53
16. Free-Oscillation Data Recording Equipment	54
17. Reynolds Number per Foot versus Mach Number	56
18. Typical $\ln \theta$ versus Time	57
19. Reflection-Plane Pressure Distribution with Cavity Plugged and Unplugged, $\psi = 0$, $h = 0.9$	58
20. Reflection-Plane Pressure Distribution with Varying h , $\psi = 0$	59
21. Reflection-Plane Pressure Distribution with Varying ψ , $h = 0.9$	60
22. Aircraft Model Pressure Distribution at the Wing- Body Juncture, $\psi = -0.4$, $h = 0.9$	61
23. Aircraft Model Pressure Distribution at the Fuselage-Reflection-Plane Juncture, $\psi = -0.4$, $h = 0.9$. .	62
24. Comparison of Full- and Half-Span Pitching-Moment Characteristics of the Ogive-Cylinder Model	63
25. Comparison of Full- and Half-Span Pitching-Moment Characteristics of the Hemisphere-Cylinder Model	65
26. Comparison of Full- and Half-Span Pitching-Moment Characteristics of the Wing-Body Model	67
27. Comparison of Full- and Half-Span Pitch-Damping Characteristics of the Aircraft Model	69
28. Reynolds Number Effects on the Pitching-Moment Characteristics of the Ogive-Cylinder Model	70
29. Reynolds Number Effects on the Pitching-Moment Characteristics of the Hemisphere-Cylinder Model	72
30. Reynolds Number Effects on the Pitching-Moment Characteristics of the Wing-Body Model	74
31. Effects of Base Alterations on the Pitching-Moment Characteristics of the Ogive-Cylinder Model	76

<u>Figure</u>	<u>Page</u>
32. Effects of Oscillation Frequency on the Pitch-Damping Characteristics of the Full-Span Ogive-Cylinder Model	78
33. Effects of Oscillation Frequency on the Pitch-Damping Characteristics of the Full-Span Hemisphere-Cylinder Model	79
34. Effects of Oscillation Frequency on the Pitch-Damping Characteristics of the Half-Span Ogive-Cylinder Model	80
35. Effects of Oscillation Frequency on the Pitch-Damping Characteristics of the Half-Span Hemisphere-Cylinder Model	81
36. Effects of Oscillation Frequency on the Pitch-Damping Characteristics of the Half-Span Wing-Body Model, $M_{\infty} = 1.0$	82
37. Comparison of Static Pitching-Moment Coefficients between Tunnels 1T and 4T for the Ogive-Cylinder Model	83
38. Comparison of Static Pitching-Moment Coefficients between Tunnels 1T and 4T for the Hemisphere-Cylinder Model	84
39. Details of the Sting Flare	85
40. Effects of Sting Flare on Pitching-Moment Characteristics of the Aircraft Model	86
41. Effects of Sting Flare on Pitching-Moment Characteristics of the Hemisphere-Cylinder Model	88

TABLES

1. Test Phases	91
2. Test Conditions	91
NOMENCLATURE	92

1.0 INTRODUCTION

Frequently, pitch-damping derivatives of unconventional configurations necessarily require some special techniques in mounting the model in a wind tunnel with minimum support interference. The aerospace vehicles of today and those planned for the future often have shapes that cannot be mounted in the conventional sting arrangement. Examples are: aircraft with twin engine exhausts and no suitable rear centerbody, long-slender missiles, and reentry vehicles with control surfaces along the entire base.

The fact that support interference has large effects on dynamic stability measurements, especially in the transonic speed regime, was illustrated by Reding and Ericsson (Ref. 1). The dynamic stability of configurations with bulbous or boattail bases are particularly sensitive to support interference. Interference can not only affect the magnitude of the damping, but in some cases completely change the sign. The extremely small damping moments measured in wind tunnel testing (of the order of 10^{-3} ft-lb) also add to the complexity of the problem.

The problems faced by the aerodynamicist in search of meaningful stability derivatives are enormous; however, several interesting techniques have been devised to bypass these obstacles. Figure 1 through 5 illustrate mounting techniques that are as varied as one could imagine. Each technique depicted is described in Refs. 2 through 6, respectively.

The purposes of this investigation were to study alternate mounting techniques for transonic testing, choose one that would best meet all the requirements, and demonstrate its effectiveness. Of those techniques studied, it appeared that the half-model reflection-plane technique showed the most promise. The merits and demerits of half-models were discussed by Van der Blik in Ref. 7 where he showed that, with certain precautions, data from half-span models compare favorably with those of

full-span models. Some dynamic stability testing of semi-span models was performed as early as 1952 by Orlik-Ruckemann and Olsson. Most of the recent work has been done by Orlik-Ruckemann, Laberge, et al., of the National Research Council of Canada, and is partially reported in Refs. 8 through 14. A large part of their work has been in the supersonic and hypersonic speed ranges and has produced some exciting results that might otherwise be unobtainable. The work reported in Ref. 14 illustrates the versatility of the system to obtain data over a wide range of Mach numbers and illustrates the sensitivity of pitch-damping measurements at transonic Mach numbers. These data while impressive in the quality and repeatability show no comparisons for similar full-span models. Limited data were obtained on a full-span model of one of these configurations in the AEDC Aerodynamic Wind Tunnel (1T), and the unpublished results (Ref. 15) showed that considerable differences may result. From these results, it was obvious that to make a data comparison between full- and half-span configurations all test parameters should be matched, and all testing conducted in the same wind tunnel.

The investigation reported herein was made with these precautions in mind. A group of aerospace configurations was chosen to typify most peculiarities noted in transonic flow and both full- and half-span models of each were tested. The test program was planned such that configuration, scale, reduced frequency, test conditions, and tunnels were matched where possible. The test program ranged from selecting and optimizing a reflection-plane configuration to half-model pitch-damping tests with boundary-layer suction.

While testing in the low angle-of-attack range ($\alpha \leq 10$ deg), it became evident that the half-model technique would facilitate high angle-of-attack testing, hence the program scope was increased to include angles up to 90 deg. The survey of requirements for future dynamic stability testing by Orlik-Ruckemann (Ref. 16) also pointed out the need for high angle-of-attack testing.

Each of the tests was conducted at Mach numbers from 0.6 to 1.2, with angles of attack from -2 to 10 deg for the low-alpha tests and -2 to 90 deg for the high-alpha tests.

2.0 APPARATUS

2.1 TEST FACILITIES

2.1.1 Tunnel 1T

The Aerodynamic Wind Tunnel (1T) is a continuous-flow, nonreturn wind tunnel equipped with a two-dimensional nozzle and an auxiliary plenum evacuation system. The test section is 1 ft square and 37 in. long, and is equipped with inclined-hole, 6-percent-open, perforated walls. The Mach number range is from 0.2 to 1.5; variable nozzle contours are used above $M_{\infty} = 1.05$. The tunnel is operated at a stilling chamber total pressure of about 2,850 psfa with a ± 5 -percent variation dependent on tunnel resistance and ambient atmospheric conditions. The stagnation temperature can be varied from 80 to 120°F above ambient temperature as necessary to prevent visible condensation from occurring in the test section. The general arrangement of the tunnel and its associated equipment is shown in Fig. 6, and a detailed description of the tunnel and its capabilities is given in Ref. 17.

2.1.2 Tunnel 4T

The Aerodynamic Wind Tunnel (4T) is a closed-circuit, continuous-flow, variable-density tunnel capable of being operated at Mach numbers from 0.1 to 1.3; also nozzle blocks can be installed to provide nominal Mach numbers of 1.6 and 2.0. At all Mach numbers, the stagnation pressure can be varied from 300 to 3,700 psfa. The test section is 4 ft square and 12.5 ft long with variable porosity walls (0 to 10 percent). The test section is completely enclosed in a plenum chamber from which the

air can be evacuated, thus allowing part of the tunnel airflow to be removed through the test section walls. This design allows control of wave attenuation and blockage effects. A more extensive description of the tunnel is available in Ref. 17.

2.2 TEST ARTICLES

The initial test articles were designed to verify the half-model reflection-plane technique over the angle-of-attack range from 0 to 10 deg. Both full- and half-span models (Fig. 7) were provided of (1) an ogive-cylinder to simulate missile configurations, (2) a hemisphere-cylinder to represent more bluff bodies like bombs, and (3) a wing-body with a T-tail representing airplanes. The diameter (1.2 in.) was chosen for the maximum allowable blockage in Tunnel 1T, and the lengths for the various configurations were dictated by the diameter of the reflection plane and the physical dimensions of the existing free-oscillation sting balance. In subsequent tests at high angles of attack (-2 to 90 deg), the T-tail was removed from the wing-body model, and the length was extended to match that of the missile and bluff-body models (Fig. 7c). All of the half-models were fabricated with the base closed, which made the models more easily statically balanced about the pivot axis. One half-model afterbody was provided with an open base that simulated the full-span models. A short dummy sting was also provided to attach to the reflection plane inside and aft of the model base to simulate the sting mounting arrangement.

The reflection plane size was limited by the size of Tunnel 1T; however, the shape (Fig. 8) was designed to produce the least disturbance near the flat surface where the models were located.

All of the models were designed such that the oscillation frequencies for the full- and half-span models were matched within 1 Hz. The oscillation frequencies for the low angle-of-attack models were matched

at 36 Hz, which was principally determined by the spring stiffness of the available balances. During the low angle-of-attack tests, it was evident that the balance structural damping could be better controlled at a lower frequency, hence for the high angle-of-attack tests some of the model parts were replaced with more exotic materials (tungsten and titanium) to lower the frequency to 25 Hz.

A full-span rod-mounted model of the hemisphere-cylinder configuration was also fabricated to provide further comparison between test techniques.

2.3 TEST MECHANISMS

The location and orientation of the reflection plane in the tunnel was optimized by performing static pressure surveys (1) over the clean reflection plane, and (2) near the wing-body, T-tail, full-span model and comparing with similar data taken near the half-model reflection plane configuration (Fig. 9). The pressure surveys were made with a static pressure probe mounted on an adjustable head that could locate the probe at any horizontal or vertical station within the flow field of the model. For the pressure surveys, the full-span model was mounted on a long slender sting. The tunnel station of the full-span model was matched with that of the half-span model to eliminate the effect of possible variations in pressure along the tunnel centerline.

All of the full-span pitch-damping tests were conducted with a sting-type free-oscillation balance (Fig. 10), which was machined out of a single piece of steel to minimize structural damping. Model excitation was accomplished by oscillating gas jet pulses at the top and bottom, inside the model base. During the low angle-of-attack tests in Tunnel 1T, the balance was mounted directly to the tunnel pitch mechanism which allowed angle-of-attack variations from -2 to 10 deg (Fig. 11). In the high angle-of-attack tests in Tunnel 4T, an additional mini-sector (Fig. 12) was mounted on the tunnel pitch sector to allow angle-of-attack variations

up to 90 deg. A special adapter was provided for low angles of attack (-2 to 28 deg) to reduce aerodynamic interference from the mini-sector (Fig. 12c).

The half-model tests were conducted on a wall-mounted balance which was attached to the top wall of Tunnel 1T. A schematic of the balance used in the low angle-of-attack tests is shown in Fig. 13. The balance consisted of a shaft that protruded through the tunnel wall and on which the reflection plane and model were attached. The shaft was attached to the inside shell through three sets of cross flexures that allowed rotation of the shaft about a fixed axis through its center. Model excitation was accomplished with a pneumatic cock-and-release mechanism. The inside shell was attached to an outside shell through a set of ball bearings that allowed angle-of-attack variations. Movement between the inner and outer shells during the cock-and-release cycle was prevented with a pneumatic clamp ring.

The low angle-of-attack tests uncovered several problems that required solution before the high angle-of-attack tests could be started. The principal problem was repeatability of structural damping. This problem was solved by redesigning a large portion of the balance (Fig. 14) and decreasing the model oscillation frequency. Particular emphasis was placed on securing all joints that could produce damping if they were allowed to move. The cocking mechanism was moved to the top of the balance to allow installation of a labyrinth seal that bridged the balance for the purpose of boundary-layer suction through the reflection plane. Oscillation frequency was made variable with the inclusion of inertia disks at the top of the balance.

Two configurational modes were available for the half-model free-oscillation tests. They were (1) rigid connection between the model and reflection plane such that they oscillated as a single unit, and (2) the reflection plane mounted rigidly to the balance frame and the model allowed

to oscillate, separated from the plane by a 0.02-in. gap. The first technique was provided as an alternate to technique 2 which has been used in most previous half-model tests (Orlik-Ruckemann, et al.). It was thought that technique 1 would eliminate viscous damping in the gap. For the high-alpha tests, approximately 75 percent of the reflection-plane area was fitted with interchangeable, sintered, stainless-steel surfaces. Plates consisting of 5-, 10-, and 20-micron filter grades and a solid plate were available.

The previously described side-wall balance also has the capability of performing free-oscillation tests on full-span models mounted from the side on a rod (Fig. 15). The clutch-face disconnect juncture allows quick changeover from one technique to another.

2.4 INSTRUMENTATION

The static pressure surveys were made with a probe that was especially designed for this study (Fig. 9). The probe had a hemisphere nose and four pressure ports that were manifolded together and located six probe diameters aft of the nose. The ports were connected to a 5-psid, strain-gage transducer that was referenced to the tunnel plenum pressure. The probe horizontal and vertical positions were set manually (Section 2.3), and the axial traverses were controlled remotely.

All of the pitch-damping tests used the free-oscillation technique, and model position was measured with a strain-gaged beam. A signal proportional to the model deflection was conditioned and recorded on an oscillograph, on a damping system that automatically indicated the number of cycles to decay to one-half amplitude, and on magnetic tape for future off-line data reduction. A schematic and photograph of the data acquisition system including the automatic gas pulse-drive control system used on the full-span tests are shown in Fig. 16. The half-span test data system was the same except that model excitation was accomplished with a pneumatic cocking mechanism (Section 2.3).

3.0 PROCEDURE

3.1 TEST CONDITIONS AND PROCEDURES

The tests were conducted in three phases, which consisted of (1) pressure surveys, (2) low angle-of-attack pitch damping, and (3) high angle-of-attack pitch damping. A summary of the nominal test conditions for the various phases is presented in Tables 1 and 2 and in Fig. 17.

In the pressure survey phase, the system described in Section 2.3 was used first on the sting-mounted full-span model and then on the wall-mounted half-span reflection plane model. Probe position relative to the model axial centerline was held constant while axial-pressure surveys were made.

The procedure for recording data during the full-span pitch-damping tests was to excite the model with the gas pulse system and, when the oscillation amplitude reached ± 3 deg, turn the gas supply off and record data during the free-decay cycle to the steady-state trim position. The procedure was essentially the same for the half-span tests and the full-span rod pitch-damping test except for the pneumatic cocking mechanism which initially deflected the model 4 deg.

3.2 PRECISION OF MEASUREMENTS

Instrument errors in the basic tunnel parameters, total pressure, and total temperature were used along with the standard deviations in Mach number, which were determined from test section flow calibrations, in the Taylor series method of error propagation to determine the following uncertainties:

M_∞	Tunnel	Percent			
		δM_∞	δq_∞	δRe	δV_∞
0.6	1T	± 0.67	± 1.03	± 1.55	± 0.770
0.6	4T	± 0.35	± 0.55	± 1.65	± 0.408
0.8	1T	± 0.59	± 0.72	± 1.35	± 0.710
0.8	4T	± 0.29	± 0.37	± 1.60	± 0.348
0.9	1T	± 0.56	± 0.58	± 1.30	± 0.698
0.9	4T	± 0.31	± 0.35	± 1.60	± 0.375
1.0	1T	± 0.60	± 0.51	± 1.33	± 0.740
1.0	4T	± 0.39	± 0.37	± 1.62	± 0.440
1.2	1T	± 0.62	± 0.29	± 1.35	± 0.780
1.2	4T	± 0.80	± 0.39	± 1.98	± 0.820
1.3	1T	± 0.68	± 0.19	± 1.46	± 0.860

Coefficient uncertainties include errors in balance calibrations, test conditions, and instrument errors resulting from data transfer from the analog tape system to the digital system. The estimated uncertainties for the various coefficients are as follow:

M_∞	Tunnel	Percent			
		$\delta(\omega d/2V_\infty)$	$\delta(C_{mq} + C_{m\dot{\alpha}})$	δC_m	$\delta(p/p_\infty)$
0.6	1T	± 1.26	± 10.0	± 1.43	± 0.136
0.6	4T	± 1.08	± 10.0	± 1.14	
0.8	1T	± 1.23	± 10.0	± 1.23	± 0.167
0.8	4T	± 1.06	± 10.0	± 1.07	
0.9	1T	± 1.22	± 10.0	± 1.16	± 0.187
0.9	4T	± 1.07	± 10.0	± 1.06	
1.0	1T	± 1.24	± 10.0	± 1.12	± 0.208
1.0	4T	± 1.09	± 10.0	± 1.07	
1.2	1T	± 1.27	± 10.0	± 1.04	± 0.266
1.2	4T	± 1.29	± 10.0	± 1.07	
1.3	1T	± 1.32	± 10.0	± 1.02	± 0.300

3.3 DATA REDUCTION

The equation of motion for a model performing one-degree-of-freedom pitch oscillations with damping is

$$I_y \ddot{\theta} + M_{\dot{\theta}} \dot{\theta} + M_{\theta} \theta = 0 \quad (1)$$

The solution to this equation is

$$\theta = \theta_0 e^{-\{M_{\dot{\theta}}/2I_y\}t} \cos(Wt - \phi) \quad (2)$$

where θ_0 and θ are arbitrary constants. When $\cos(\omega t - \phi) = 1$, the envelope encompassing the points of tangency with the displacement is described by

$$\theta = \theta_0 e^{-\{M_{\dot{\theta}}/2I_y\}t} \quad (3)$$

With the aid of the logarithmic decrement and the assumption that C_{yR} cycles are required to damp to a given amplitude ratio, $R = \theta_2/\theta_1$. The following equation for damping moment is derived:

$$M_{\dot{\theta}} = - \frac{2I_y f}{C_{yR}} \ln R \quad (4)$$

Equation (4), which assumes a linear restoring moment, is derived in detail in Ref. 18. An additional correction for models with slightly nonlinear restoring moments is also derived, and Eq. (4) now becomes

$$M_{\dot{\theta}} = - \frac{2I_y f}{C_{yR}} \ln \left\{ R \left(\frac{\omega_2}{\omega_1} \right)^{1/2} \right\} \quad (5)$$

Rewriting Eq. (5) using the relationships from Fig. 18 gives

$$M_{\dot{\theta}} = - \frac{2I_y}{\Delta t} \ln \left\{ \left(\frac{\theta_2}{\theta_1} \right) \left(\frac{\omega_2}{\omega_1} \right)^{1/2} \right\} \quad (6)$$

Further reduction using logarithmic identities gives

$$M_{\dot{\theta}} = - 2I_y \left\{ \frac{\ln \theta_2 - \ln \theta_1}{\Delta t} + \frac{1}{2} \frac{\ln \omega_2 - \ln \omega_1}{\Delta t} \right\} \quad (7)$$

In the limit as $\Delta t \rightarrow 0$, Eq. (7) becomes

$$M_{\dot{\theta}} = -2I_y \left\{ \frac{d \ln \theta}{dt} + \frac{1}{2} \frac{d \ln \omega}{dt} \right\} \quad (8)$$

The model oscillation amplitude decay signals, which were recorded on analog tape, were converted to digital signals at a rate of approximately 60 samples per cycle. A digital computer was used to define the decay envelope, oscillation frequency, and static trim angle. Least-squares curve fits of $\ln \theta$ and $\ln \omega$ versus time were used to determine the slopes $d \ln \theta / dt$ and $d \ln \omega / dt$ for use in Eq. 8.

Calculations were made using wind-on and wind-off values to determine the aerodynamic damping:

$$M_{\dot{\theta}_a} = M_{\dot{\theta}_\omega} - M_{\dot{\theta}_T} \left(\frac{\omega_T}{\omega_\omega} \right) \quad (9)$$

The aerodynamic coefficients were calculated as follows:

$$C_{m_q} + C_{m_{\dot{a}}} = M_{\dot{\theta}_a} \left\{ \frac{2V_\infty}{q_\infty S d^2} \right\} \quad (10)$$

In the case where the model and reflection plane were oscillated together, special wind-on runs were made with the reflection plane alone, and the resulting pitch-damping coefficients were subtracted directly to obtain net coefficients for the model. In some cases, the reflection-plane damping amounted to 50 percent of the total damping. Pitching moments referenced to the model pitch center were calculated for each steadystate trim position. The moments were reduced to coefficients by

$$C_m = \frac{M}{q_\infty S d} \quad (11)$$

4.0 RESULTS

4.1 REFLECTION-PLANE PRESSURE SURVEYS

The results of the reflection-plane pressure surveys are presented in Figs. 19 through 23. In Ref. 7, convincing evidence was presented that

the volume of the support behind the reflection plane would present enough blockage to cause spillage over the front surface of the reflection plane thereby affecting the flow field around the model. The tunnel wall was provided with a step cavity with a volume approximately equal to the volume of the support behind the reflection-plane surface. A comparison was made of the flow field pressure distribution in front of the reflection plane in the area where the model would be located with and without the cavity plugged. The results presented in Fig. 19 show that, with the cavity plugged, the disturbances extend farther downstream, especially around Mach number one.

It was desired that the reflection plane be located as near the tunnel wall as possible to alleviate model loading on the balance. Previous tunnel boundary-layer measurements had shown that boundary-layer thickness was less than one inch. A comparison of pressure distributions over the reflection plane located 0.9 and 1.4 in. away from the wall (Fig. 20) showed essentially no differences.

Tunnel flow angle measurements indicated that small flow angles occurred on the tunnel centerline and generally were greater away from the centerline. The reflection plane was positioned at three yaw attitudes relative to the tunnel wall, and pressure surveys were made. In Fig. 21, it can readily be seen that yawing the reflection-plane leading edge slightly away from the free stream gave the best pressure distribution in the area where the model would be located.

These tests showed conclusively that the reflection plane, when properly orientated, was suitable for simulating free-stream conditions near the model. Based on these results, the reflection plane was set at $h = 0.9$ in. and $\psi = -0.4$ deg and provided with a cavity at the reflection plane wall juncture for the remainder of the tests.

The aircraft model was installed on the reflection plane, and pressure surveys were made at two critical areas near the model. They included (1)

near the wing-body juncture (Fig. 22), and (2) near the reflection plane-body juncture (Fig. 23). In both cases, agreement between the full- and half-span models was excellent.

4.2 PITCH DAMPING TESTS

4.2.1 General

The order of testing was as follows: full- and half-span tests in Tunnel 1T in the angle-of-attack range from -2 to 10 deg, full-span tests in Tunnel 4T with angles of attack up to 75 deg, and half-span tests in Tunnel 1T with angles of attack from -2 to 90 deg. One rod-mounted model was also run in the last test phase. The combined plots of static pitching-moment coefficient and pitch-damping coefficient versus angle of attack from the last two phases are discussed in Section 4.2.2, as well as aircraft model pitch-damping data from the first phase (low-alpha full- and half-span tests). These data also show comparison of the two half-model mounting techniques which were discussed in Section 2.3.

The comparison plots in Section 4.2.2 are discussed with all variables matched except Reynolds number. A reduction in Reynolds number was required in Tunnel 4T in order to obtain full-span pitch-damping data above $\alpha = 10$ deg. This was necessary to keep the deflection due to static-trim angle within the balance limits. An attempt was made to determine the effects of Reynolds number on C_m and $C_{mq} + C_{m\dot{\alpha}}$ at low angles of attack, and the results are analyzed in Section 4.2.3.

One difference between the full- and half-span models was that the half-span models had closed bases, while the full-span models had open bases and a sting inserted. A study was made on one half-span model (gapped-ogive-cylinder) of the effects of opening the base and inserting a dummy sting, and the results are discussed in Section 4.2.4.

When the half-model balance was modified to the high angle-of-attack capability, the reduction in frequency that resulted gave an excellent opportunity to compare two oscillation frequencies on both the full- and half-span models. The results of these comparisons are described in Section 4.2.5.

In a test to determine an acceptable shape for the sting aft of the model, an interesting comparison was made of the effects of a large angle flare just behind the model. The results of this test are given in Section 4.2.6.

The data reduction procedure described in Section 3.3 gave damping data for oscillation amplitudes (θ) from ± 0.6 to ± 3.8 deg for the half-models and ± 0.6 to ± 3 deg for the full models. In many cases, significant variations of $C_{mq} + C_{m\dot{\alpha}}$ with θ were noted, especially for $\alpha > 30$ deg; however, for simplicity, all comparisons made in this report are for $\theta = \pm 1$ deg.

Considerable time and effort were expended to determine if boundary-layer suction through the reflection plate would help make the half-model flow field more like that of the full model. One porous plate was installed (20 micron), and suction rates up to 0.19 percent of the total tunnel flow were applied. These flow rates correspond to suction flow coefficients (C_Q) from 0 to 0.0019. The results showed no tendency to change the half-model damping data. The results were not conclusive enough, however, to state that boundary-layer suction would not help. A more detailed study which includes various porosity patterns, more suction, and even varying suction rates over the reflection plate could prove useful.

4.2.2 Full- and Half-Model Comparisons

The variations of C_m and $C_{mq} + C_{m\dot{\alpha}}$ with α for full- and half-span ogive-cylinder, hemisphere-cylinder, and wing-body models are presented

in Figs. 24 through 26, respectively. In these figures, the case where the half-span model was oscillated independently of the reflection plane is denoted by "half-span (gapped)." Again, it must be emphasized that, in the comparison between full- and half-span, Reynolds number was not matched (Fig. 17). Pitch-damping data for the aircraft model over the angle-of-attack range from -2 to 12 deg are presented in Fig. 27 where the Reynolds number was matched for all cases.

The variation of C_m with angle of attack for the ogive-cylinder model (Fig. 24a) showed agreement in the data between full-span and both half-span techniques below $\alpha = 20$ deg. Above $\alpha = 20$ deg, the data from the two half-span techniques disagreed with the full-span data and the gapped model showed lower pitching moments than the ungapped model. This was attributable to a loss in lift caused by the gap. The comparison of $C_{mq} + C_{m\dot{\alpha}}$ for the three ogive-cylinder models in Fig. 24b showed good agreement for all three cases up to $\alpha = 30$ deg except for $M_\infty = 1.0$. For $\alpha > 30$, the agreement deteriorated. The general opinion that pitch damping is affected by the attachment and separation points on the model appears to hold true in this case. Orlik-Ruckemann in Ref. 19 experimented with full- and half-span cones and found that the presence of the reflection plane caused displacement of both attachment and separation points for $\alpha > 20$ deg. The pattern of vortex shedding, which also affects the pitch damping, was also altered by the presence of the reflection plane.

In Fig. 25, similar comparisons are made for the hemisphere-cylinder models. An additional configuration consisting of a full-span model mounted on a rod through the pitch axis is also included. The comparison of C_m for the sting-mounted full-span model and the two half-model configurations showed approximately the same results as seen with the ogive-cylinder models. The rod model data showed larger differences in C_m from the other configurations at Mach numbers above 0.8 (Fig. 25). For $M_\infty \geq 1.0$, the rod model C_m showed a break from

the other cases at $\alpha = 10$ deg. In Ref. 20, schlieren photographs of a model mounted on a rod indicated that the normal shock ahead of the rod influenced the flow field on the model in front and back of the rod for $M \geq 1.0$. Pitch-damping comparisons (Fig. 25b) showed fair agreement between full- and half-span data up to $\alpha = 20$ deg. No explanation can be made for the apparent random but repeatable spikes that occurred throughout the angle-of-attack range for the half-models. Note that the ungapped half-model exhibited dynamic instability above and below $\alpha = 0$ at $M_\infty = 0.9$. This phenomenon will be discussed in greater detail in Section 4.2.3.

Static pitching-moment characteristics of the wing-body model shown in Fig. 26a are somewhat different from those of the axisymmetric models. The ungapped half-model showed good agreement at $M_\infty = 0.6$, $\alpha \leq 35$ deg and $M_\infty = 1.2$, $\alpha \leq 50$ deg; however, in general, the half-model configurations showed considerably smaller C_m values at the larger angles of attack than the full-span model. Differences of this magnitude were unique to these half- full-span comparisons; hence, other differences such as Reynolds number must be investigated. It will be shown in Section 4.2.3 that Reynolds number mismatch caused the differences. The largest disagreement occurred at $M_\infty = 1.0$, and here again the loss of lift incurred by the gapped model was evident. The comparison of full- and half-span pitch-damping data shown in Fig. 26b indicated, if the same criteria used for the axisymmetric models were used in this case, that a fair comparison only up to $\alpha = 20$ deg was evident for $M_\infty < 1.0$ and $\alpha = 10$ deg for $M_\infty \geq 1.0$.

In Fig. 27, the comparison of pitch-damping characteristics of the full- and half-span aircraft models showed good agreement at subsonic Mach numbers over the angle-of-attack range shown. Significant differences, however, were noted at the transonic Mach numbers. Also considerable differences were seen between the gapped and ungapped half-models, especially for $M_\infty \geq 1$.

A special note about the comparison of the two half-model mounting techniques concerning the pitch-amping differences noted in the previous section is in order. Two sources of differences are immediately evident, and they include viscous damping between the gapped model and the reflection plane, and the loss of lift due to gap. The latter was predicted theoretically by Judd in Ref. 21 where the loss of lift theory was extended to the case of a wing with a root gap undergoing pitch oscillations. In this test, each of the models used was susceptible to both sources of error, and it appears that the effects cancel each other on the ogive-cylinder, hemisphere-cylinder and wing-body models (Figs. 24b, 25b, and 26b, respectively). The aircraft model which derived most of its damping from the T-tail was more susceptible to the loss of lift caused by the gap; hence, the gapped model should have less damping which was precisely the case in Fig. 27.

4.2.3 Effects of Reynolds Number

The effects that Reynolds number had on the static and dynamic pitching-moment characteristics of the three full-span models are shown in Figs. 28 through 30. The ogive-cylinder model (Fig. 28) showed no effects of Reynolds number change on C_m (Fig. 28a) and significant effects on $C_{mq} + C_{m\dot{\alpha}}$ (Fig. 28b). The largest differences occurred for $\alpha > 6$ deg and $M_\infty \geq 1$. The hemisphere-cylinder model showed Reynolds number effects on both C_m and $C_{mq} + C_{m\dot{\alpha}}$ (Fig. 29). Here the largest differences in $C_{mq} + C_{m\dot{\alpha}}$ occurred for $\alpha > 4$ deg and $M_\infty \geq 1$. Another significant difference is at $M_\infty = 0.9$ and for $0 \leq \alpha \leq 3$ deg where the high Reynolds number case exhibited a dynamic instability (Fig. 29b) and the low Reynolds number case did not. The wing-body model (Fig. 30) showed significant differences in both C_m and $C_{mq} + C_{m\dot{\alpha}}$ for the two Reynolds numbers. In general, C_m showed greater differences as angle of attack was increased (Fig. 30a). These differences in C_m are consistent with those observed in Fig. 26a where comparisons were made for full- and half-span models that were tested

at different Reynolds numbers. The pitch damping of the wing-body model showed Reynolds number effects at most angles of attack with no definite trends (Fig. 30b).

With these observations, further conclusions were reached concerning previously discussed occurrences. The dynamic instability experienced by the hemisphere-cylinder full-span model and not by the half-models (Fig. 25b) closely resembled that produced by an increase in Reynolds number (Fig. 29b). The conclusion may be drawn that the half-models were subjected to a flow field that was effectively reduced in Reynolds number from the free stream. Another observation is that the same effects of Reynolds number on the pitch damping of the wing-body model (Fig. 30b) was observed in the comparison of full- and half-span models in Fig. 26b where the Reynolds number was not matched. One could conclude that the comparison might be better to a higher angle-of-attack if Reynolds number were matched.

4.2.4 Effects of Base Alterations

All of the previously discussed half-models were tested with closed bases. However, the full-span models had open bases and a sting entering at the base. A study was made to determine the effects of the base alterations (Fig. 14a), and the results are shown in Fig. 31. The static pitching-moment coefficients showed only minor effects of the base changes (Fig. 31a). In Fig. 31b, the only effect of base changes on the pitch-damping coefficients was an increase in pitch-damping above $\alpha = 15$ deg at $M_\infty = 0.6$ that quickly disappeared as angle of attack and Mach number were increased.

4.2.5 Effect of Oscillation Frequency

Data were obtained on full-span models at identical conditions in Tunnels 1T and 4T except at a lower frequency in Tunnel 4T. Comparisons of half-span data at identical conditions in Tunnel 1T at two frequencies

were also made. Comparison of $C_{mq} + C_{m\dot{\alpha}}$ at two oscillation frequencies for the full-span ogive-cylinder and hemisphere-cylinder models is presented in Figs. 32 and 33. The ogive-cylinder model showed more variations in $C_{mq} + C_{m\dot{\alpha}}$ with angle of attack at all Mach numbers at the lower frequency (Fig. 32). The differences became more apparent as Mach number was increased. The identical results were noted on the hemisphere-cylinder model (Fig. 33) except the largest $C_{mq} + C_{m\dot{\alpha}}$ differences were noted for $0.8 \leq M_\infty \leq 1.0$. Frequency had no effect on the dynamic instability at $M_\infty = 0.9$.

Comparison of pitch-damping data at two oscillation frequencies on the ogive-cylinder, hemisphere-cylinder, and wing-body half-models is presented in Figs. 34 through 36, respectively. The ogive-cylinder model data showed only minor effects of frequency except at $M_\infty = 1$. One unstable spike at $M_\infty = 1.2$ was seen at the lower frequency that was not observed at the higher frequency (Fig. 34). The hemisphere-cylinder model (Fig. 35) showed some frequency effects at all Mach numbers. The most notable was the difference at $M_\infty = 0.9$ where the dynamic instability was observed on the full-span model (Fig. 33). For the half-span model, the lower frequency showed dynamic instabilities on either side of $\alpha = 0$, while the higher frequency did not.

A different type of frequency change was made on the wing-body model in that the moment of inertia was changed on the balance with the inertia disk (Fig. 14a). A single Mach number ($M_\infty = 1.0$) was chosen to show the effects of frequency at large angles. The effects were found to be minimal (Fig. 36) except at the largest angles ($\alpha > 75$ deg).

Pitching moment was derived from the static trim angle of the model; hence oscillation frequency would not affect the results. Values of C_m for the ogive-cylinder and hemisphere-cylinder models are presented, however, to show data repeatability between the two tunnels (Figs. 37 and 38).

4.2.6 Effect of Sting Shape

During the full-span damping tests, it became necessary to check the effects of sting shape on the model pitch damping. Data were taken on the sting balance, one with a flare located immediately aft of the model base (Fig. 39), and with a slender sting (Figs. 10 and 11). The results are illustrated in Figs. 40 and 41 for the aircraft and hemisphere-cylinder models, respectively. In Fig. 40a, the aircraft static pitching moments were altered at all Mach numbers, particularly at $M_\infty = 0.9$. The aircraft pitch-damping coefficients in Fig. 40b showed almost no effects of the flare addition. The hemisphere-cylinder model also showed effects of the flare on the static pitching-moment coefficients (Fig. 41a) at all Mach numbers except $M_\infty = 0.6$ and almost no effects on the pitch-damping coefficients (Fig. 41b). The addition of the flare had no effect on the dynamic instability at $M_\infty = 0.9$.

5.0 CONCLUDING REMARKS

On the basis of comparison with full-span test results, the half-model, reflection-plane technique was found to give fully reliable results for the configurations tested only at subcritical speeds and angles of attack below 20 deg. In tests at higher Mach numbers in the transonic range and higher angles of attack up to 90 deg, it was not demonstrated that the half-model technique can provide better than qualitative, order of magnitude results.

REFERENCES

1. Reding, Peter J. and Ericsson, Lars E. "Dynamic Support Interference." Journal of Spacecraft and Rockets, July 1972.
2. Shadow, T. O. and Paulk, R. A. "Dynamic Stability Characteristics of Bluff Bodies of Revolution at Transonic Mach Numbers." AEDC-TR-72-110 (AD902214L), August 1972.

3. Orlik-Ruckemann, K. J., LaBerge, J. G., Adams, P. A., and Conlin, L. T. "A Wind Tunnel Apparatus for Dynamic Stability Experiments on Sting-Mounted Slender Bodies." National Research Council of Canada, NAE LTR-UA-13, 1970.
4. Millard, W. A. and Curry, W. H. "A Thin Strap Support for the Measurement of Dynamic Stability Characteristics of High-Fineness-Ratio, Wind Tunnel Models." Journal of Spacecraft and Rockets, July 1970.
5. Crain, C. D., et al. "Design and Initial Calibration of a Magnetic Suspension System for Wind Tunnel Models." AEDC-TR-65-187 (AD470147), September 1965.
6. Orlik-Ruckemann, K. J. "Measurement of Aerodynamic Damping and Stiffness Derivatives in Free Oscillation with Automatically Recycled Feedback." National Research Council of Canada, NAE LR-246, 1959.
7. Van der Blik, J. A. "Notes on Half-Model Testing in Wind Tunnels." AGARDograph 298, 1959.
8. Orlik-Ruckemann, K. J. and LaBerge, J. G. "Static and Dynamic Longitudinal Stability Characteristics of a Series of Delta and Sweptback Wings at Supersonic Speeds." National Research Council of Canada, NAE LR-396, January 1966.
9. Orlik-Ruckemann, K. J. and LaBerge, J. G. "Dynamic Stability Experiments on Straight Wing Space Shuttle Abort Separation at $M = 1.80$." National Research Council of Canada, NAE LTR-UA-16, May 1971.

10. Orlik-Ruckemann, K. J. and LaBerge, J. G. "Dynamic Interference Effect on Dynamic Stability of Delta-Wing Shuttle in Abort Separation at $M = 2.00$." National Research Council of Canada, NAE LTR-UA-18, November 1971.
11. Orlik-Ruckemann, K. J., LaBerge, J. G., and Hanff, E. S. "Supersonic Dynamic Stability Experiments on the Space Shuttle." AIAA Paper No. 72-135, January 1972.
12. LaBerge, J. G. and Orlik-Ruckemann, K. J. "Aerodynamic Plume Interference on the Damping in Pitch of the Delta-Wing Shuttle Launch Configuration at Supersonic Speeds." National Research Council of Canada, NAE LTR-UA-20, June 1972.
13. Orlik-Ruckemann, K. J., LaBerge, J. G., and Iyengar, S. "Comparison of Three Oscillatory Techniques for Cones at Incidence." AIAA Paper No. 72-1015, September 1972.
14. LaBerge, J. G. "Effect of Flare on the Dynamic and Static Moment Characteristics of a Hemisphere-Cylinder Oscillating in Pitch at Mach Numbers from 0.3 to 2.0." National Research Council of Canada, NAE LR-295, January 1961.
15. Black, J. A. "A Note on the Comparison of Dynamic Stability Results between Those Obtained at the National Aeronautical Establishment and the Transonic Model Tunnel of the Propulsion Wind Tunnel Facility." Unpublished Note, September 1961.
16. Orlik-Ruckemann, K. J. "Survey of Needs and Capabilities for Wind Tunnel Testing of Dynamic Stability of Aircraft at High Angles of Attack." NASA CR-114583, 1973.
17. Test Facilities Handbook (Tenth Edition). "Propulsion Wind Tunnel Facility, Vol. 4." Arnold Engineering Development Center, May 1974.

18. Schueler, C. J., Ward, L. K., and Hodapp, A. E., Jr. "Techniques for Measurement of Dynamic Stability Derivatives in Ground Test Facilities." AGARDograph 121, October 1967.
19. Orlik-Ruckemann, K. J., and Iyengar, S. "Comparison of Three Oscillatory Techniques for Cones at Incidence." AIAA Paper No. 72-1015, September 1972.
20. Riddle, C. D. "Wind Tunnel Investigation to Determine the Feasibility of Image Model Testing at Transonic Mach Numbers." AEDC-TR-68-7 (AD828924L), March 1968.
21. Judd, M. "The Effect of a Root Gap on the Aerodynamic Forces on a Slender Delta Wing in Oscillatory Pitching Motion." The Aeronautical Quarterly, August 1963.

Ref. 2

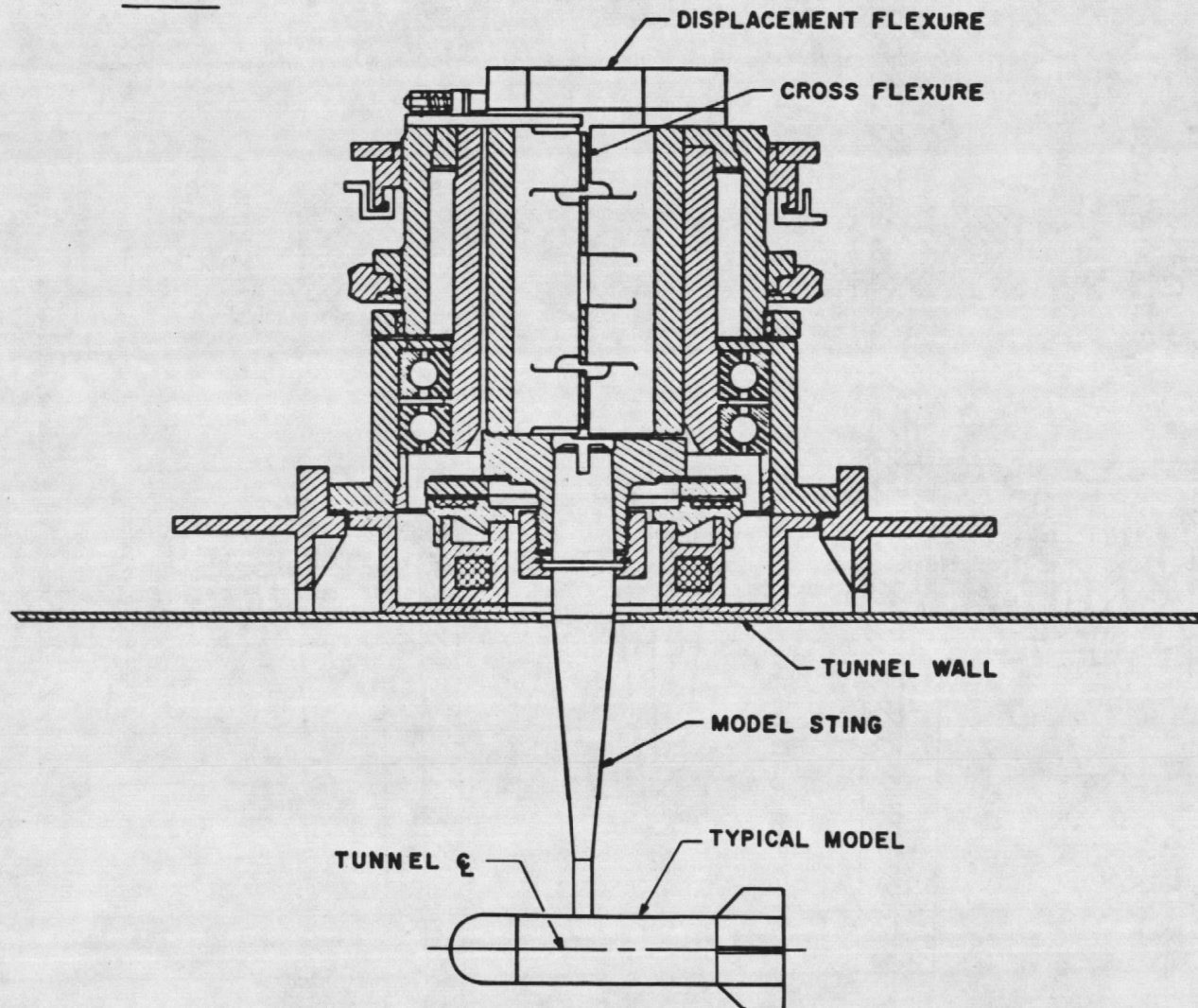


Figure 1. Rod model test mechanism.

Ref. 3

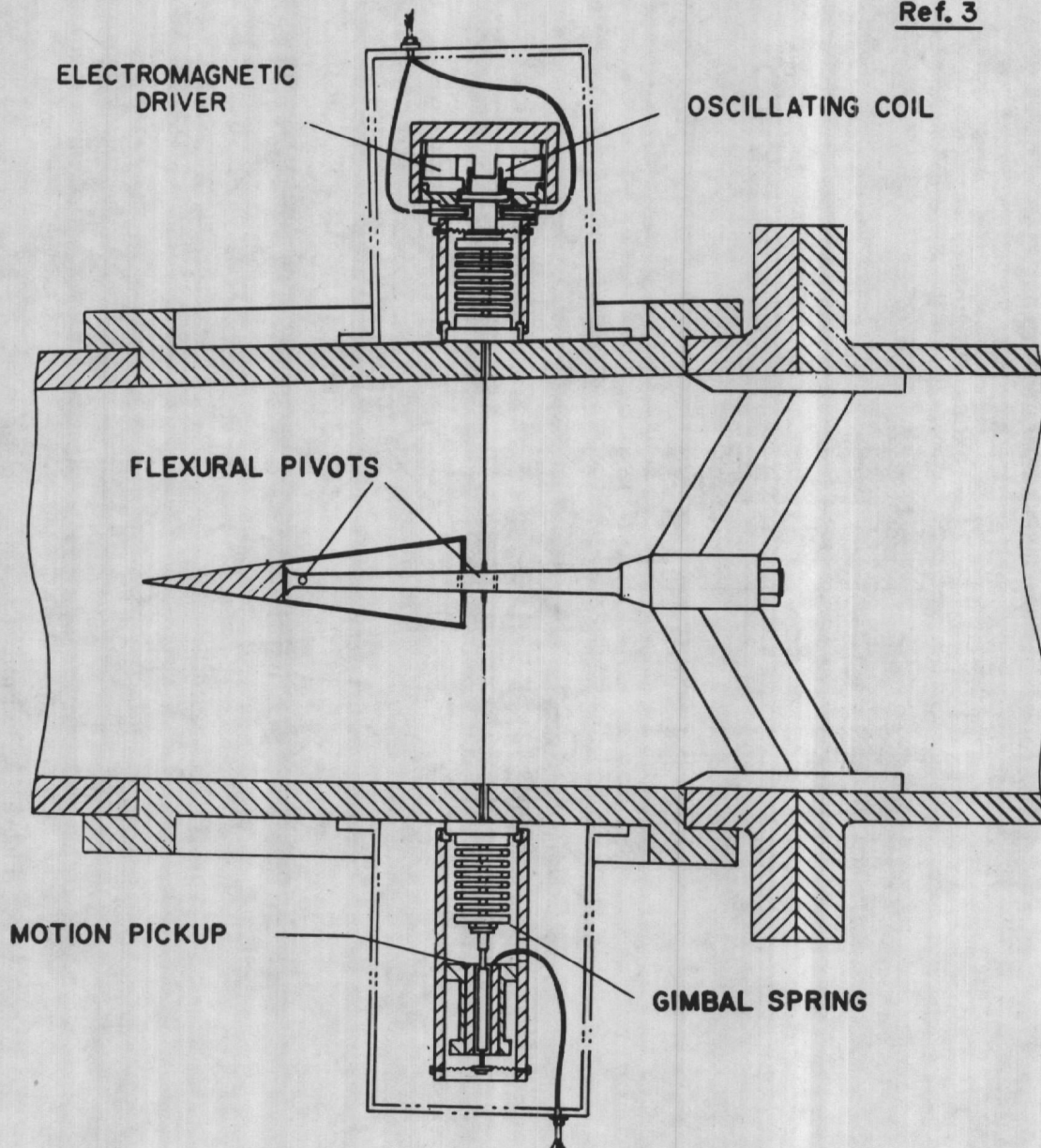


Figure 2. Sting model with external excitation.

Ref. 4

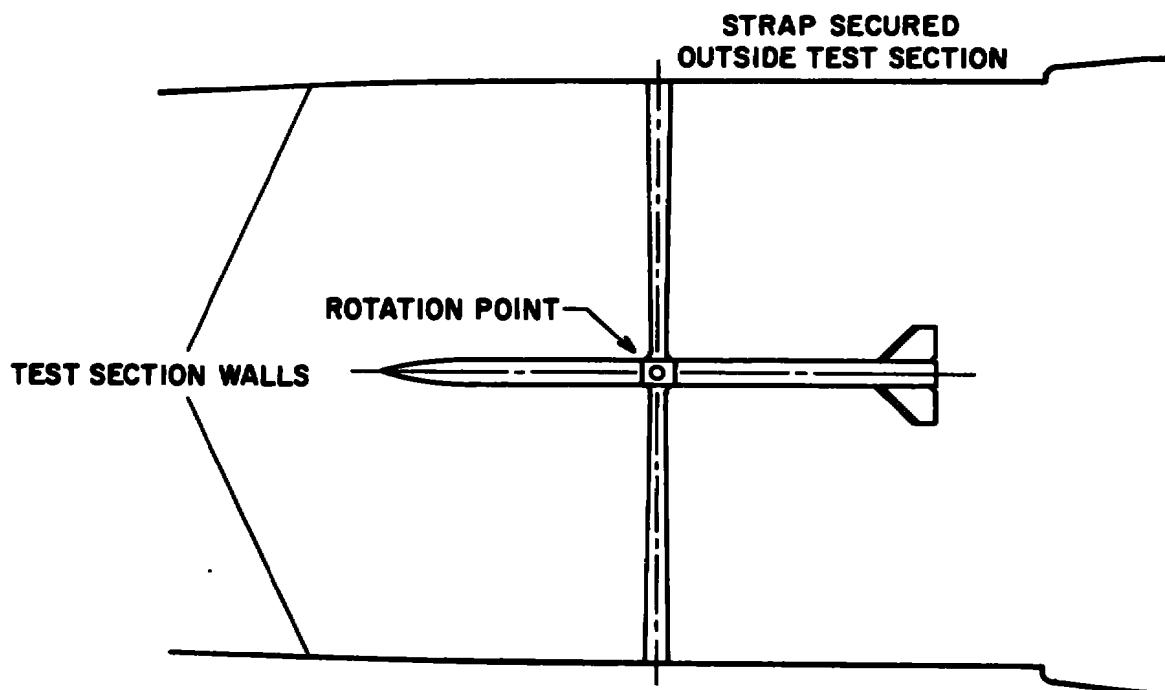


Figure 3. Ribbon-mounted model test mechanism.

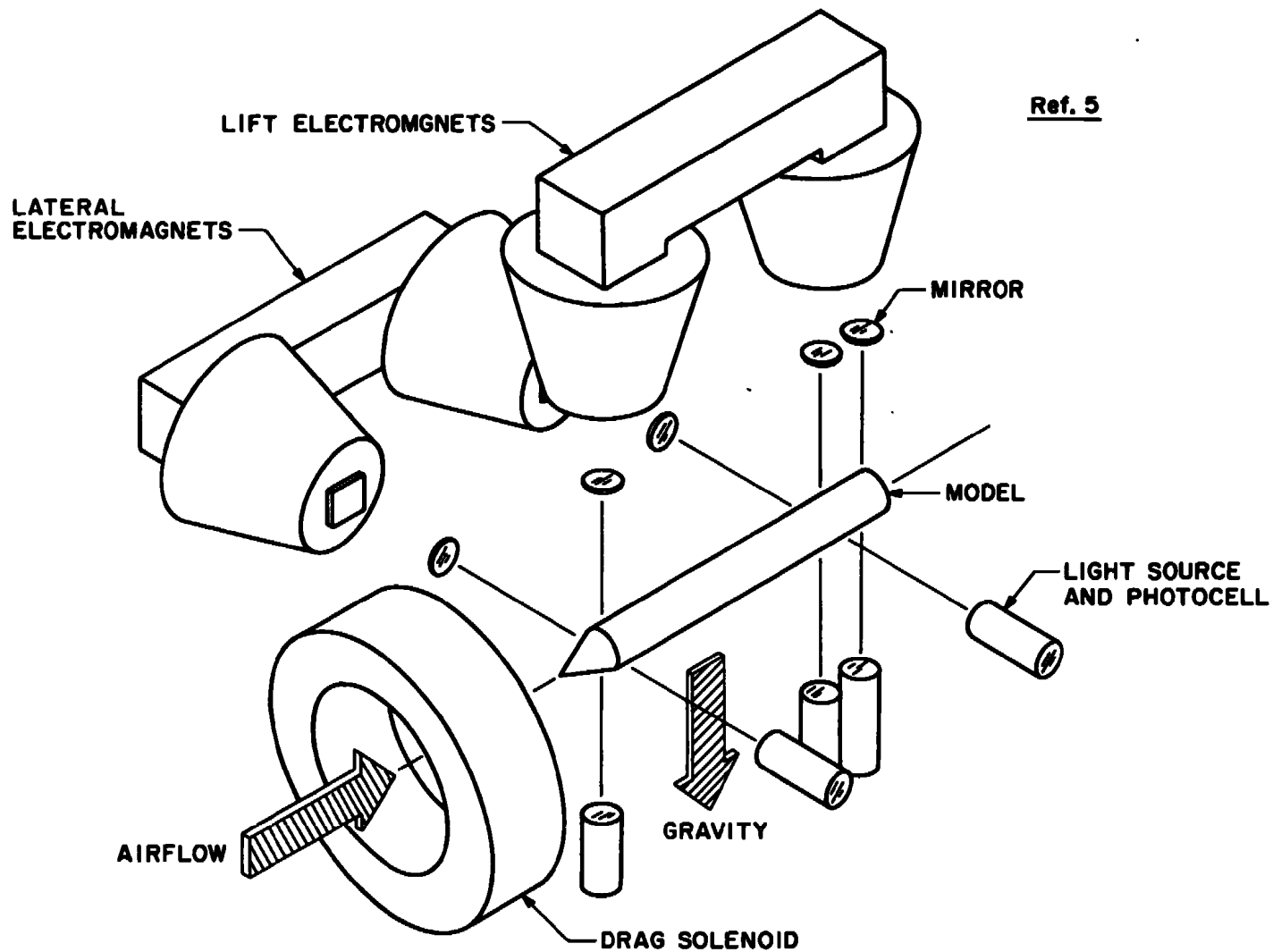


Figure 4. Magnetic suspension system.

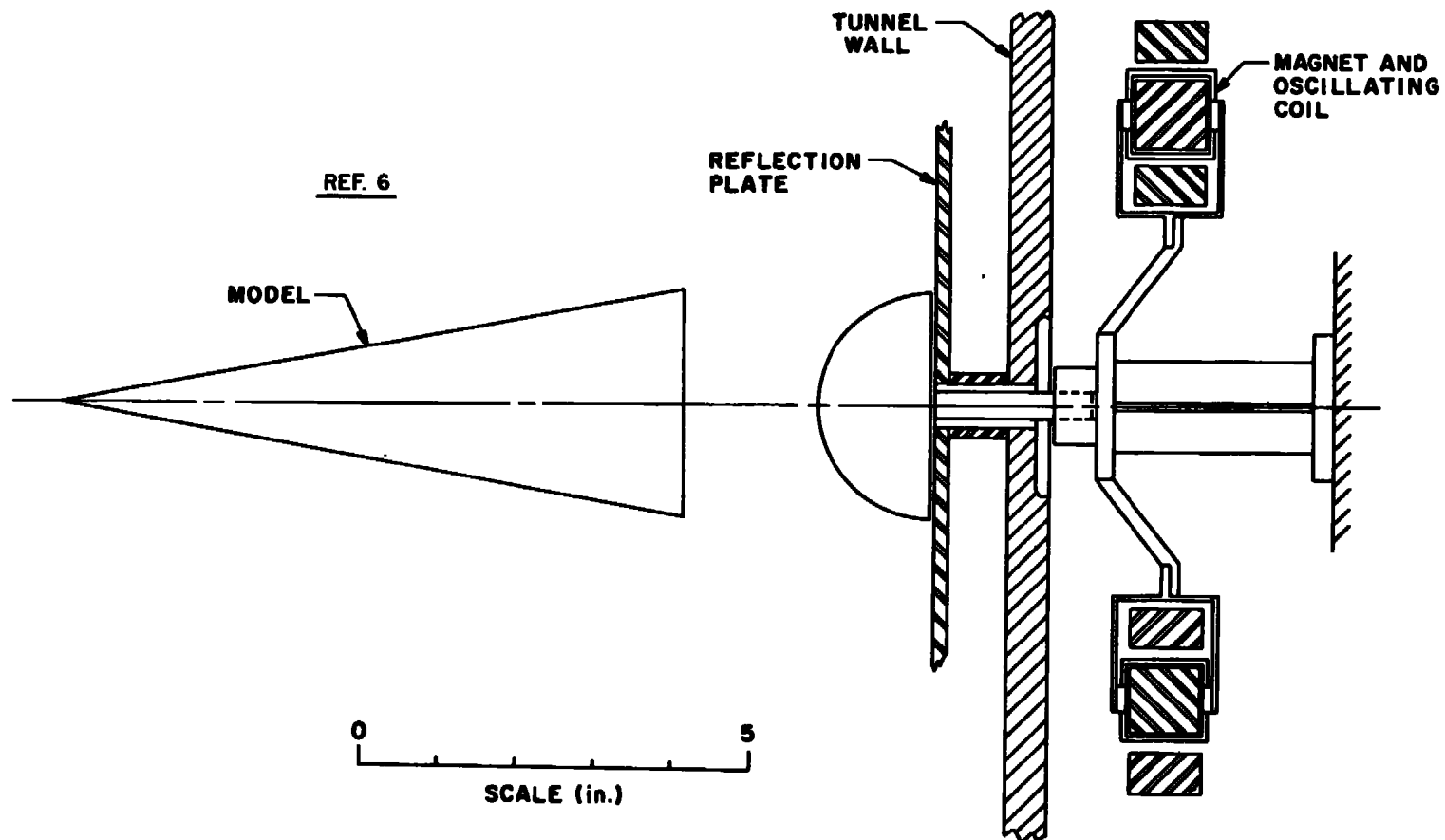


Figure 5. Half-model test mechanism.

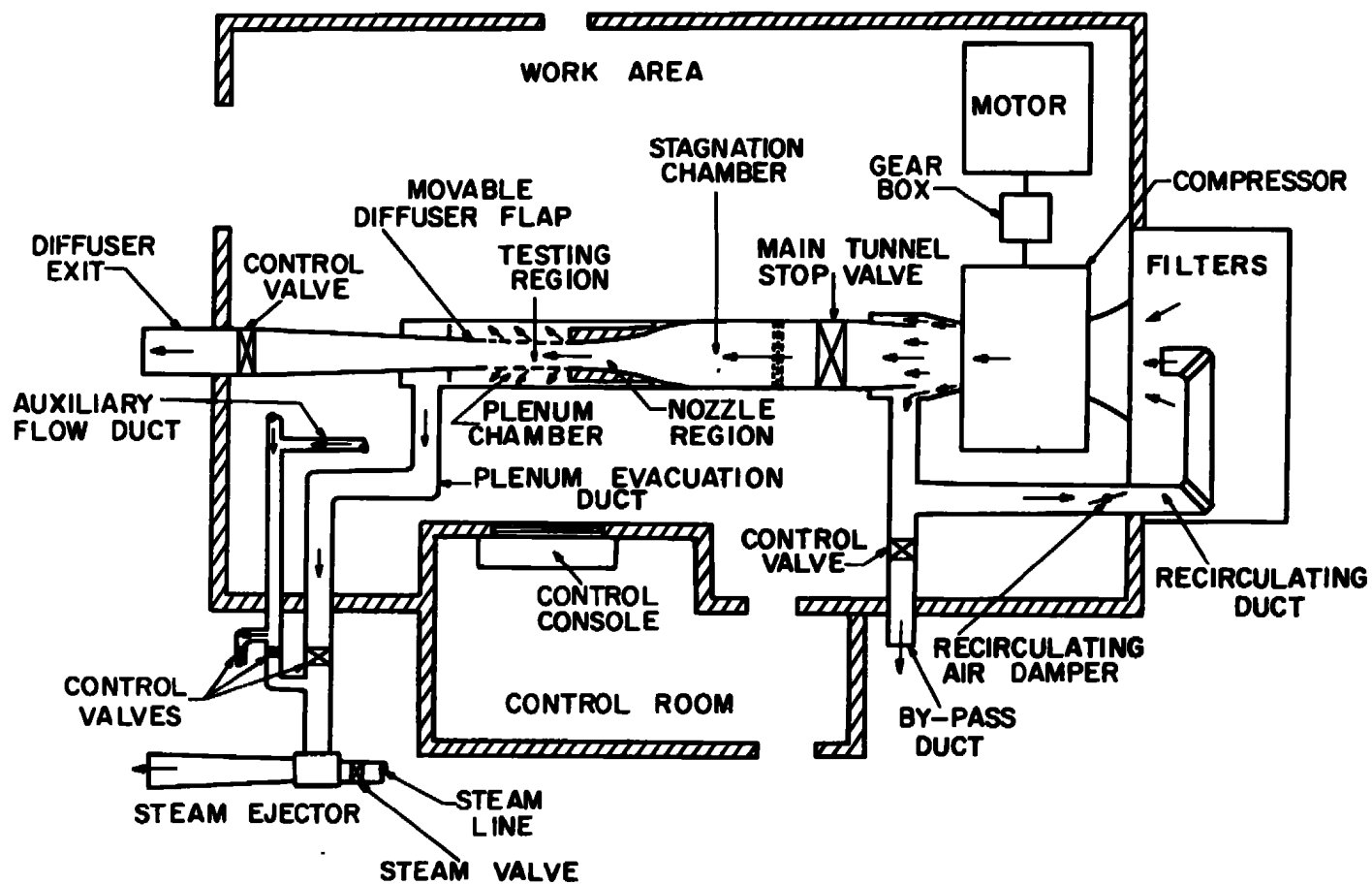
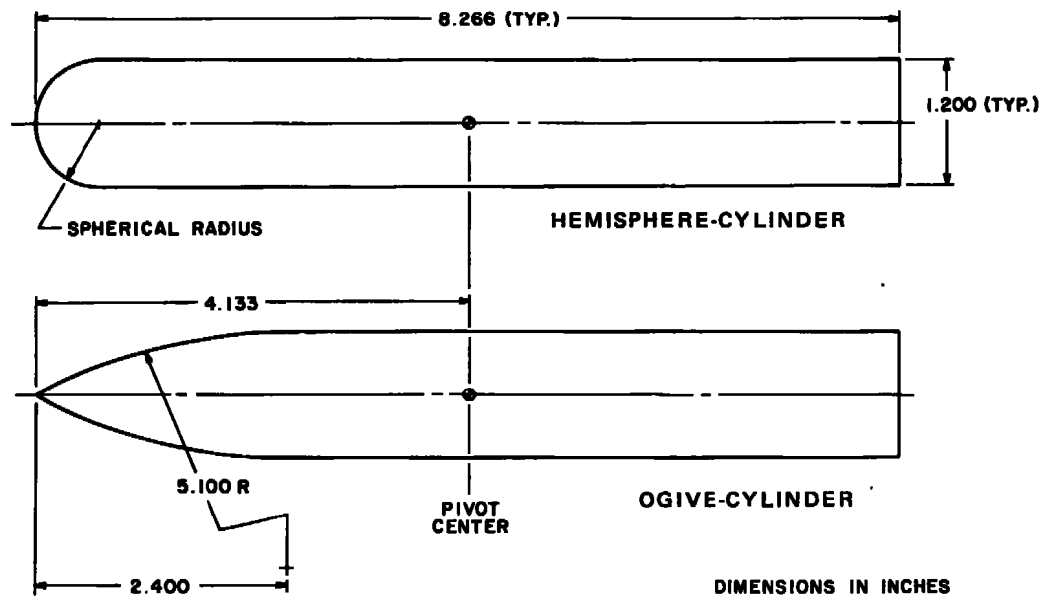


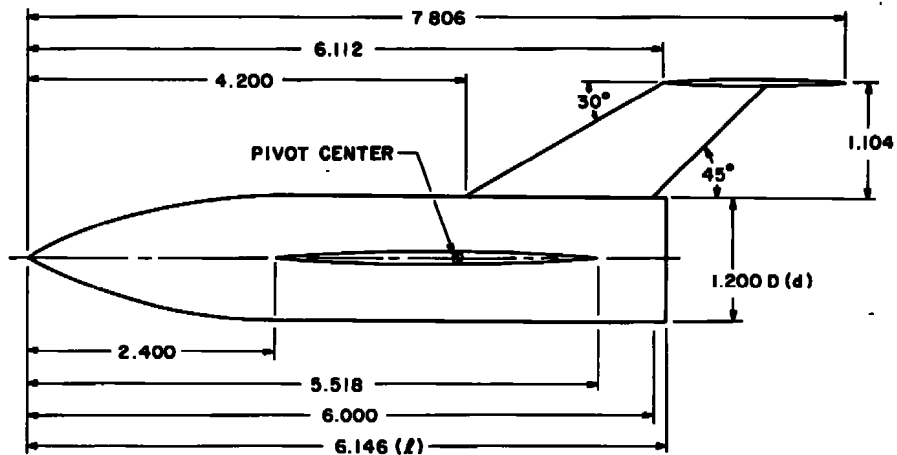
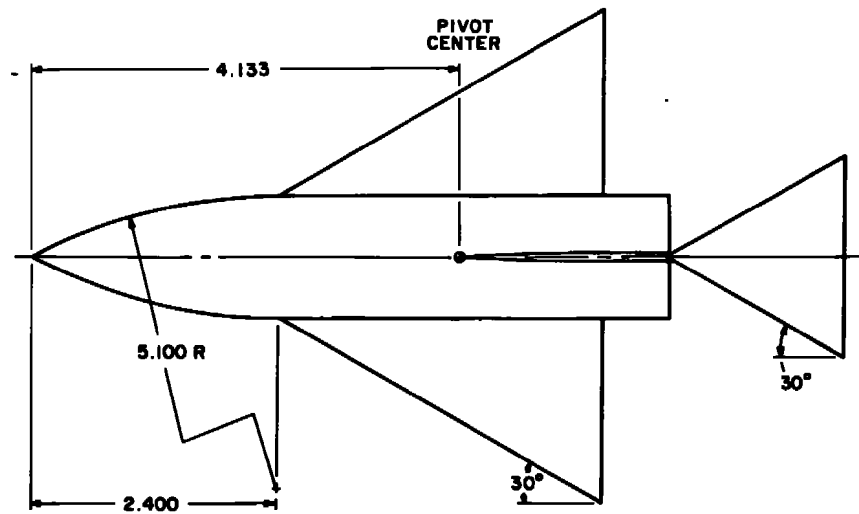
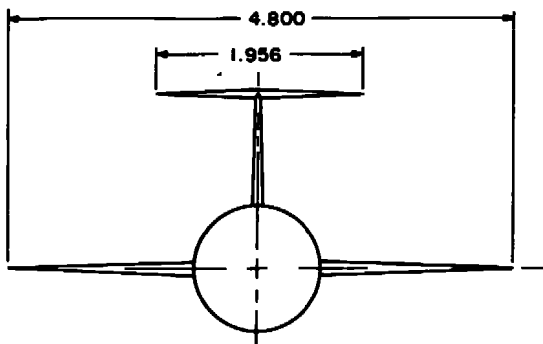
Figure 6. General arrangement of Tunnel 1T.



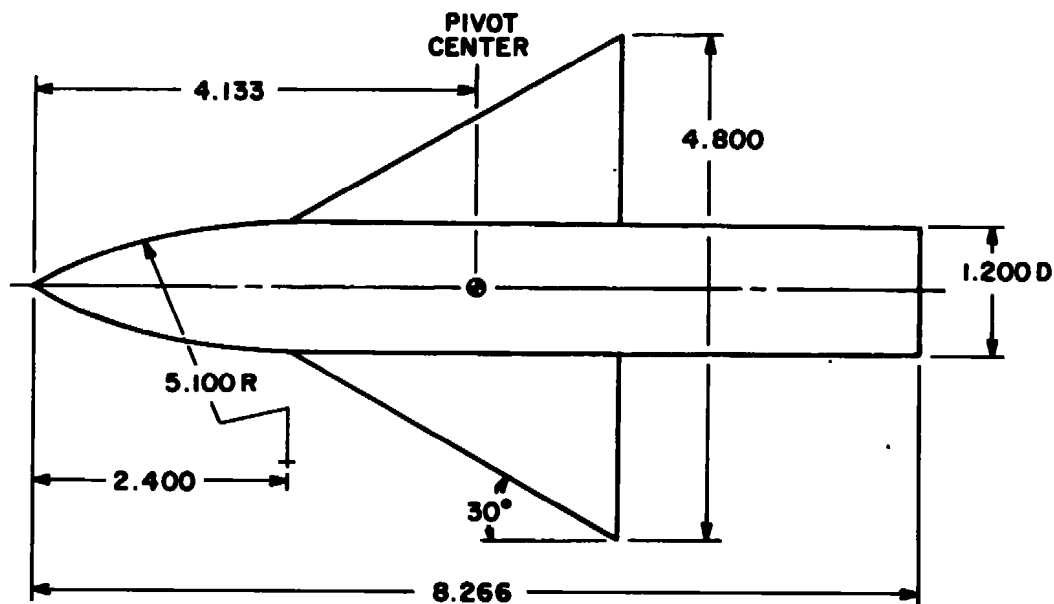
a. Axisymmetric models
Figure 7. Test models.

NOTES:

1. DIMENSIONS IN INCHES
2. AIRFOIL SURFACES - SYMMETRICAL 4 PERCENT CIRCULAR ARC

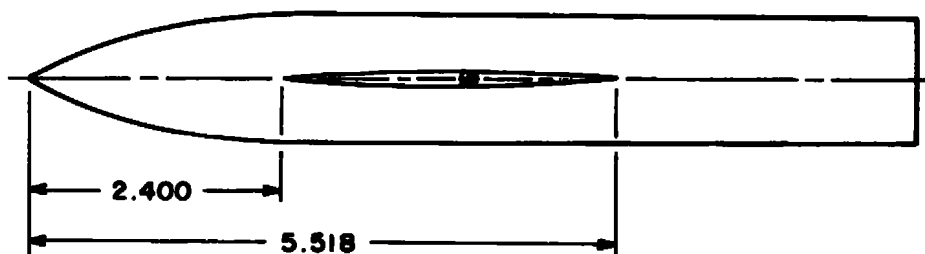


b. Aircraft model
Figure 7. Continued.



NOTES:

1. DIMENSIONS IN INCHES
2. AIRFOIL SURFACES - SYMMETRICAL 4 PERCENT CIRCULAR ARC



c. Wing-body model
Figure 7. Concluded.

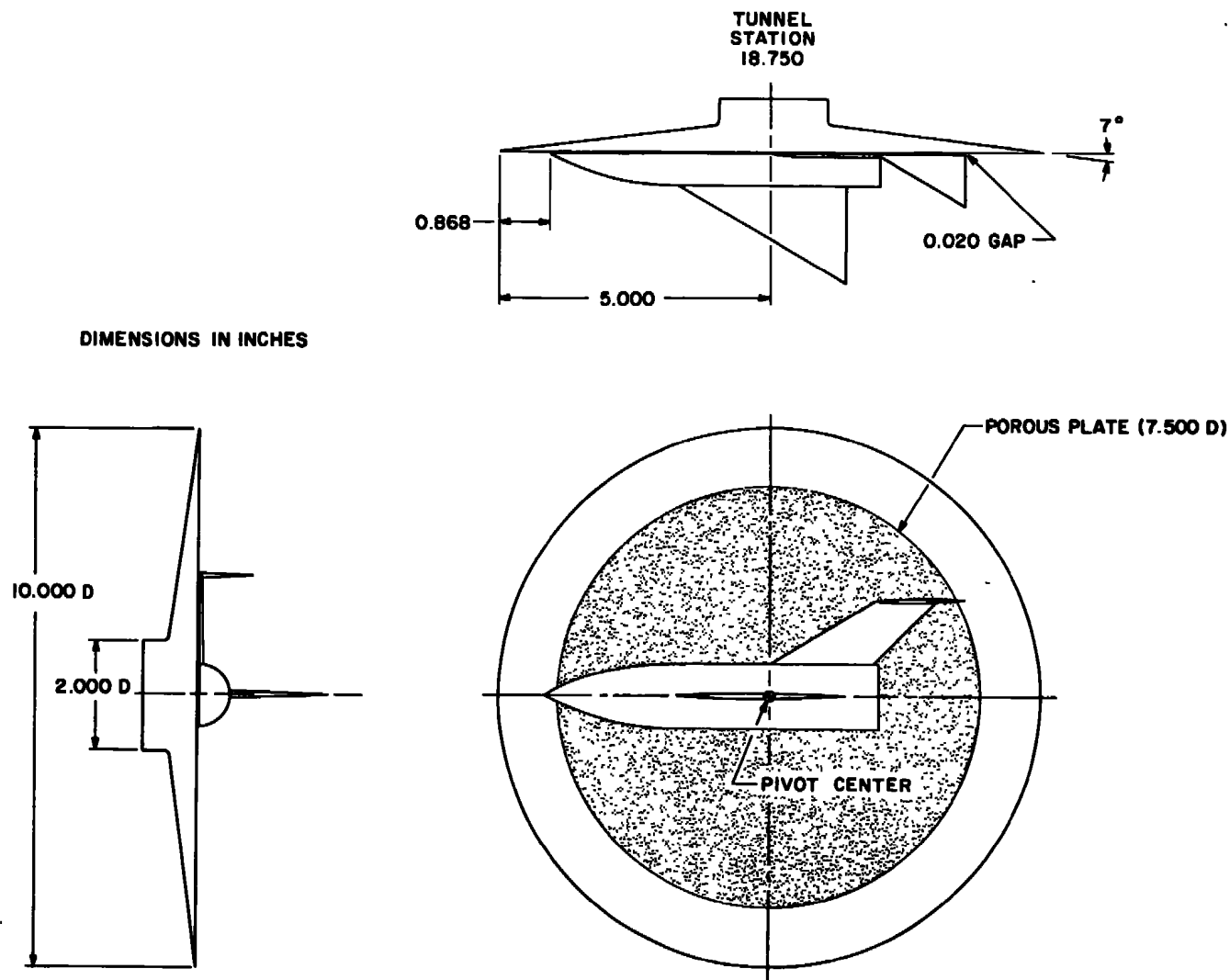
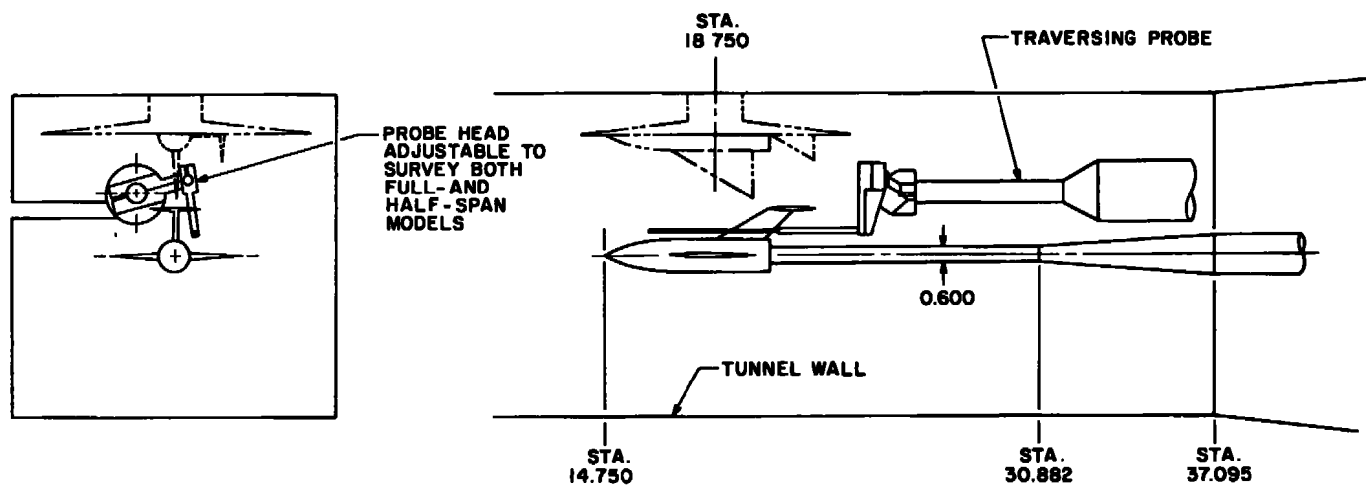
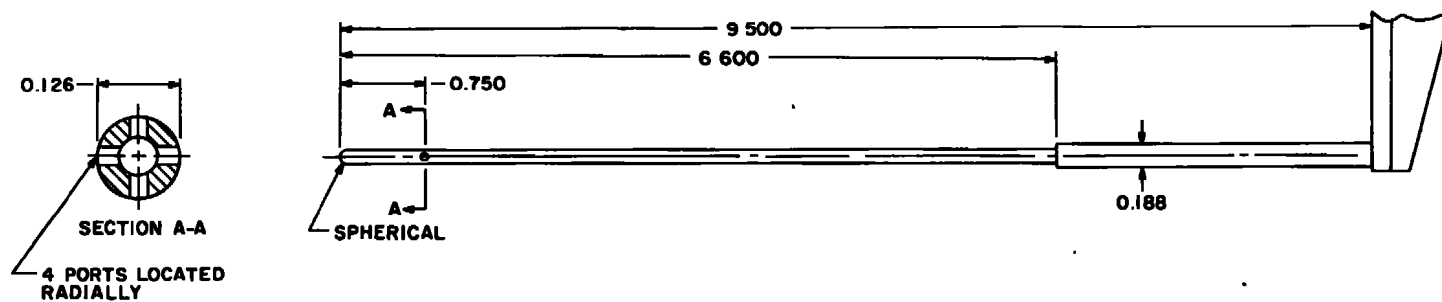


Figure 8. Reflection-plane geometry.

NOTES:

1. PROBE CAPABLE OF VARYING PRESSURE PORTS AXIAL TRANSLATION FROM TUNNEL STATIONS 12.0 THROUGH 21.1
2. TUNNEL STATIONS AND DIMENSIONS IN INCHES



a. Schematic

Figure 9. Pressure survey test mechanism.



b. Photograph
Figure 9. Concluded.

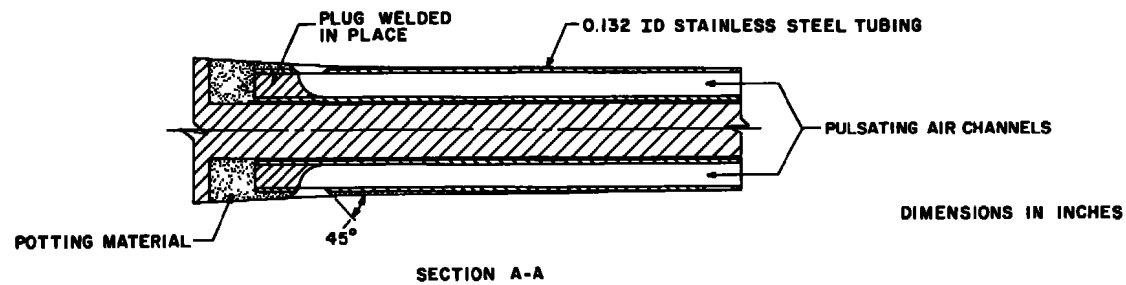
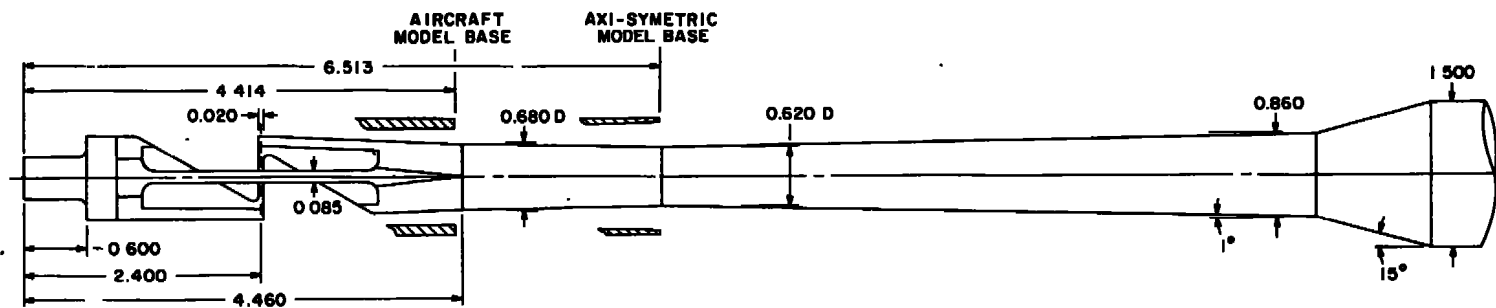
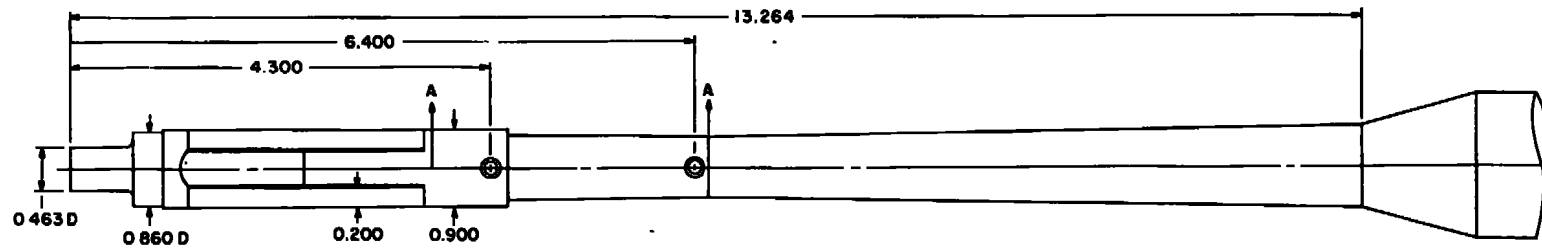
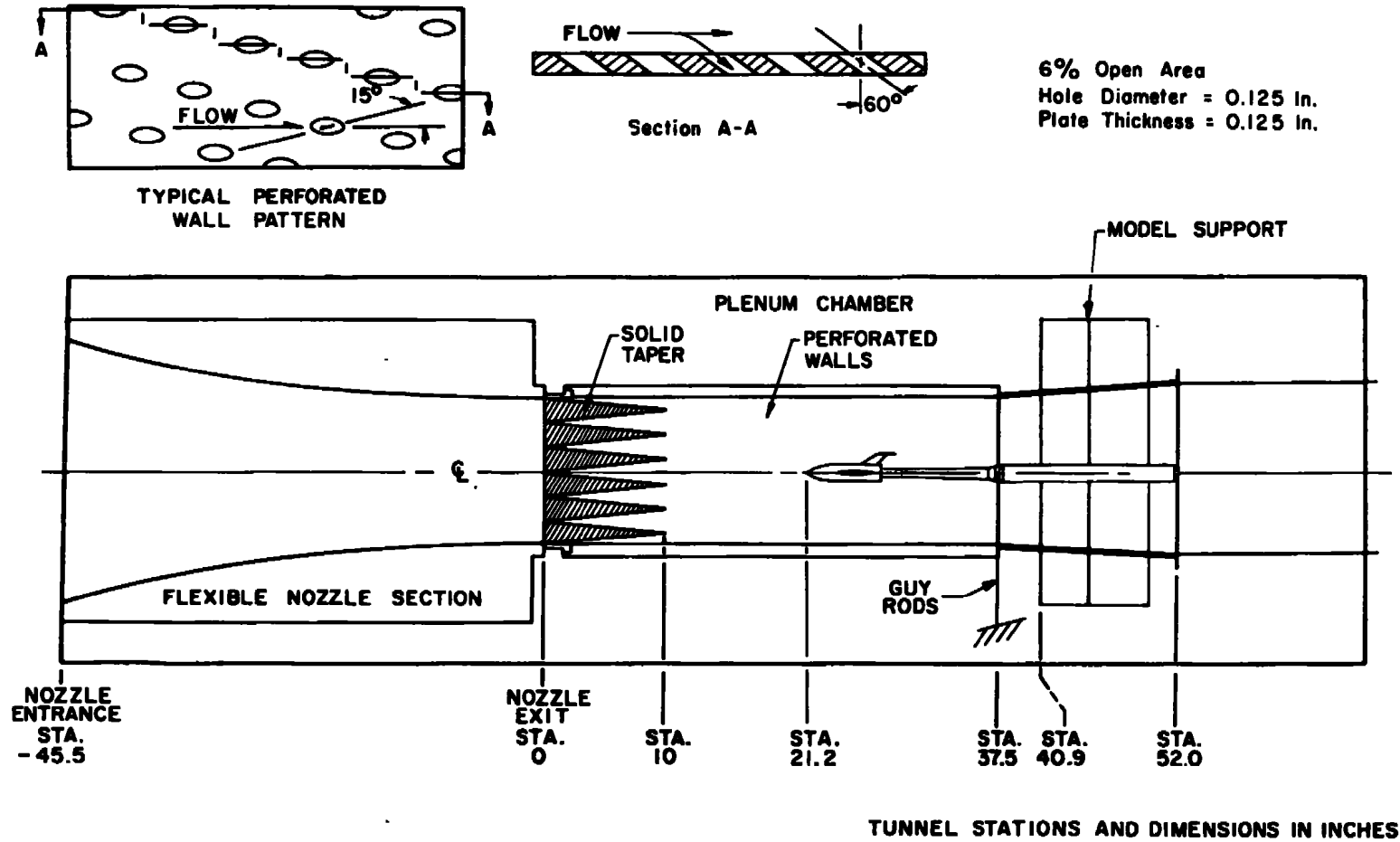
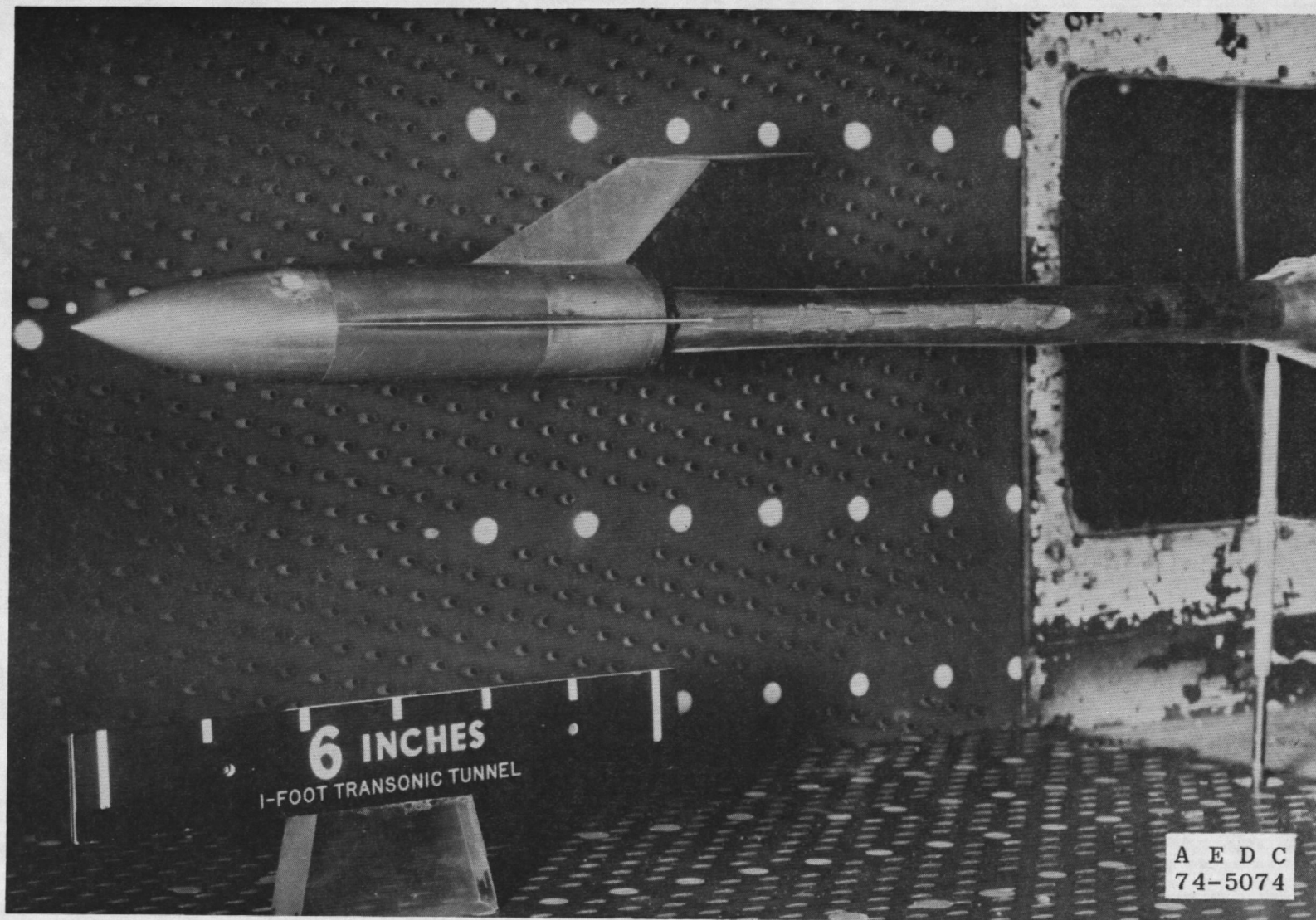


Figure 10. Sting-mounted free-oscillation balance.

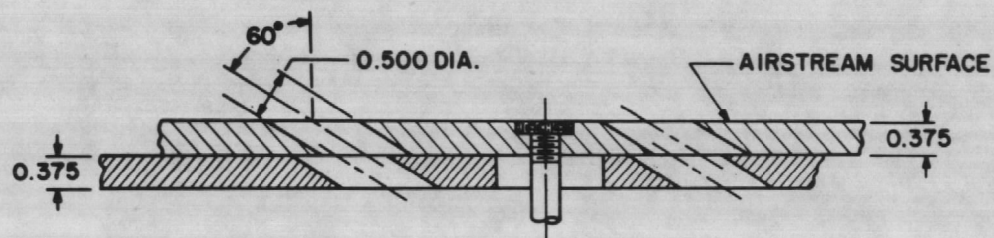


a. Schematic

Figure 11. Tunnel 1T sting support equipment.

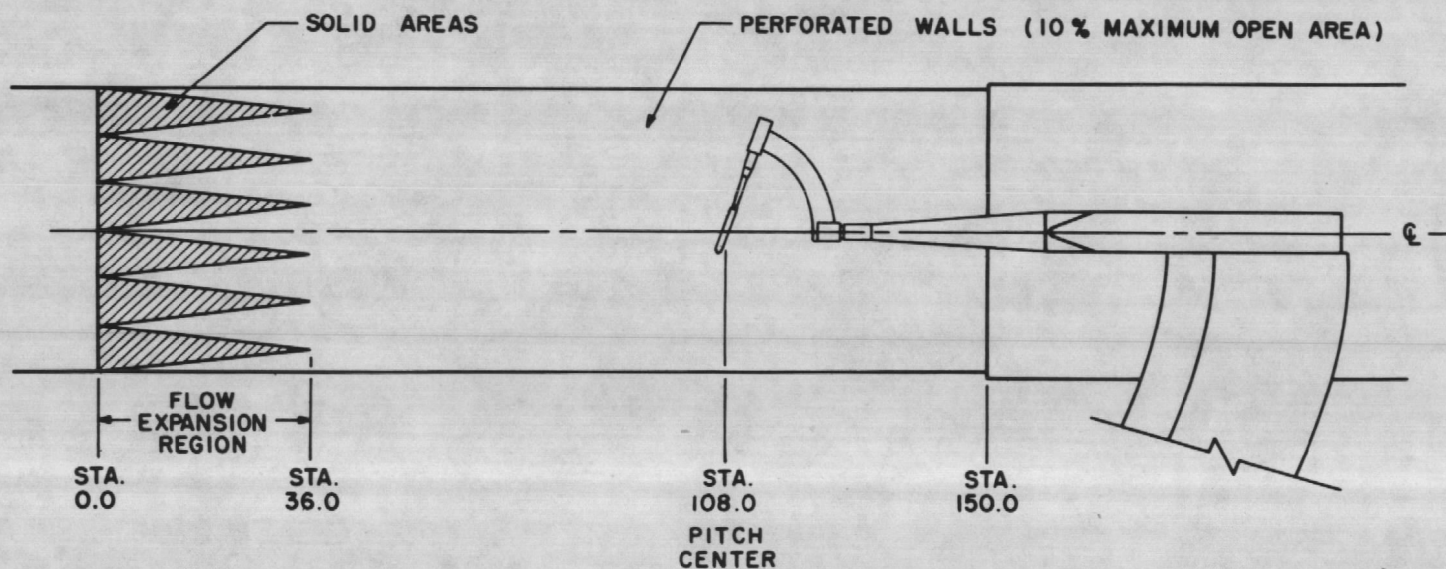


b. Photograph
Figure 11. Concluded.



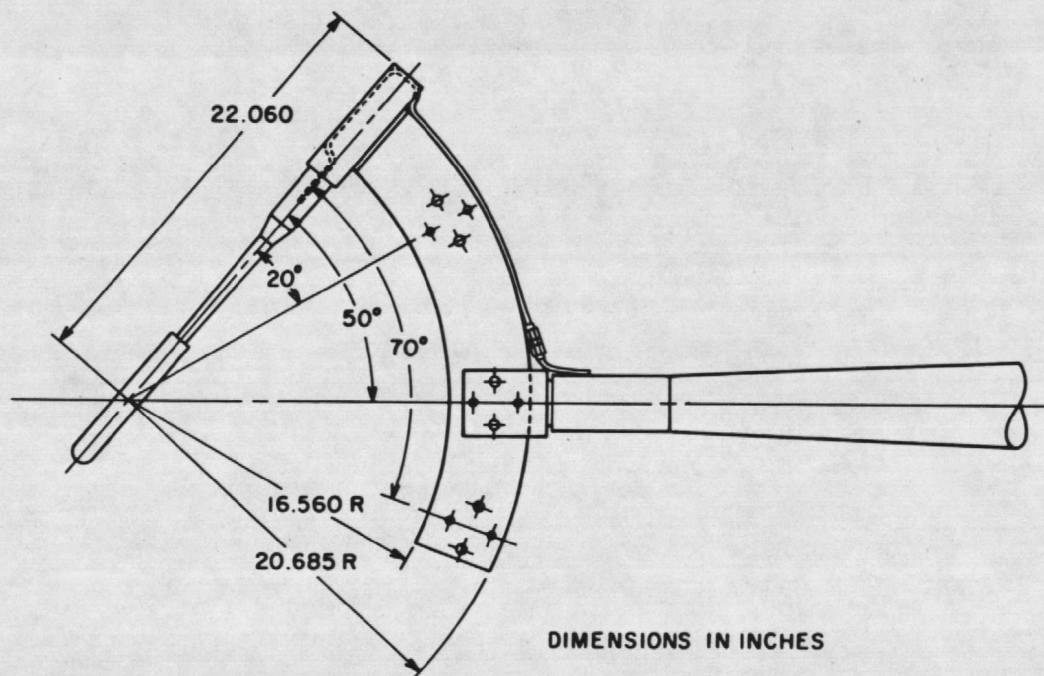
TYPICAL PERFORATED WALL CROSS SECTION

TUNNEL STATIONS AND DIMENSIONS
ARE IN INCHES

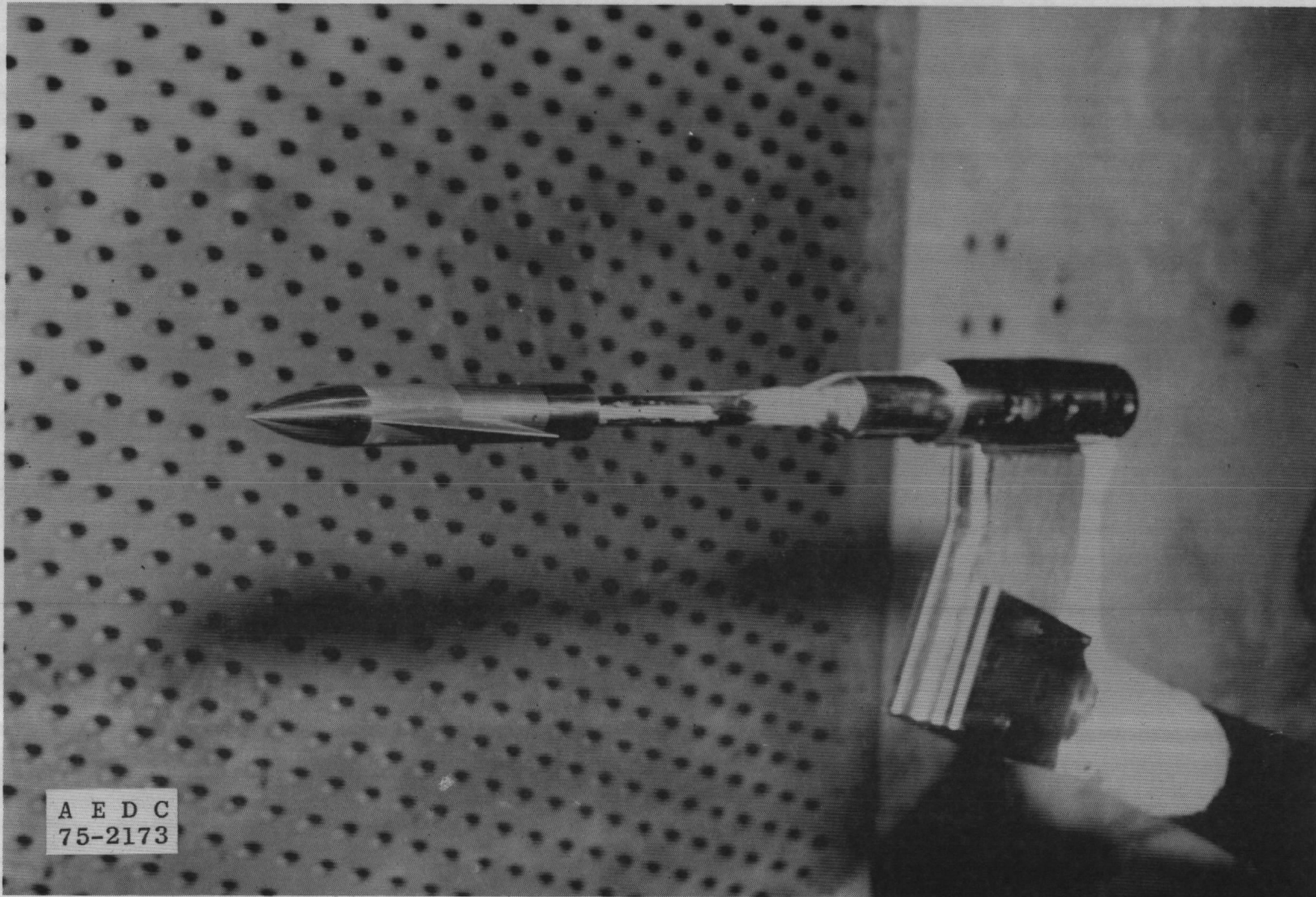


a. Pitch sector

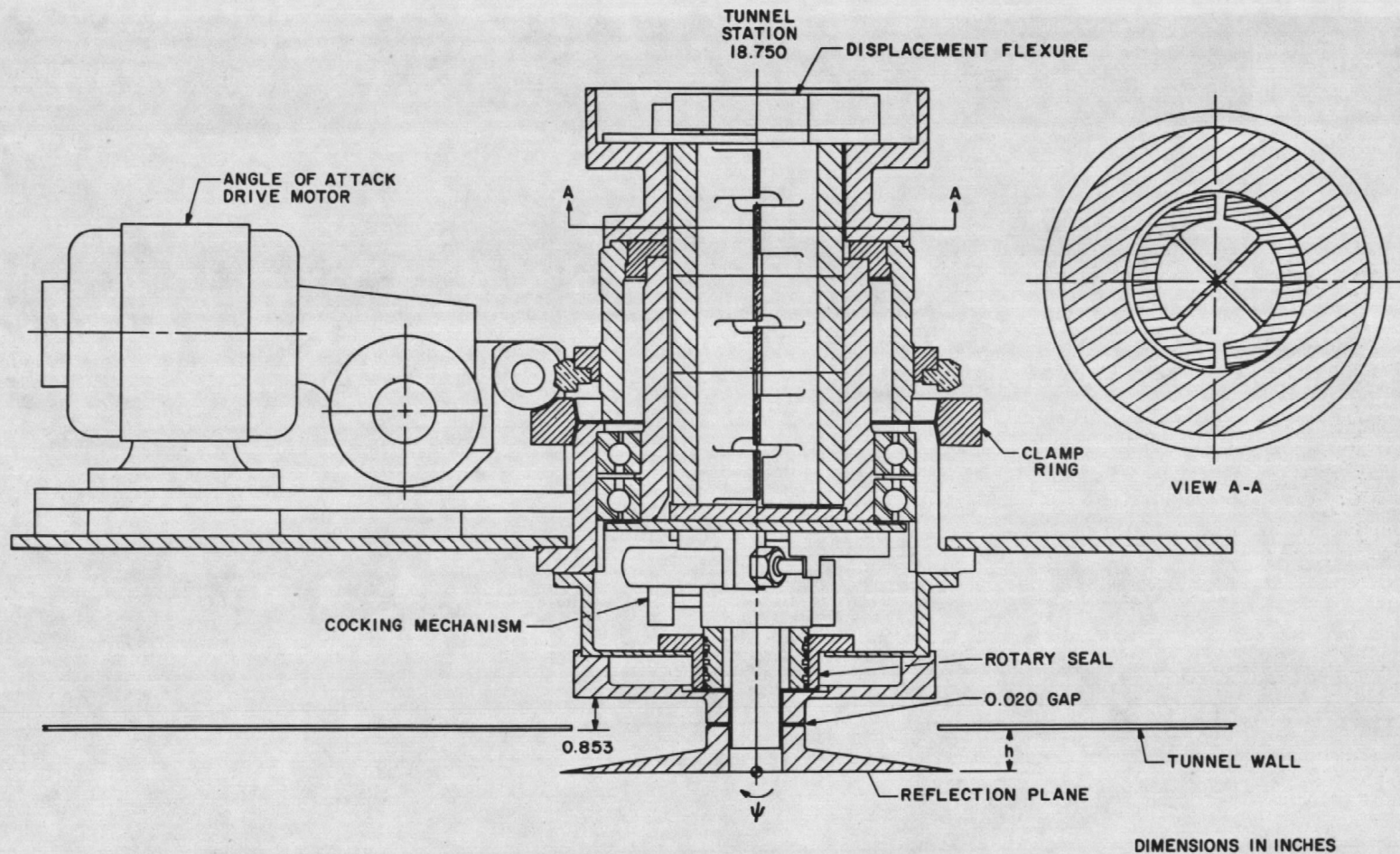
Figure 12. Tunnel 4T support equipment



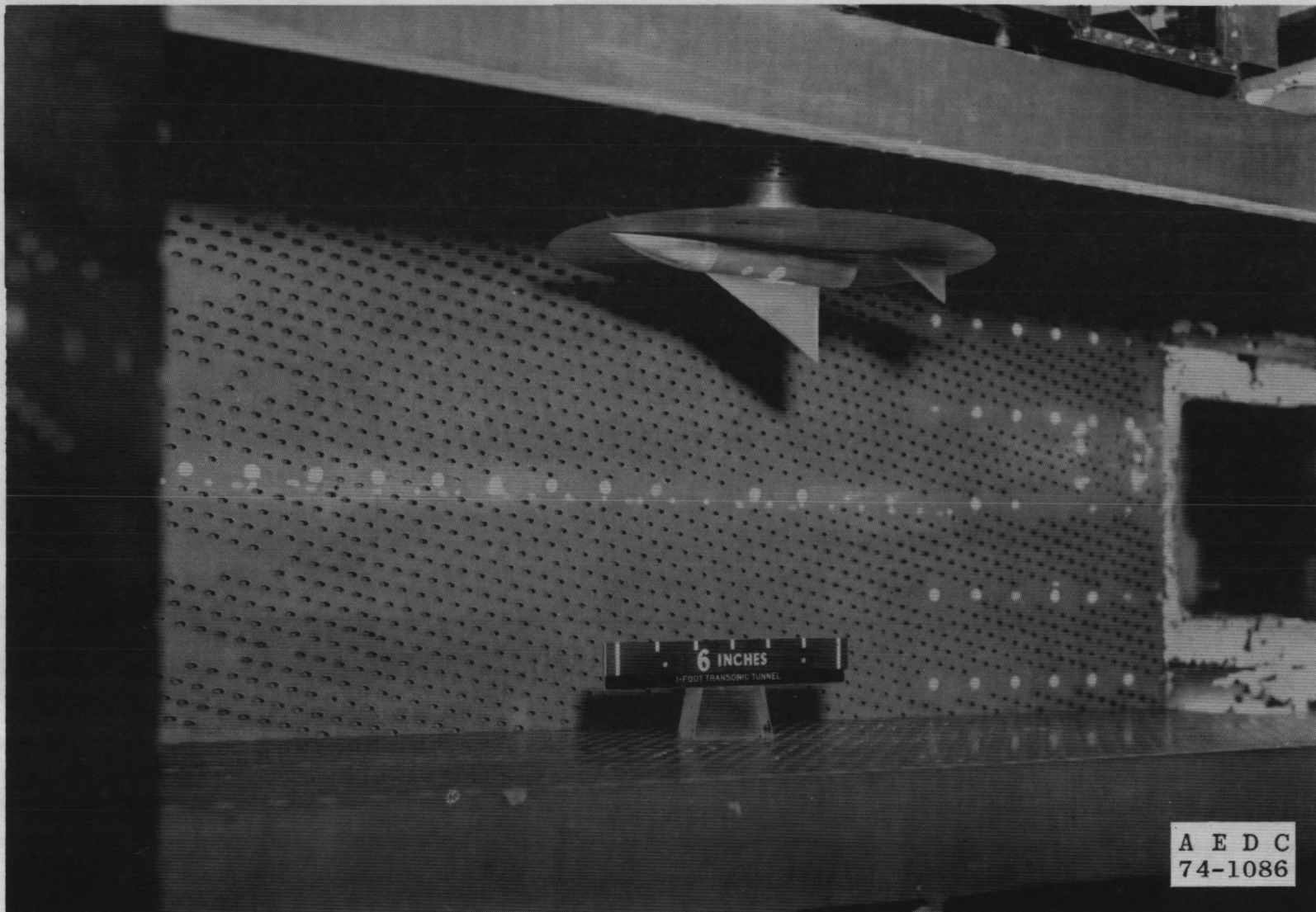
b. Mini-sector
Figure 12. Continued.



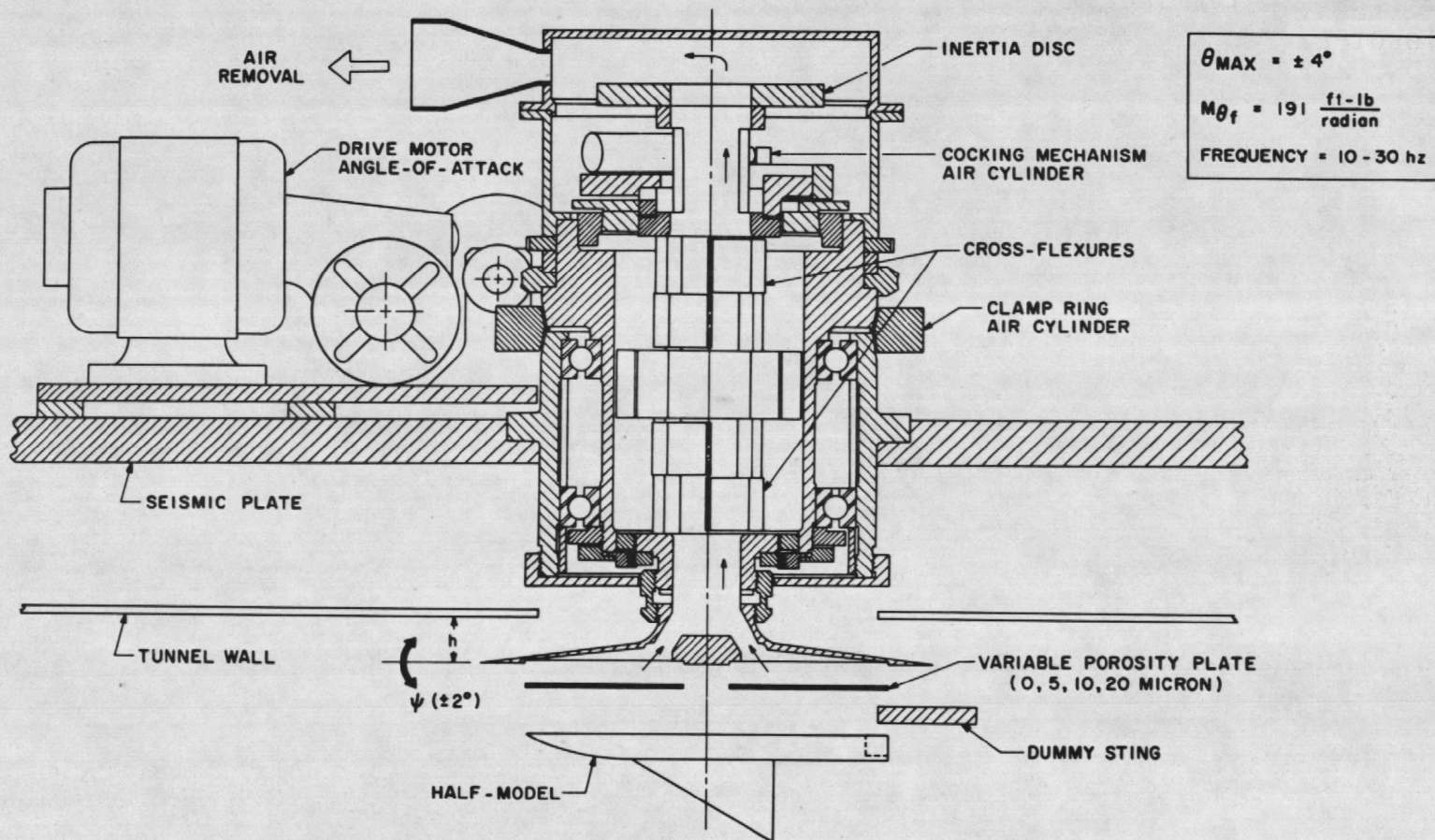
c. Photograph
Figure 12. Concluded.



a. Schematic
Figure 13. Low-alpha wall-mounted balance.

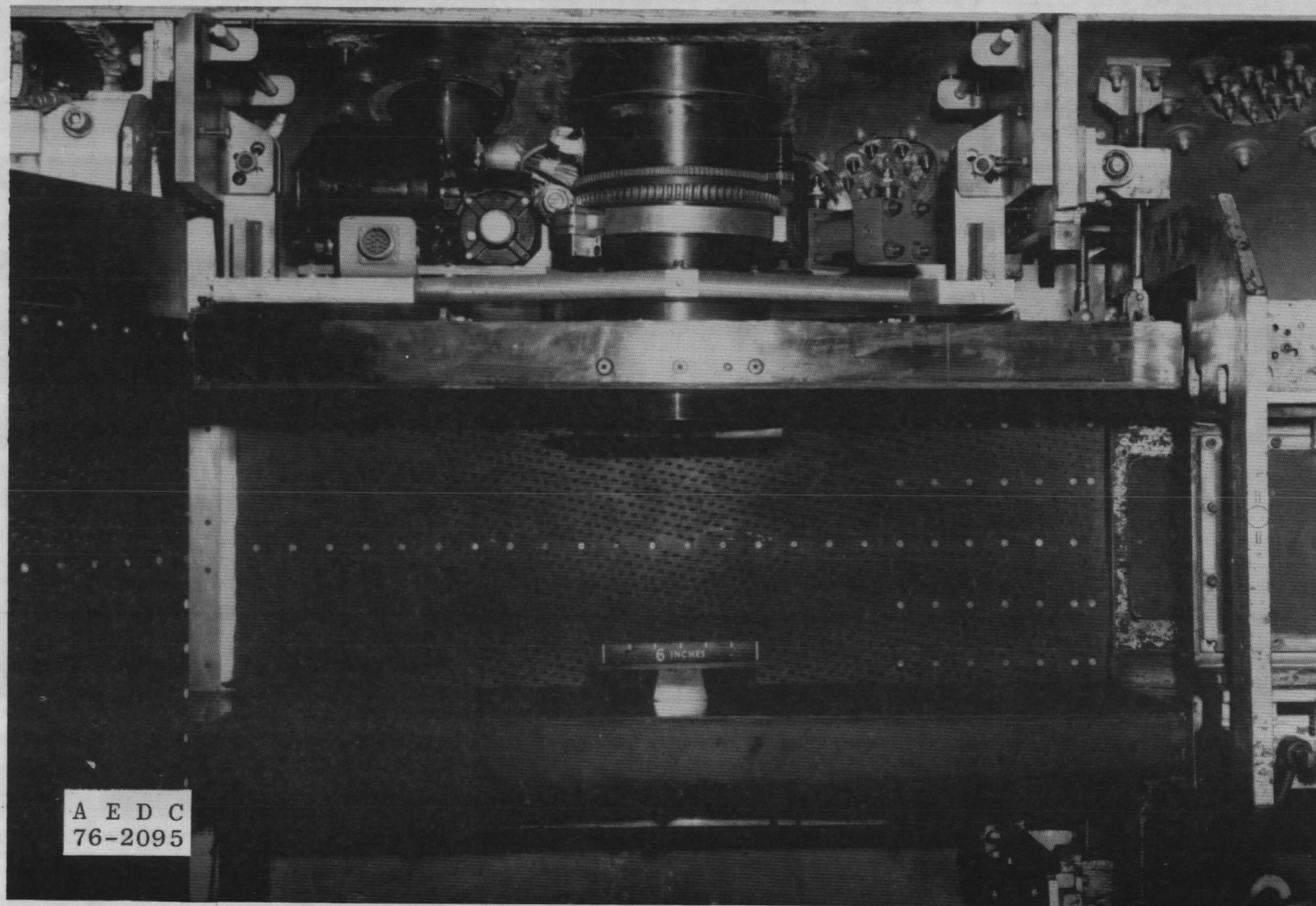


b. Photograph
Figure 13. Concluded.



a. Schematic

Figure 14. High-alpha wall-mounted balance.



b. Photograph
Figure 14. Concluded.

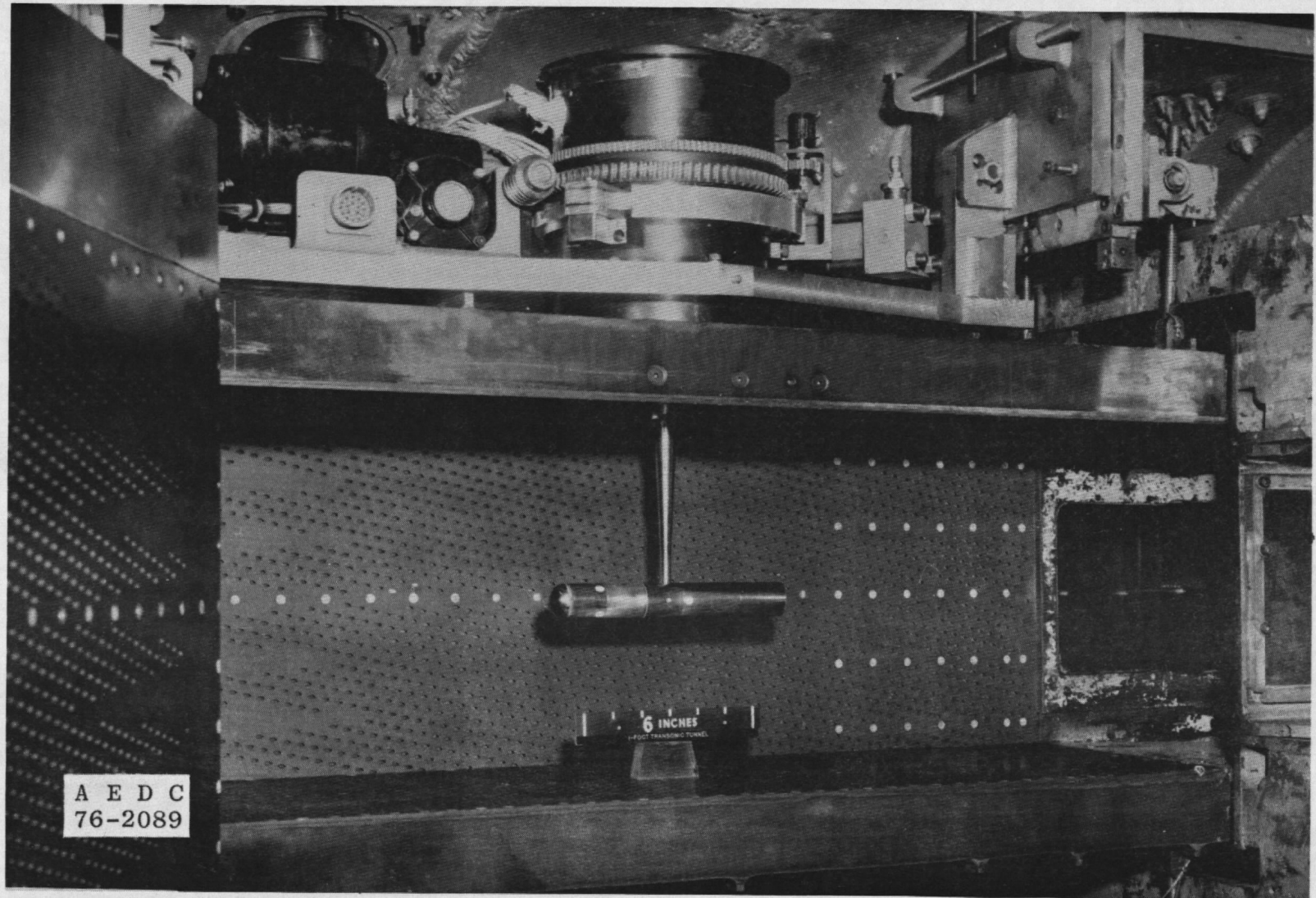
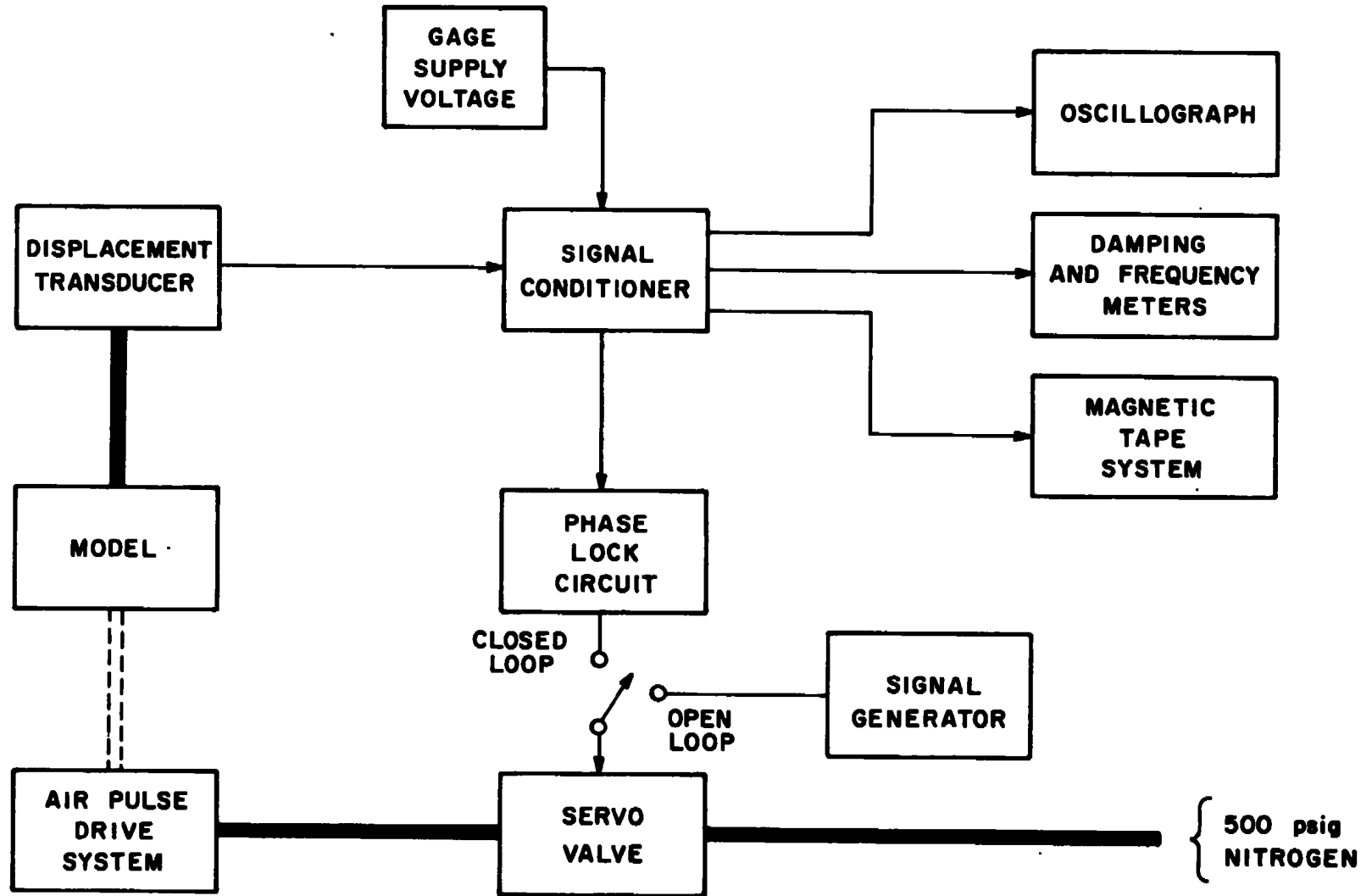
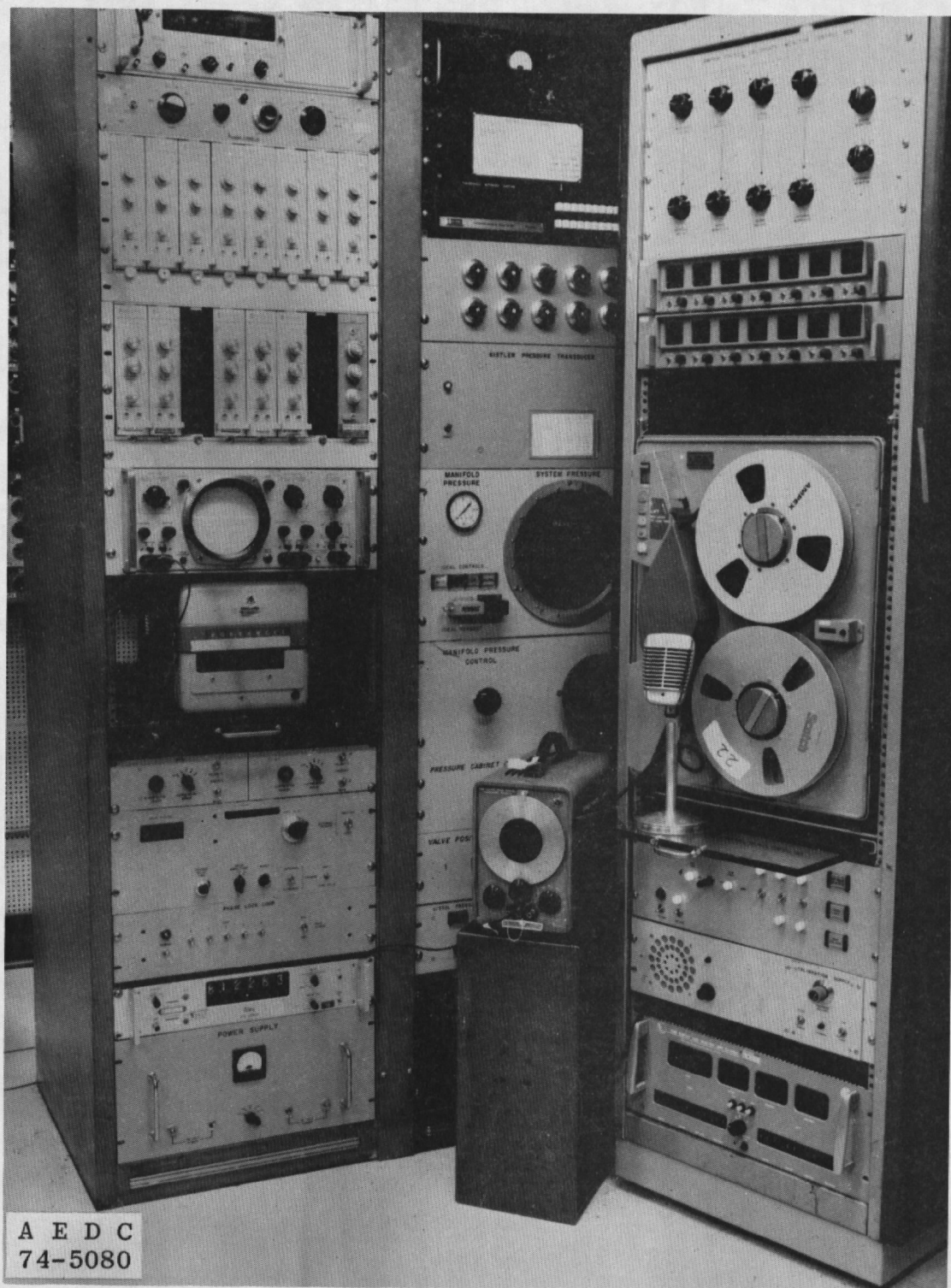


Figure 15. Rod-mounted model.



a. Schematic

Figure 16. Free-oscillation data recording equipment.



b. Photograph
Figure 16. Concluded.

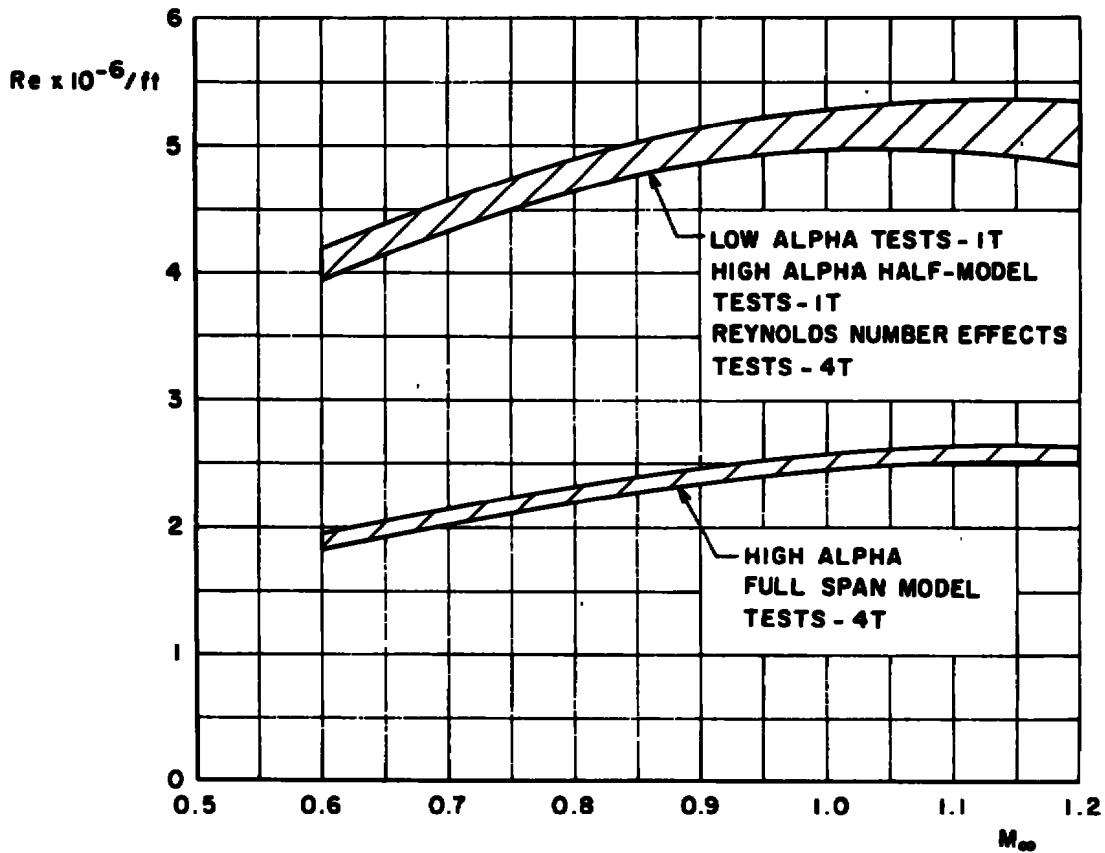


Figure 17. Reynolds number per foot versus Mach number.

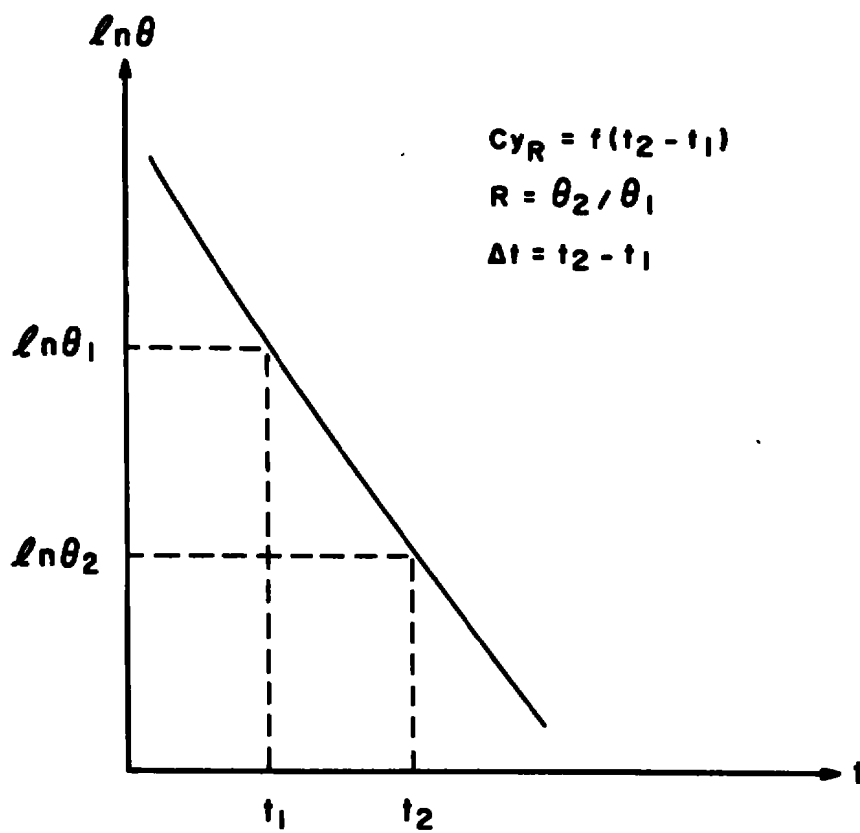


Figure 18. Typical $\ln \theta$ versus time.

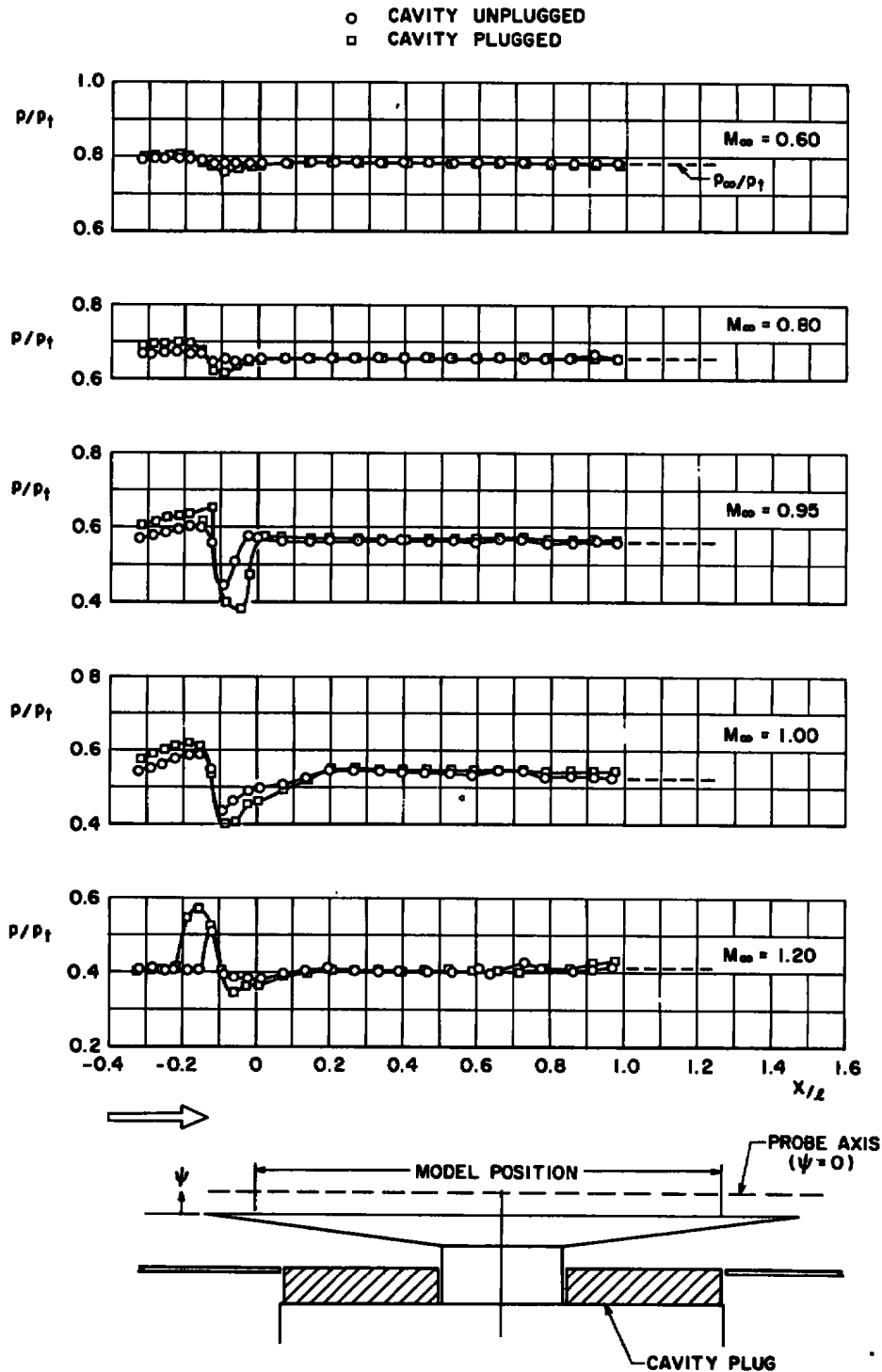


Figure 19. Reflection-plane pressure distribution with cavity plugged and unplugged, $\psi = 0$, $h = 0.9$.

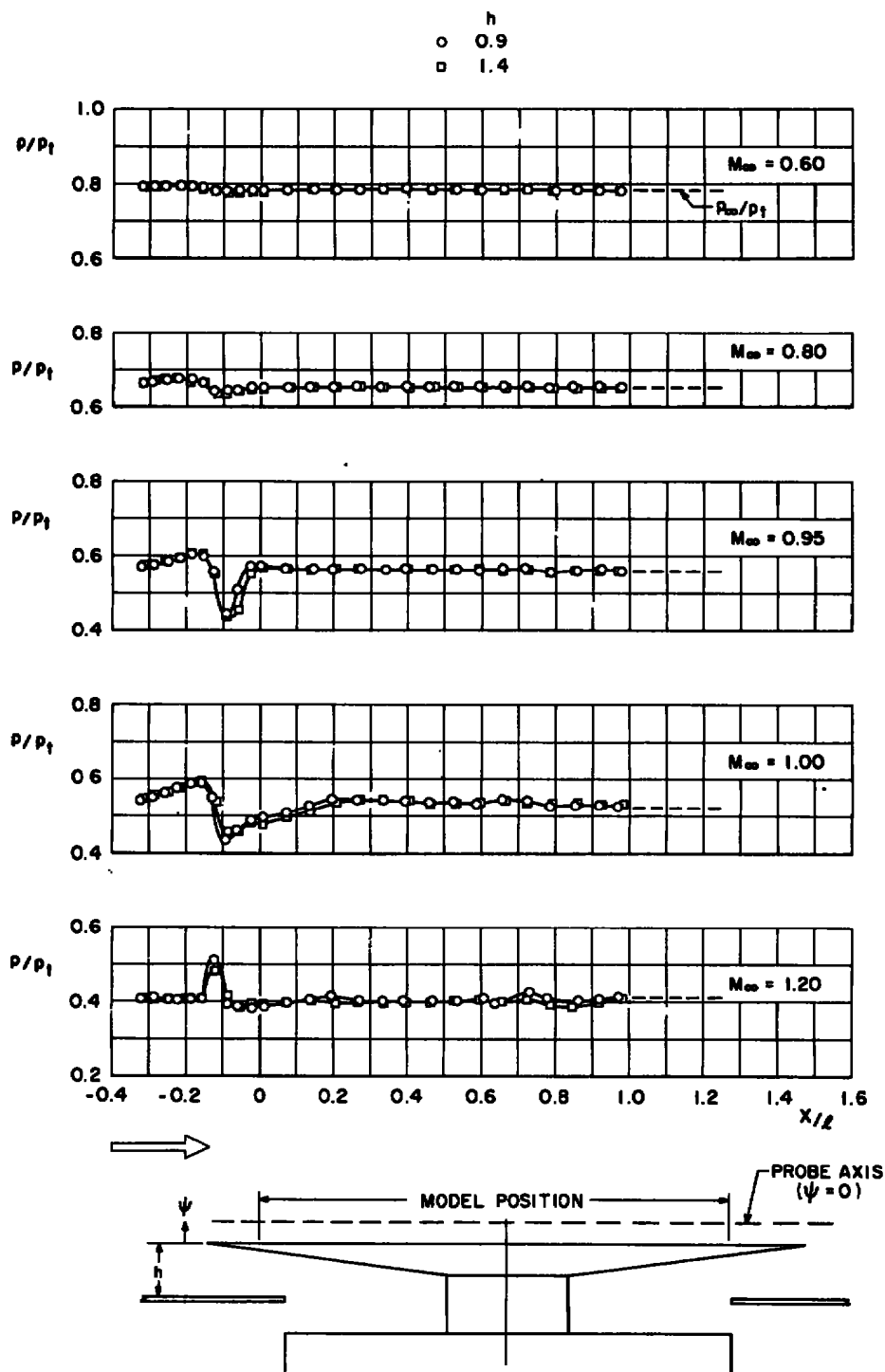


Figure 20. Reflection-plane pressure distribution with varying h , $\psi = 0$.

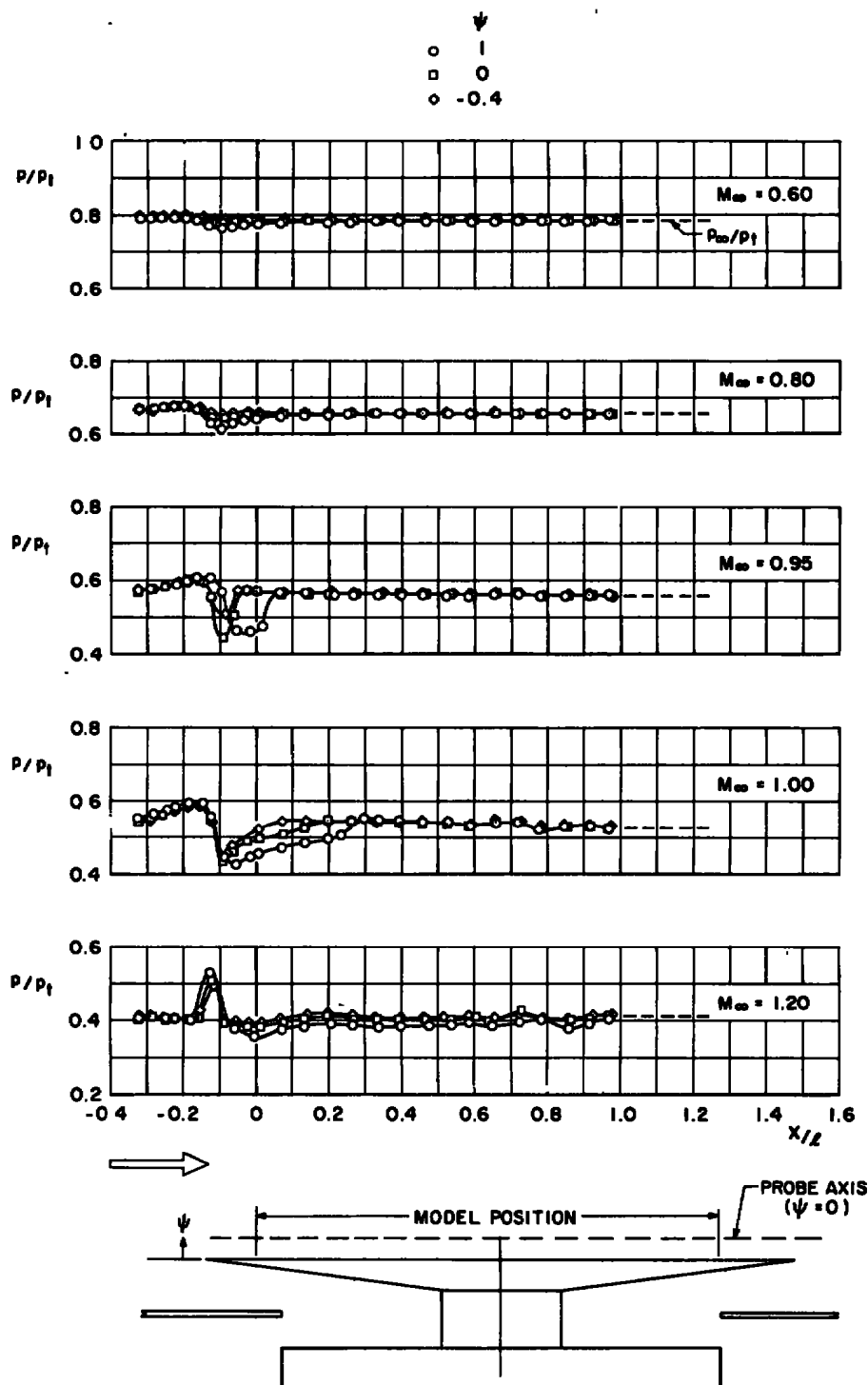


Figure 21. Reflection-plane pressure distribution with varying ψ , $h = 0.9$.

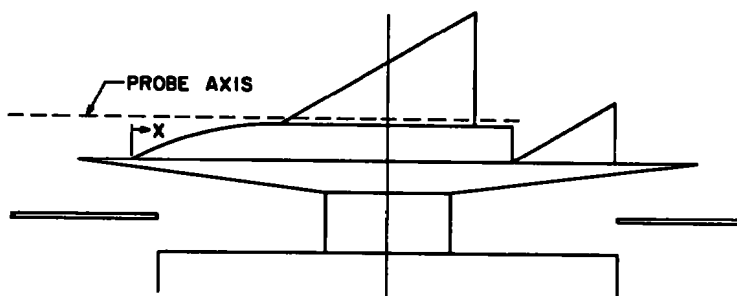
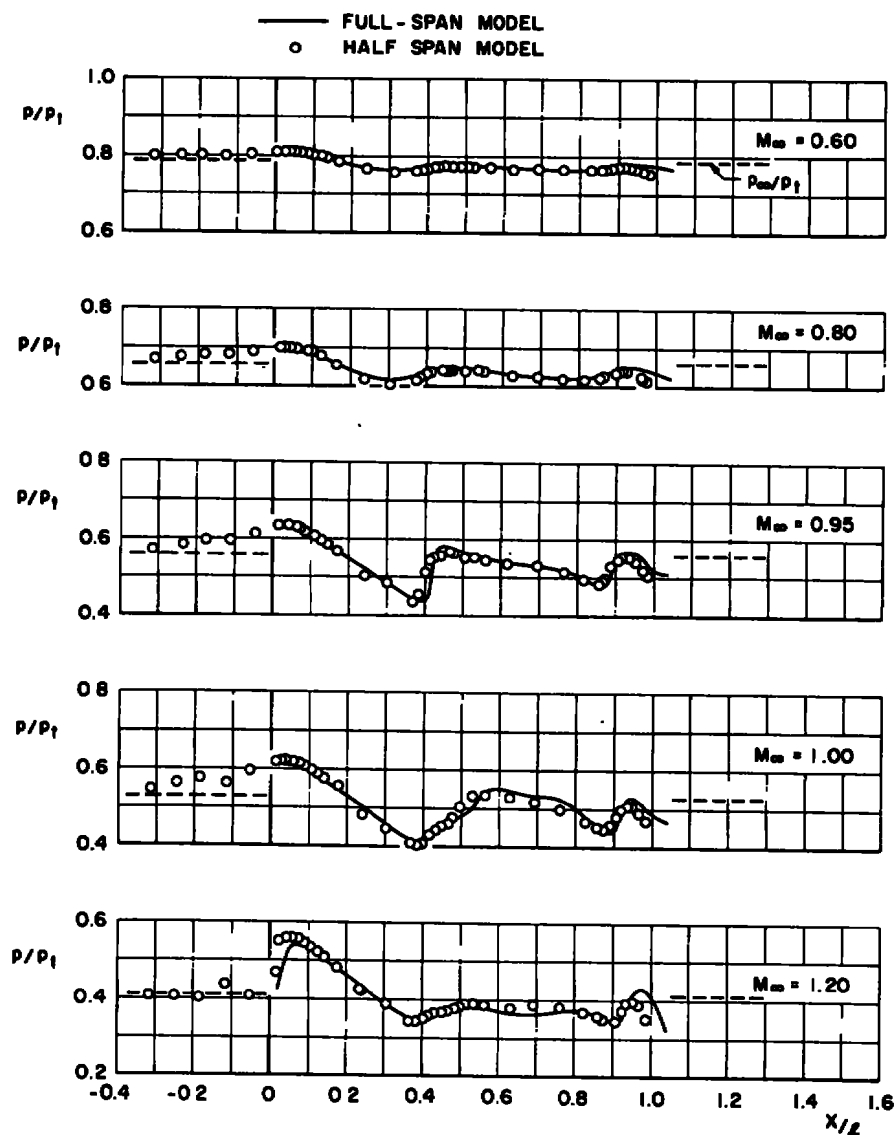


Figure 22. Aircraft model pressure distribution at the wing-body juncture, $\psi = -0.4$, $h = 0.9$.

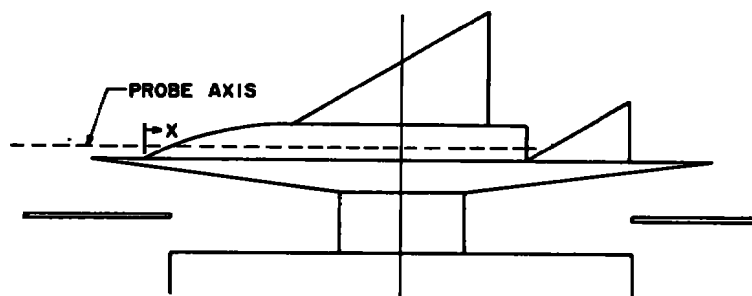
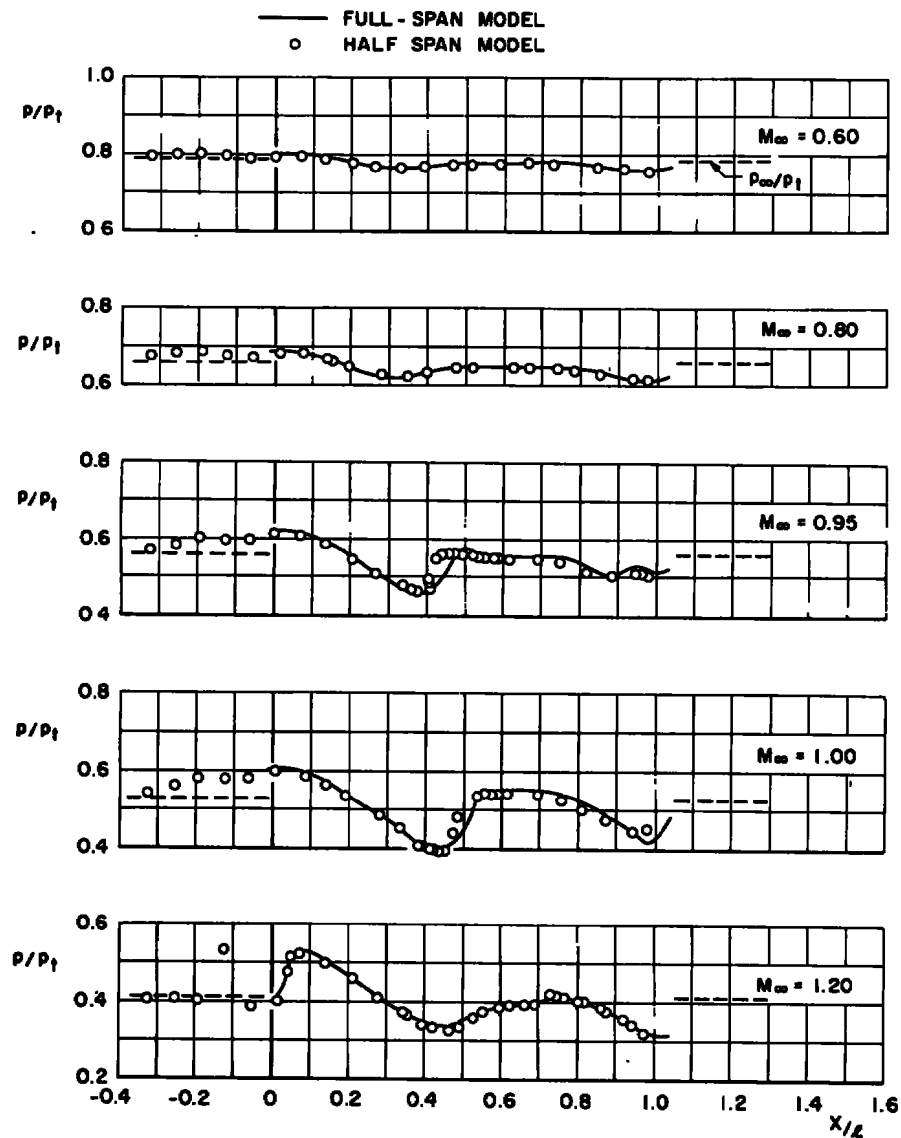
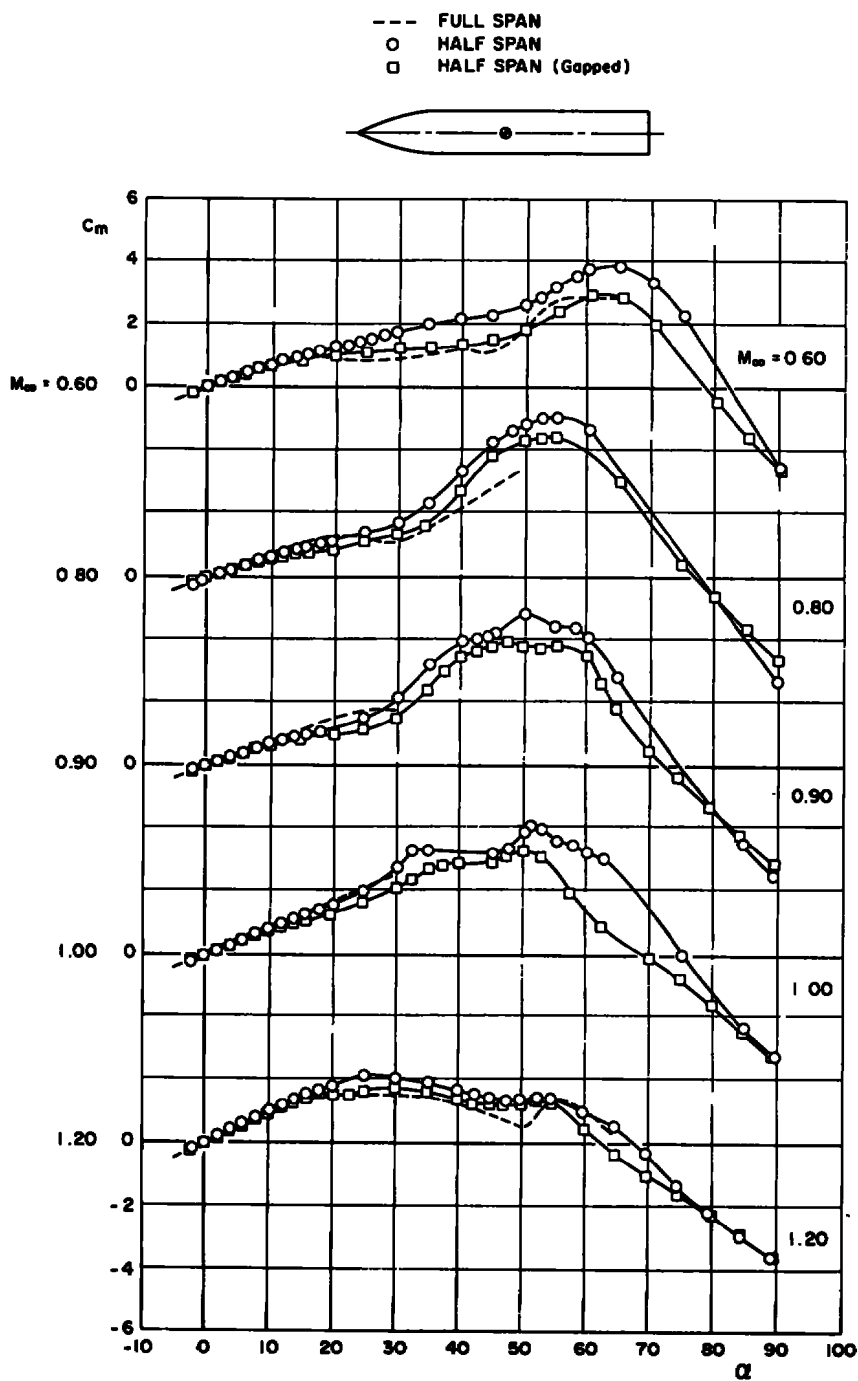
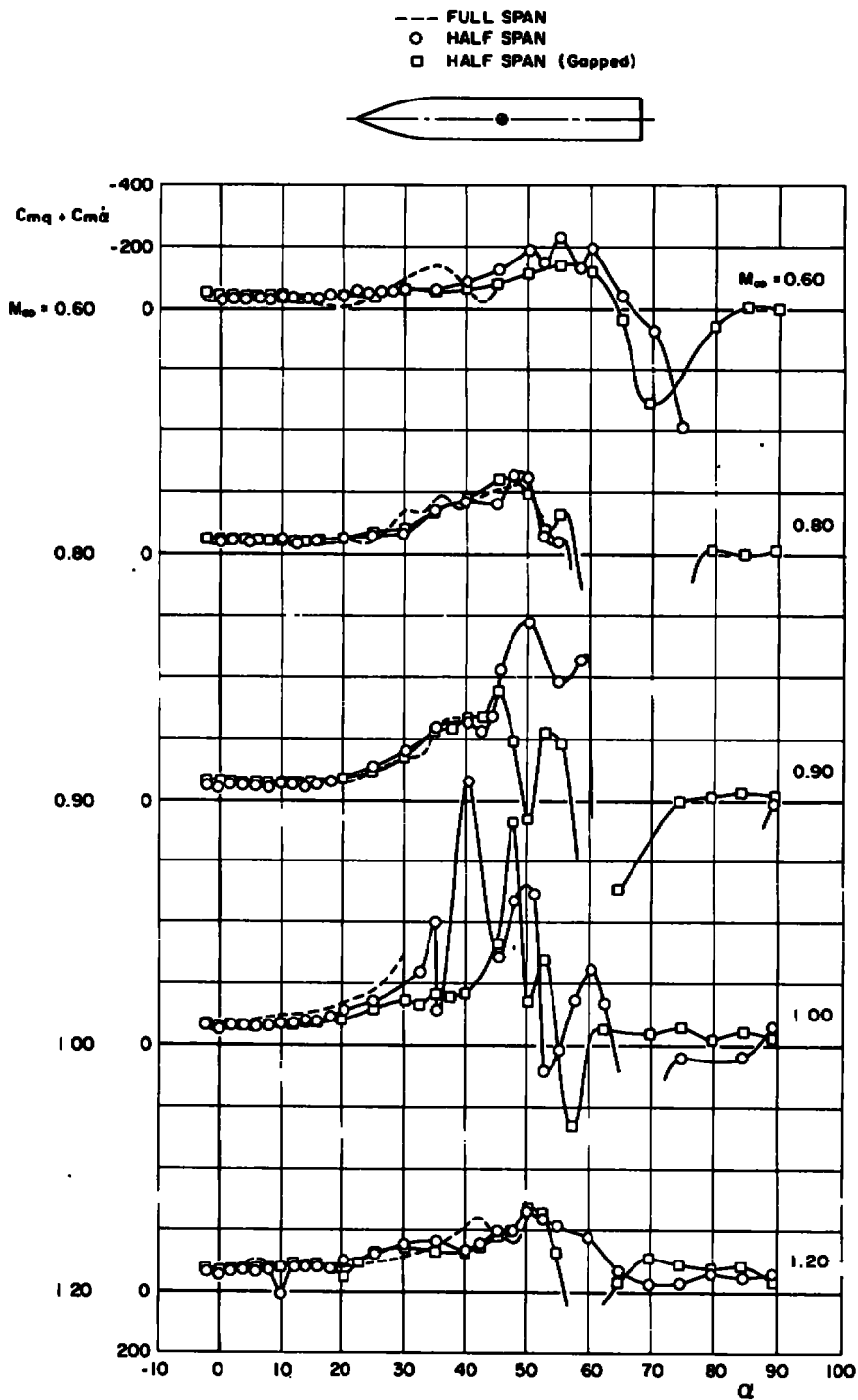


Figure 23. Aircraft model pressure distribution at the fuselage-reflection-plane juncture, $\psi = -0.4$, $h = 0.9$.

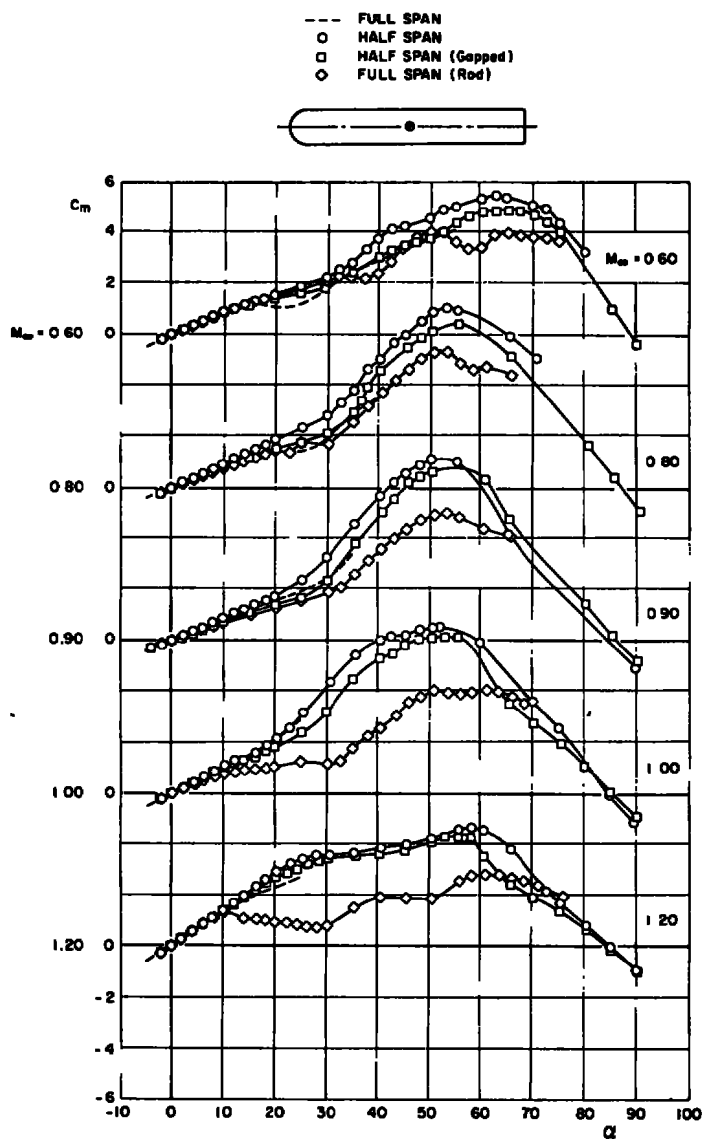


a. C_m versus α

Figure 24. Comparison of full- and half-span pitching-moment characteristics of the ogive-cylinder model.

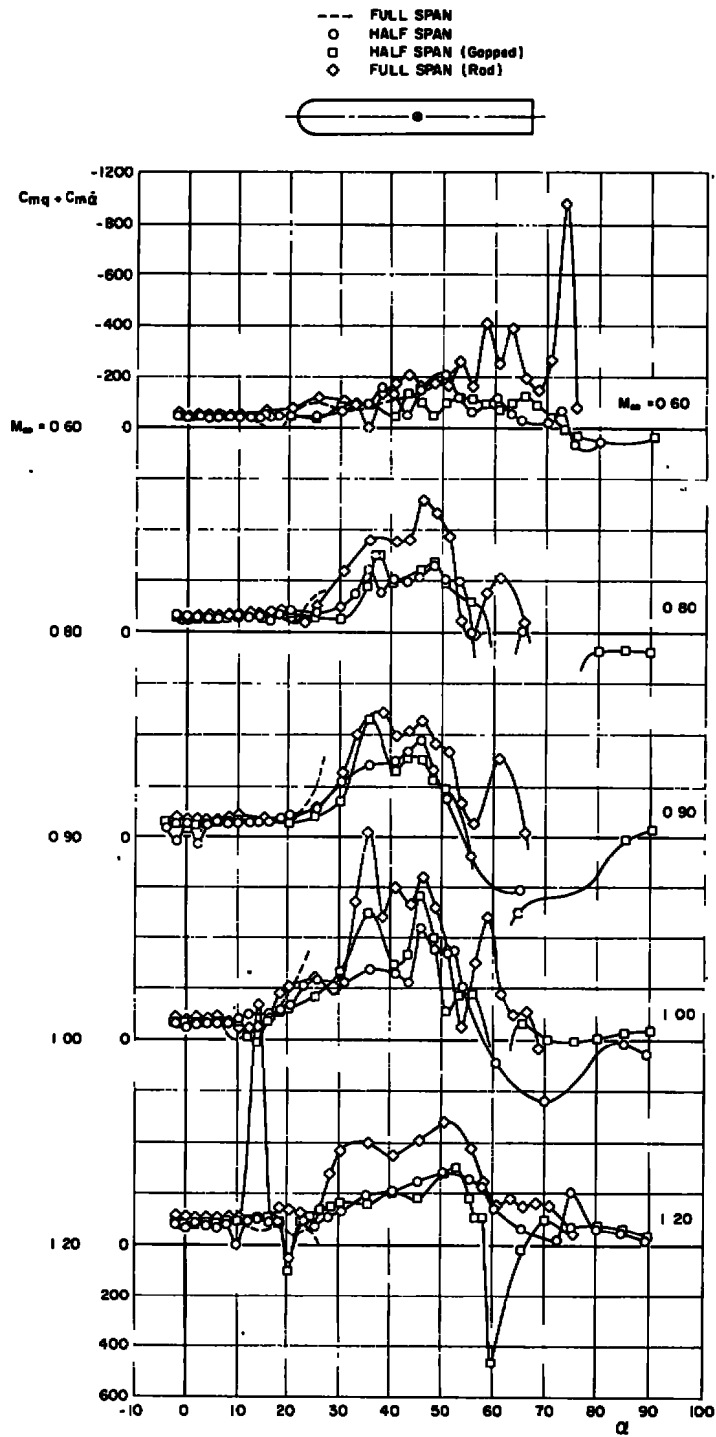


b. $C_{mq} + C_m \dot{\alpha}$ versus α
 Figure 24. Concluded.

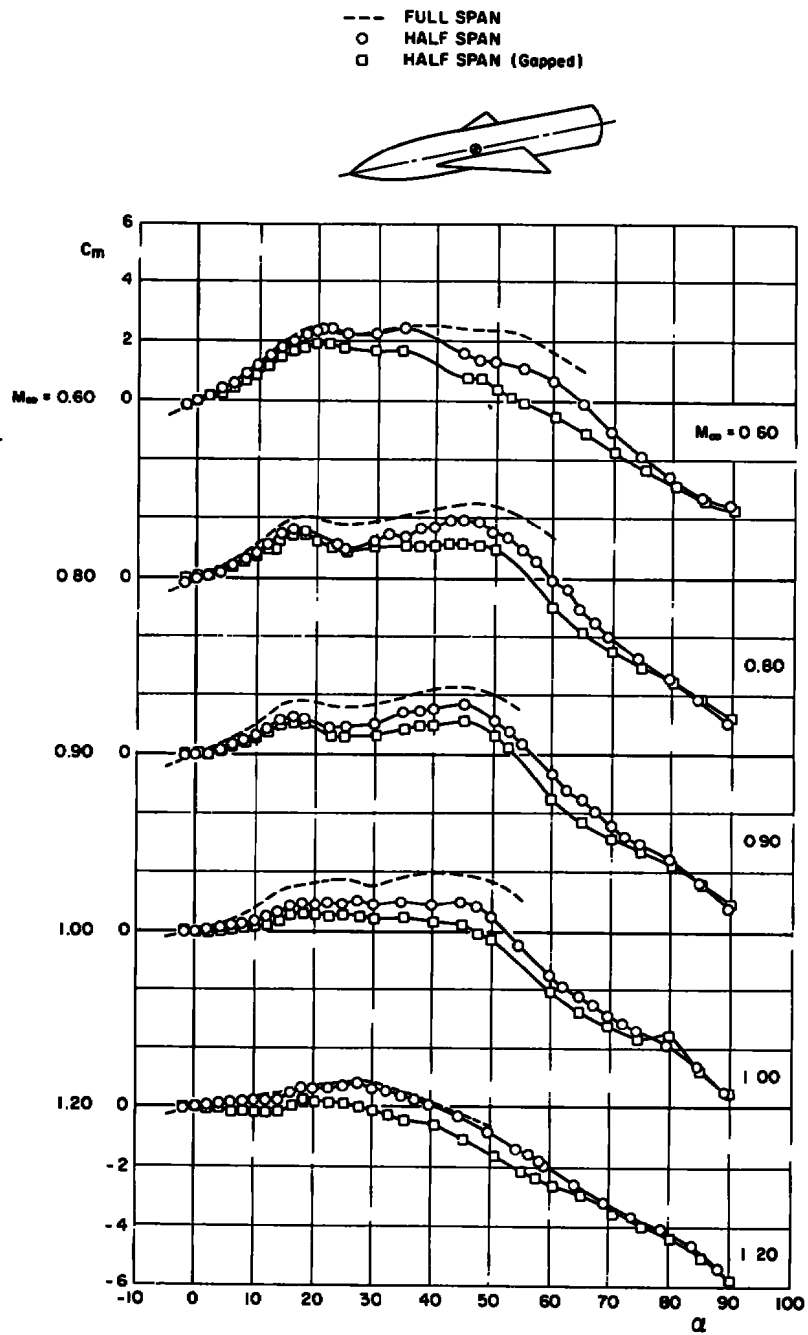


a. C_m versus α

Figure 25. Comparison of full- and half-span pitching-moment characteristics of the hemisphere-cylinder model.

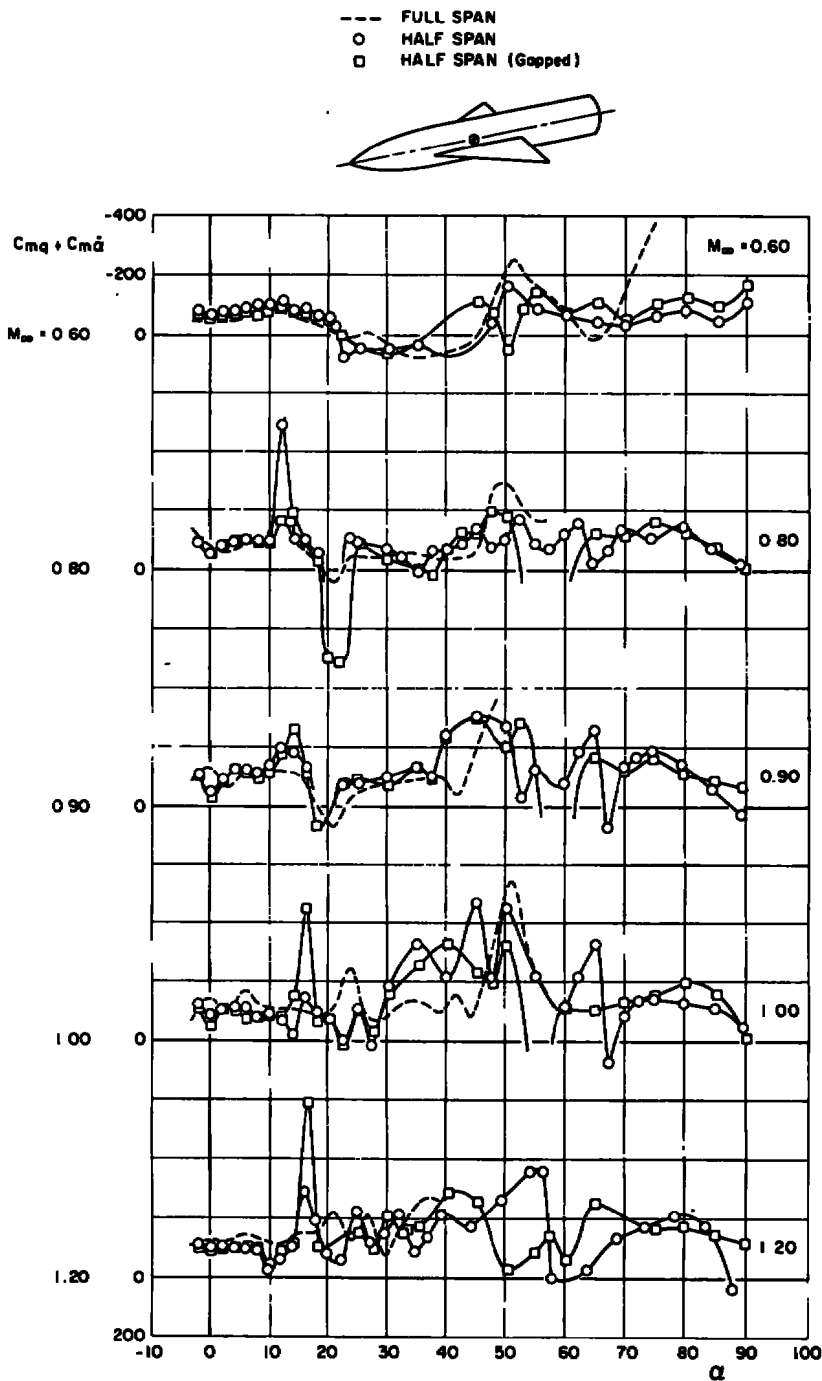


b. $C_{mq} + C_{m\dot{\alpha}}$ versus α
 Figure 25. Concluded.



a. C_m versus α

Figure 26. Comparison of full- and half-span pitching-moment characteristics of the wing-body model.



b. $C_{mq} + C_{m\dot{\alpha}}$ versus α
 Figure 26. Concluded.

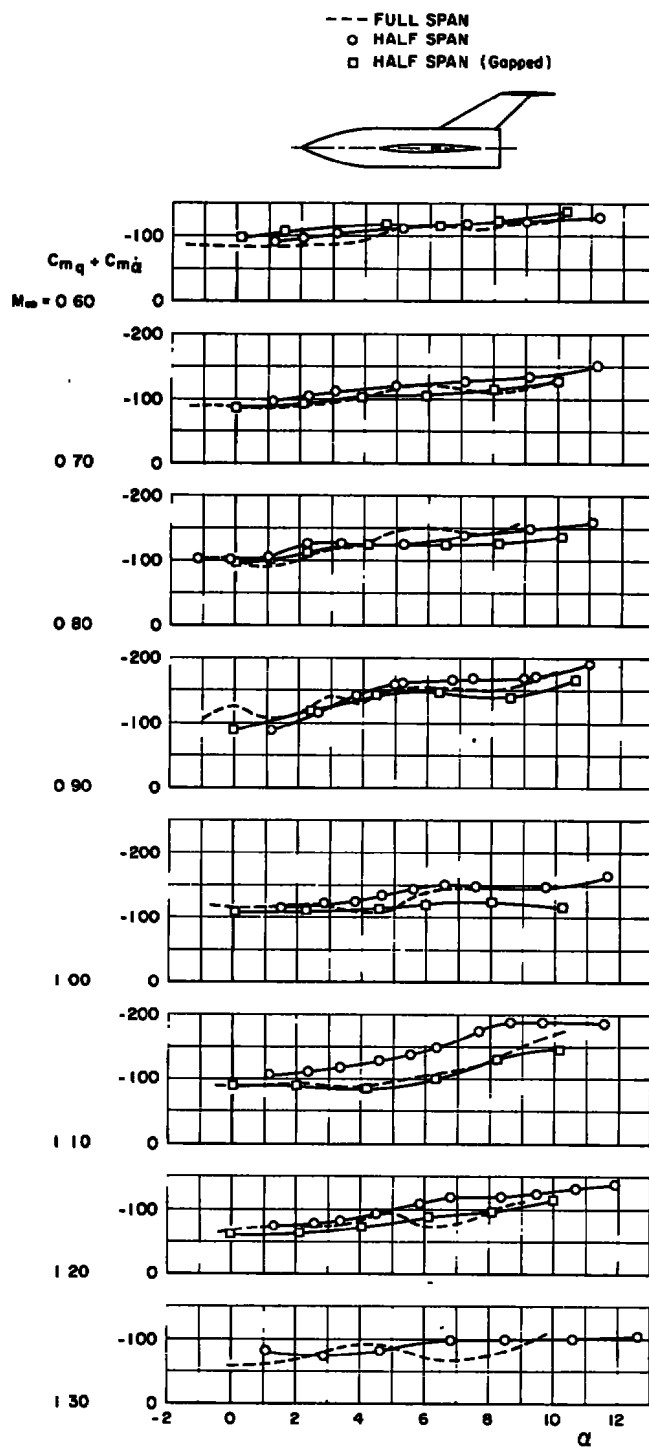


Figure 27. Comparison of full- and half-span pitch-damping characteristics of the aircraft model.

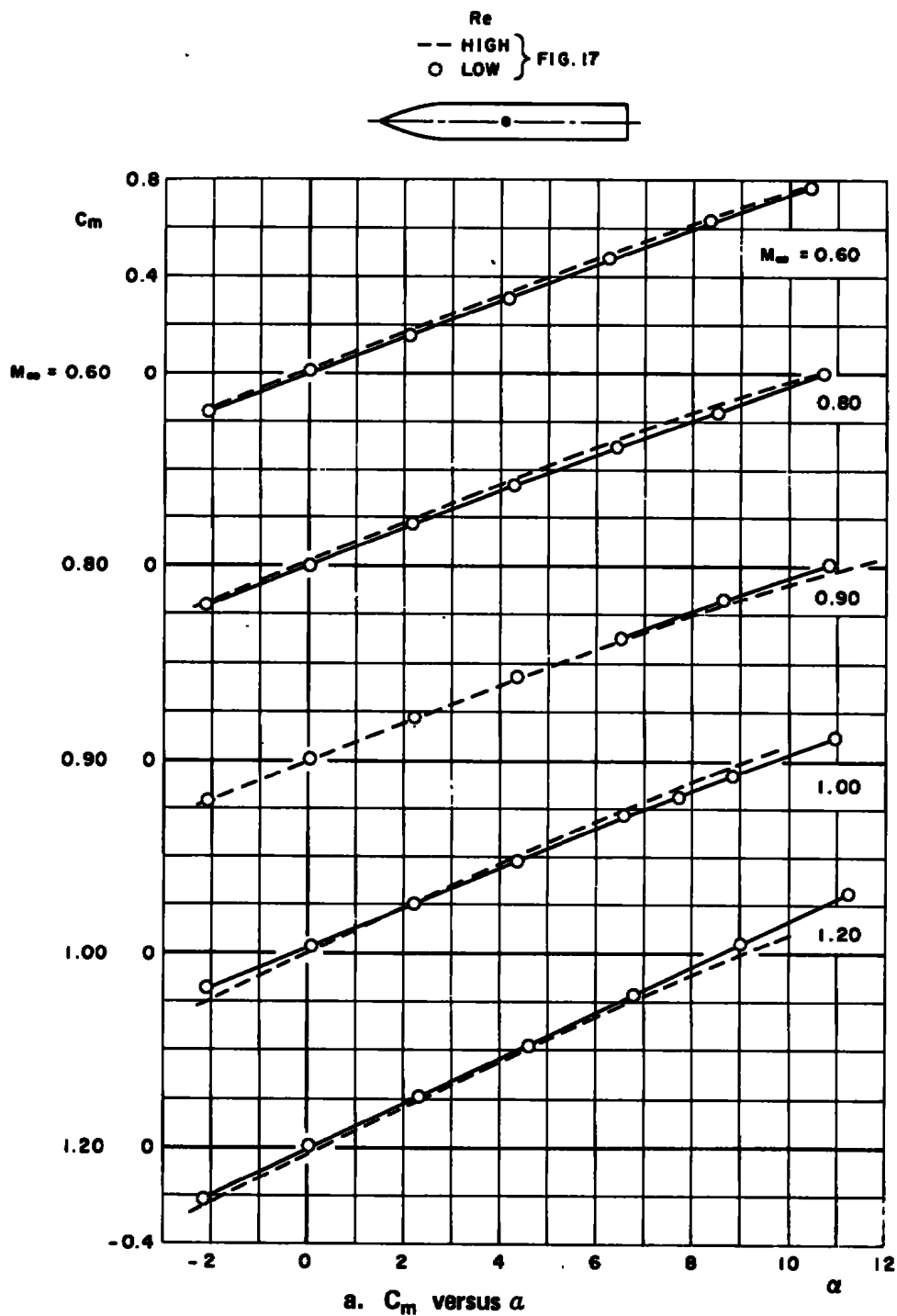
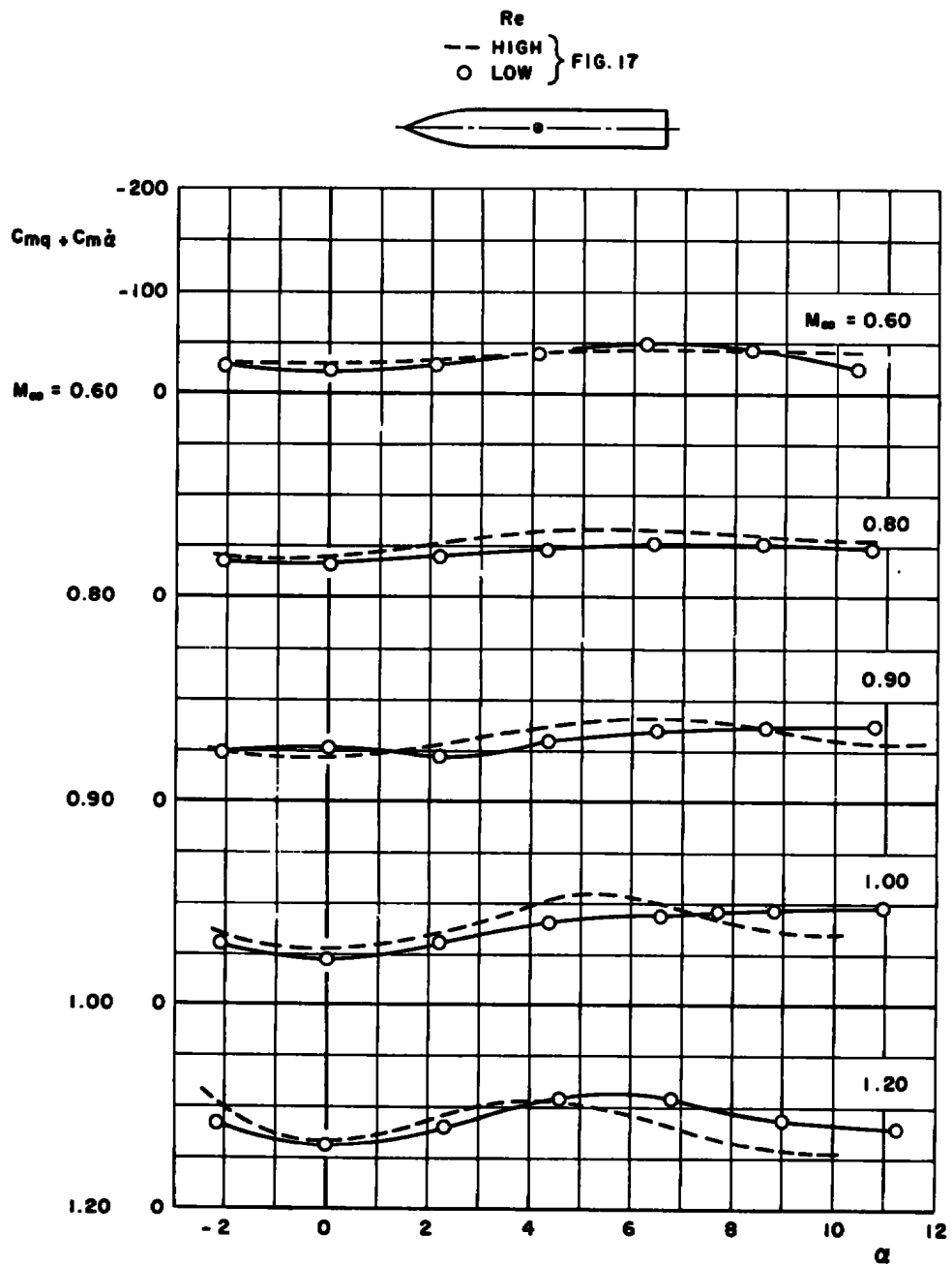


Figure 28. Reynolds number effects on the pitching-moment characteristics of the ogive-cylinder model.



b. $C_{mq} + C_m \dot{\alpha}$ versus α
 Figure 28. Concluded.

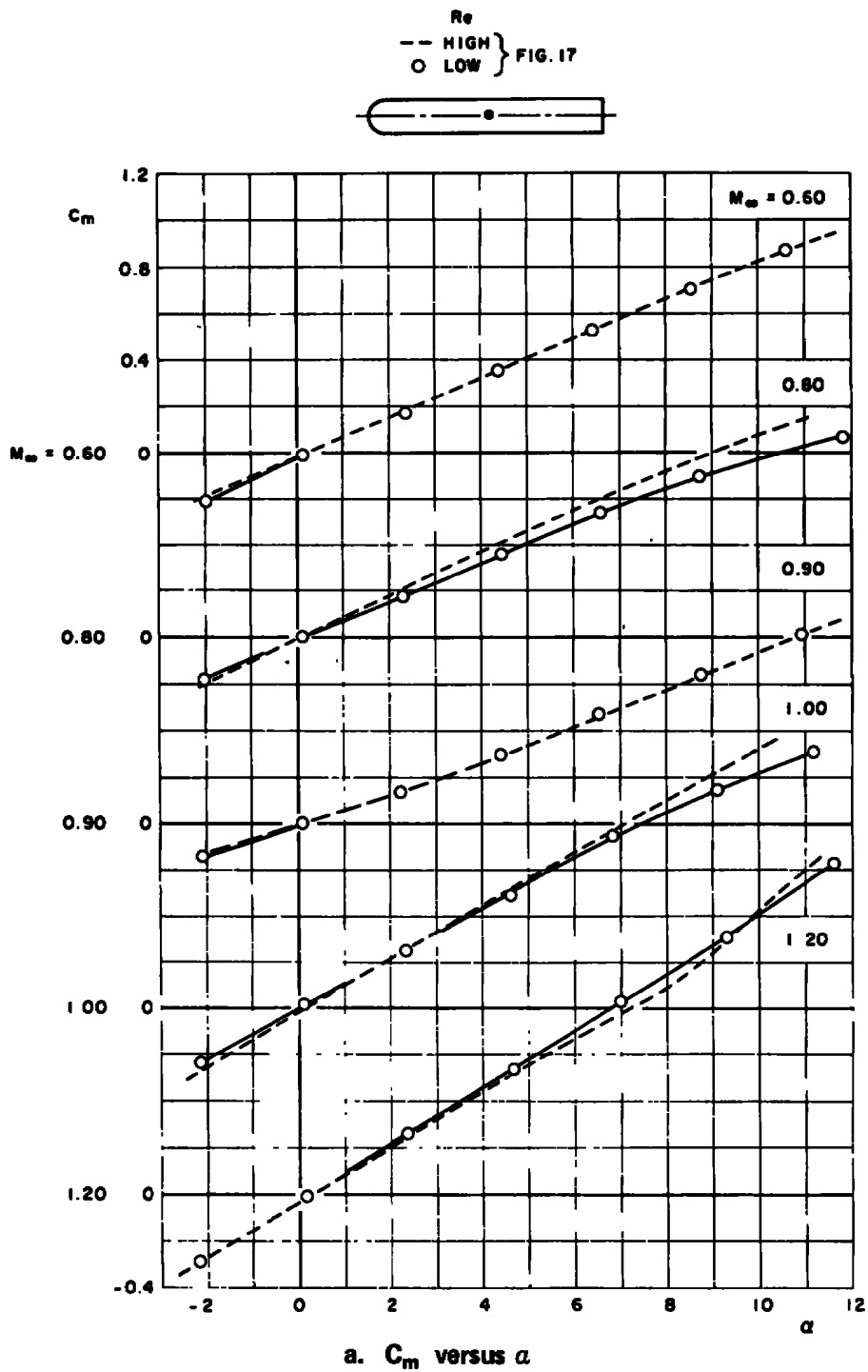
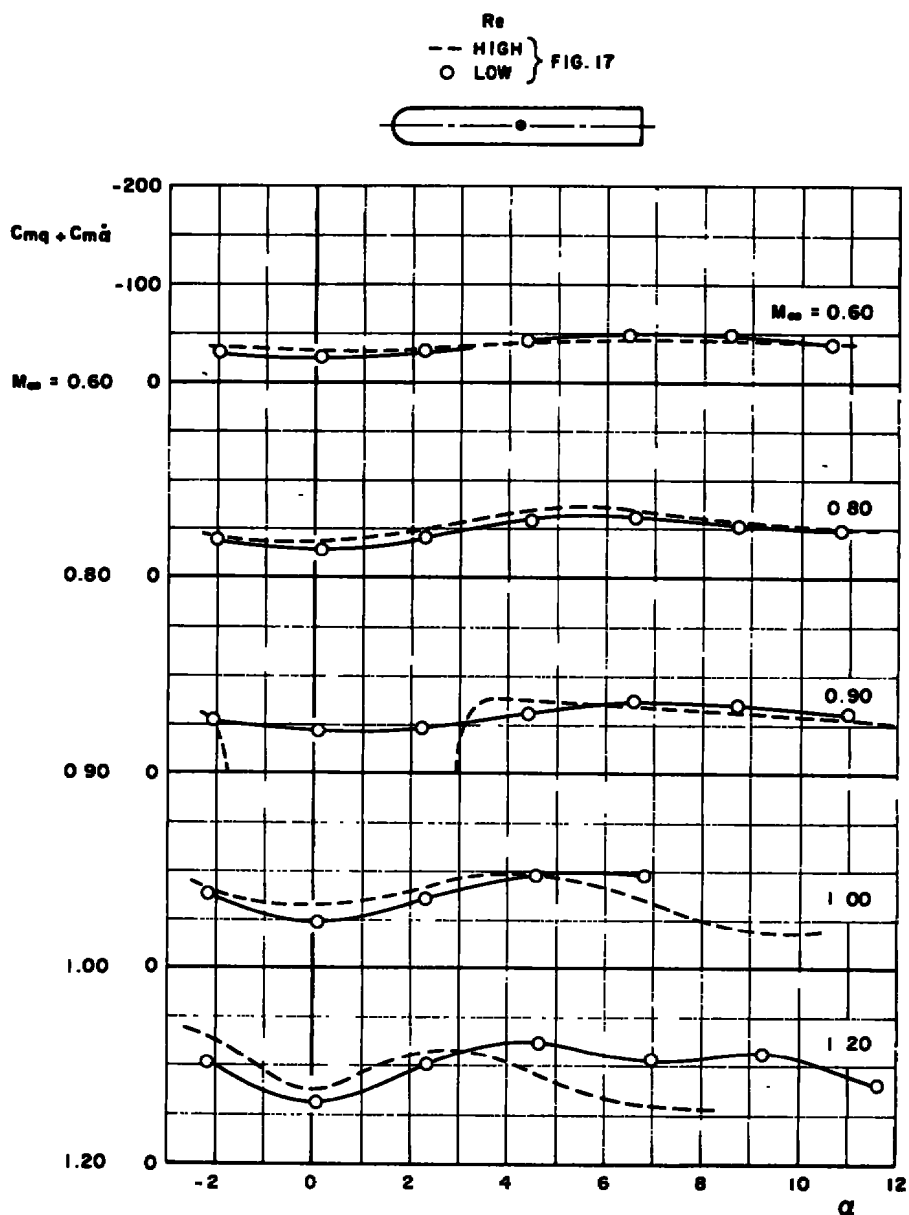


Figure 29. Reynolds number effects on the pitching-moment characteristics of the hemisphere-cylinder model.



b. $C_{mq} + C_{m\dot{\alpha}}$ versus α
 Figure 29. Concluded.

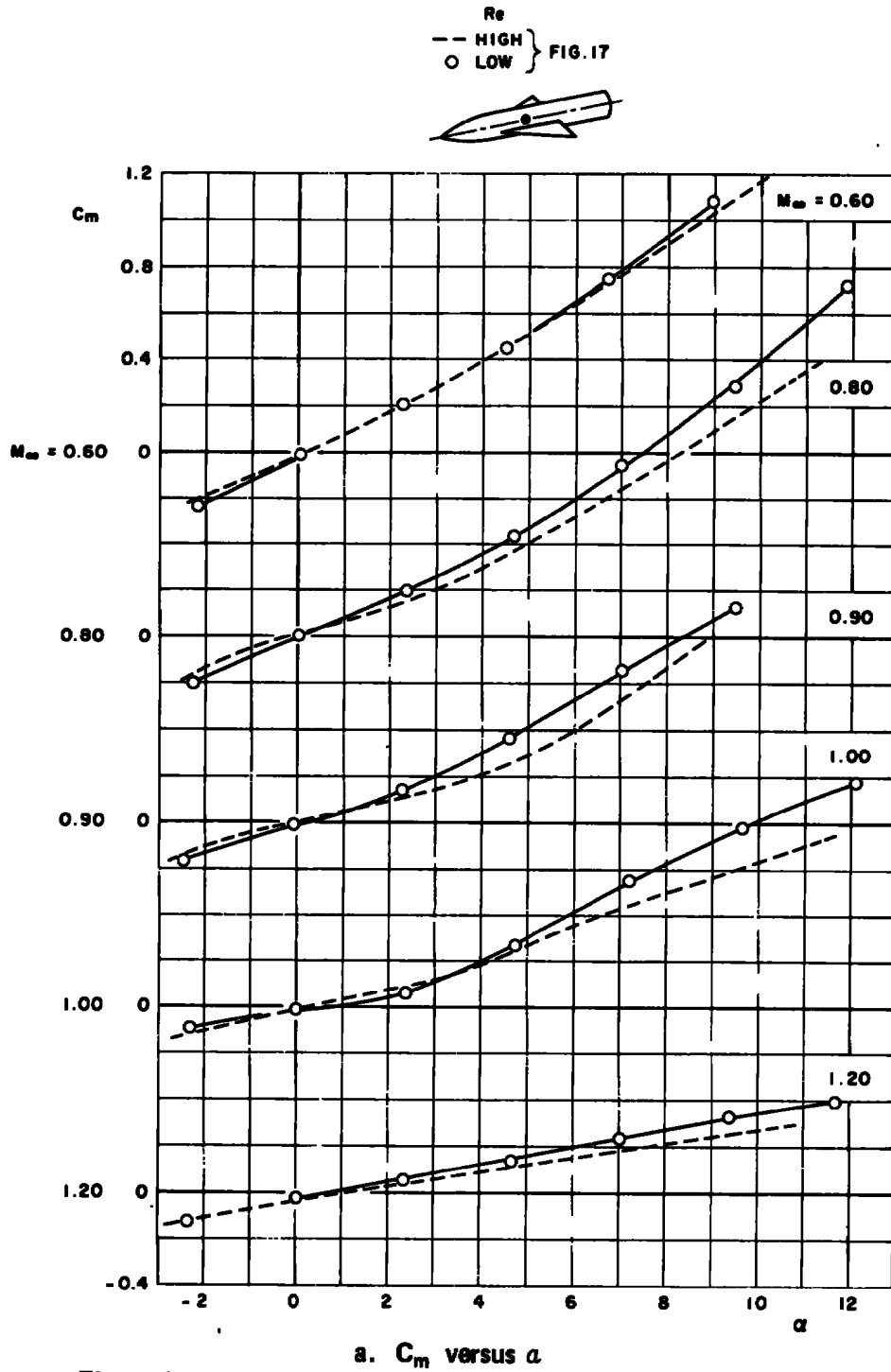
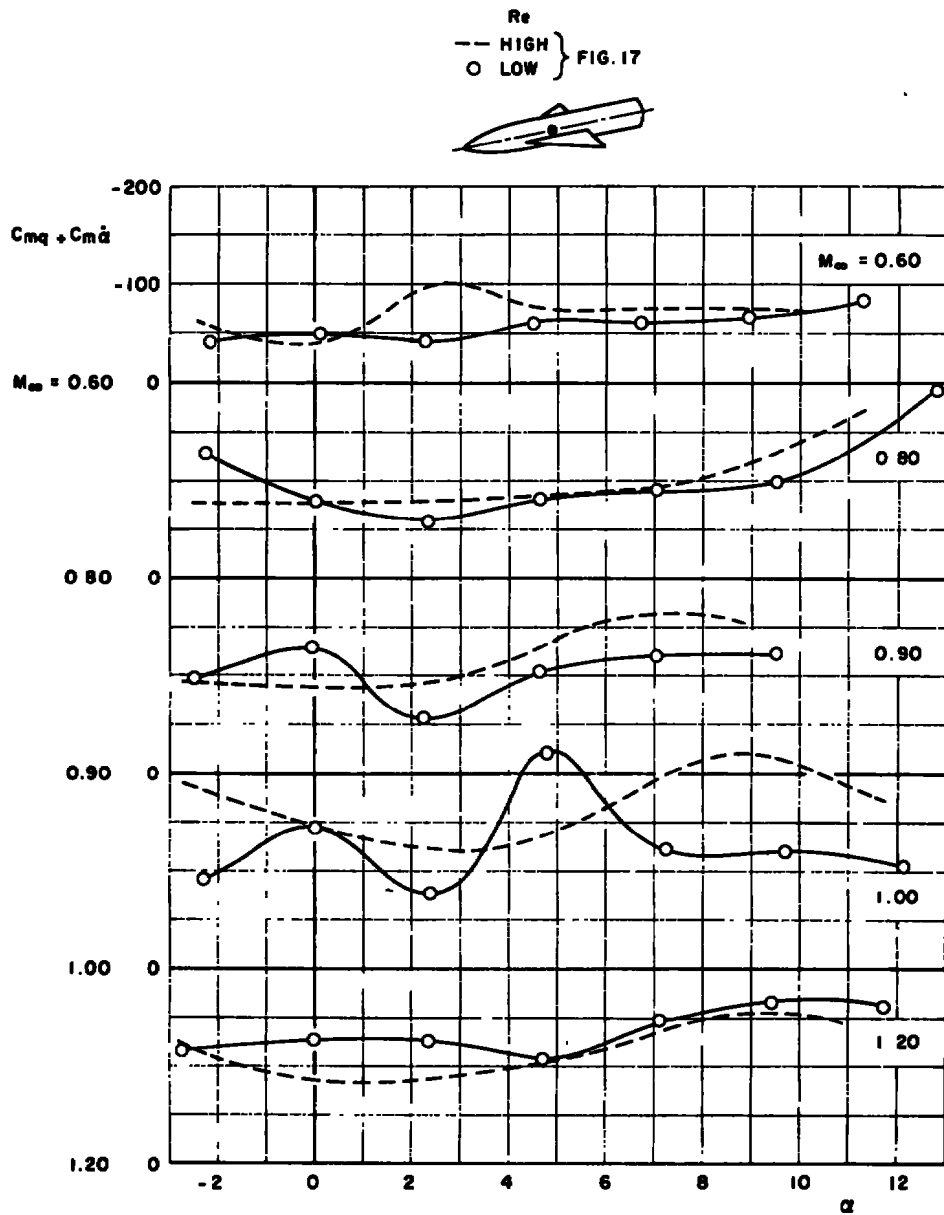


Figure 30. Reynolds number effects on the pitching-moment characteristics of the wing-body model.



b. $C_{mq} + C_m \dot{\alpha}$ versus α
Figure 30. Concluded.

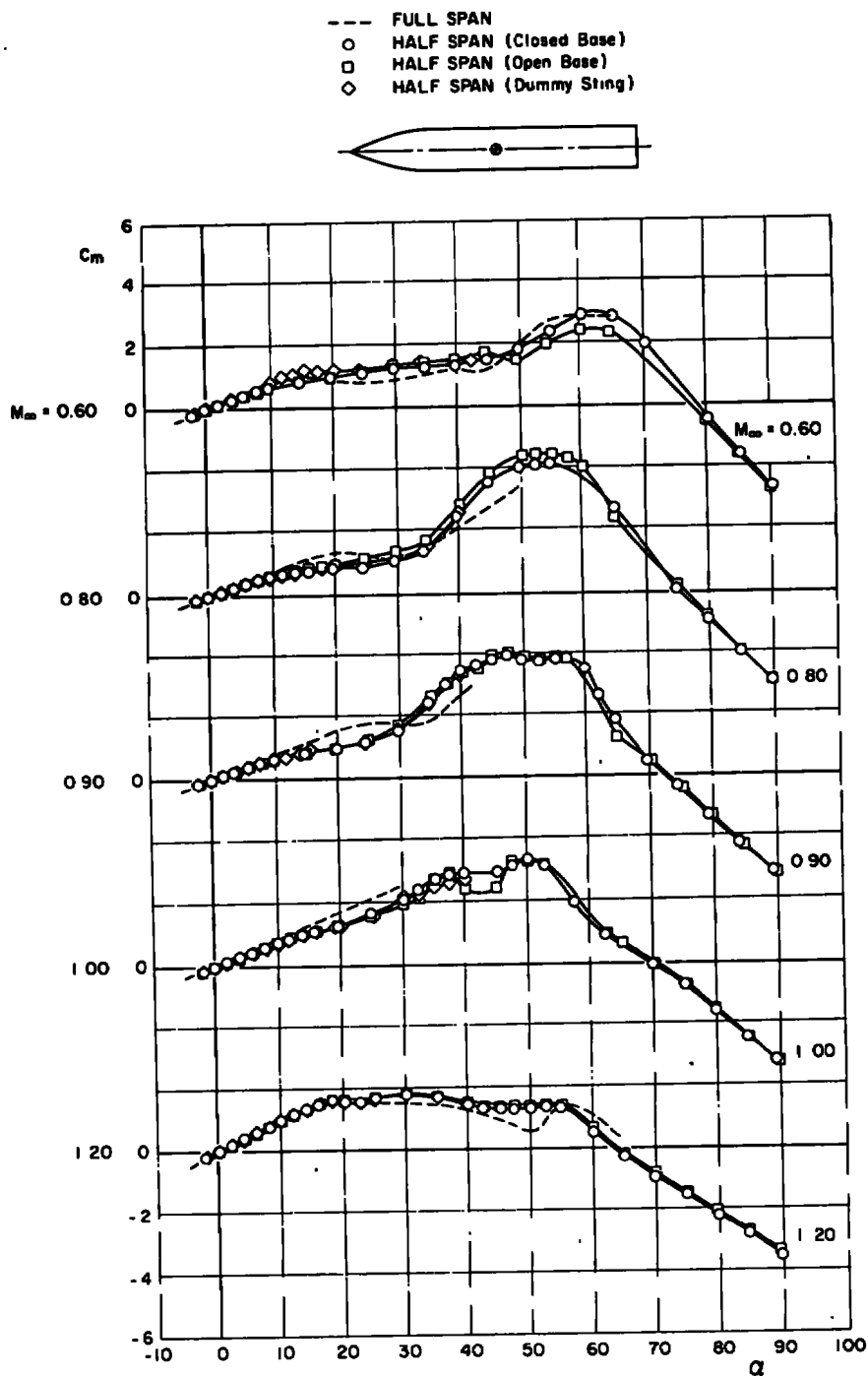
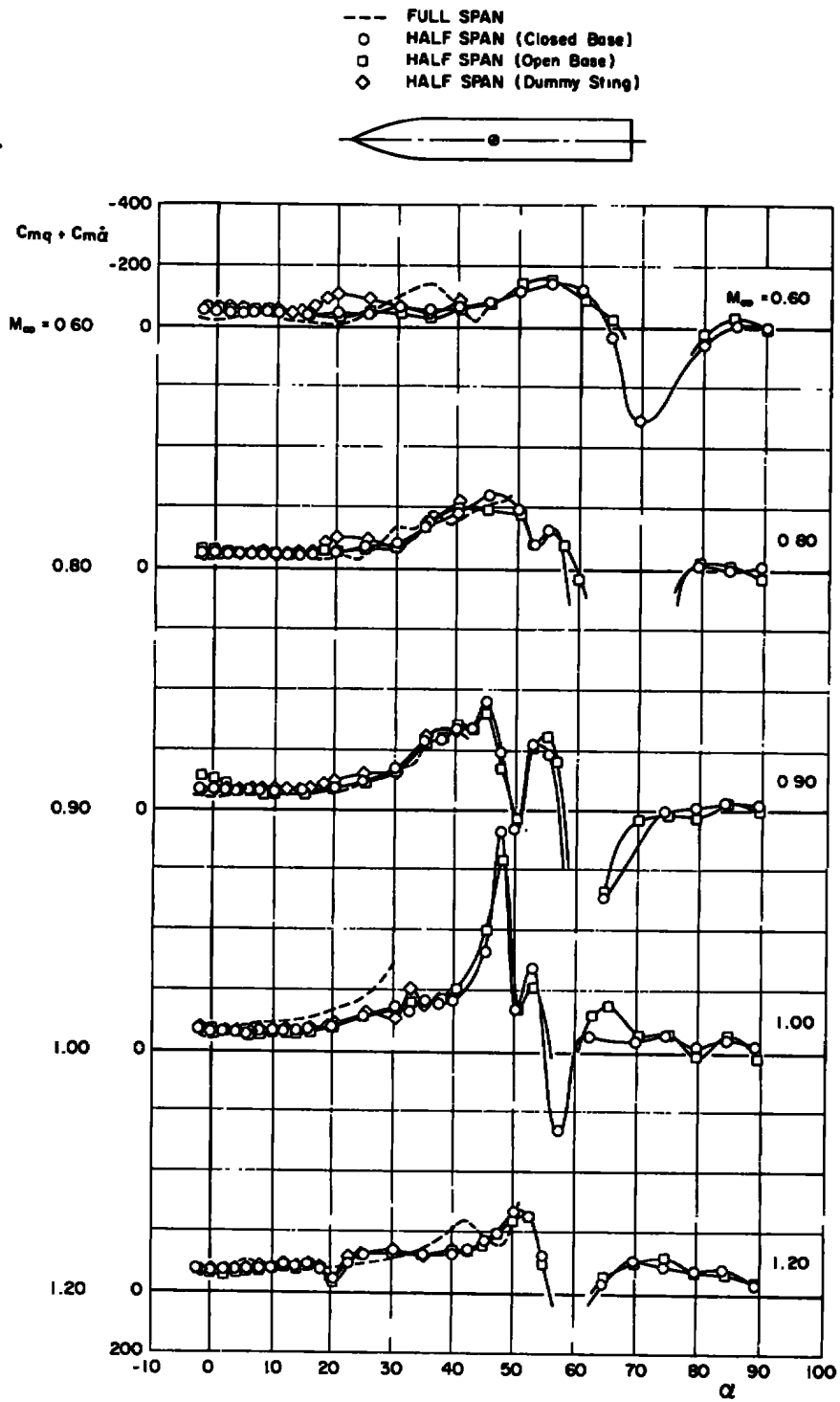
a. C_m versus α

Figure 31. Effects of base alterations on the pitching-moment characteristics of the ogive-cylinder model.



b. $C_{mq} + C_{m\dot{\alpha}}$ versus α
 Figure 31. Concluded.

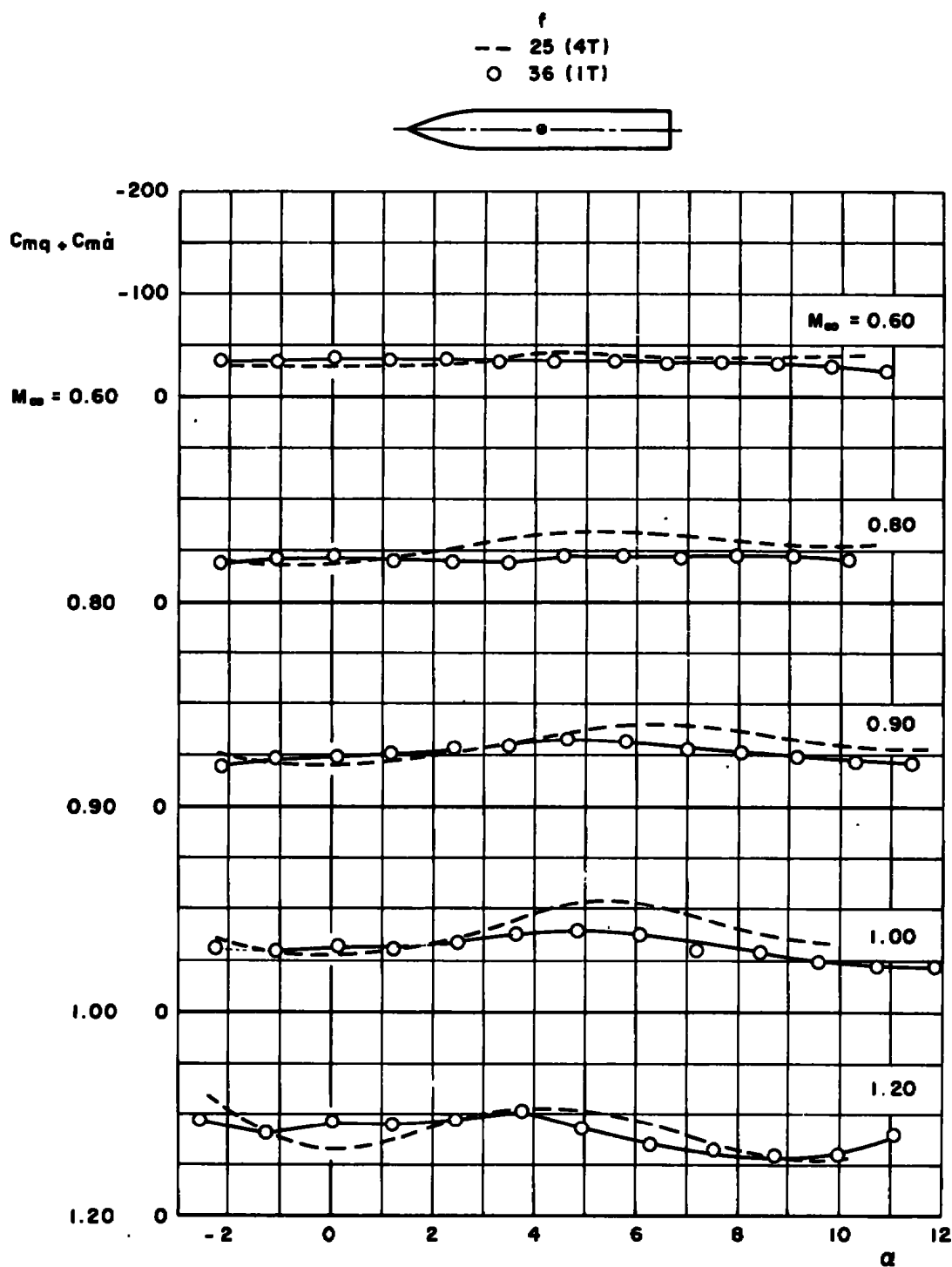


Figure 32. Effects of oscillation frequency on the pitch-damping characteristics of the full-span ogive cylinder model.

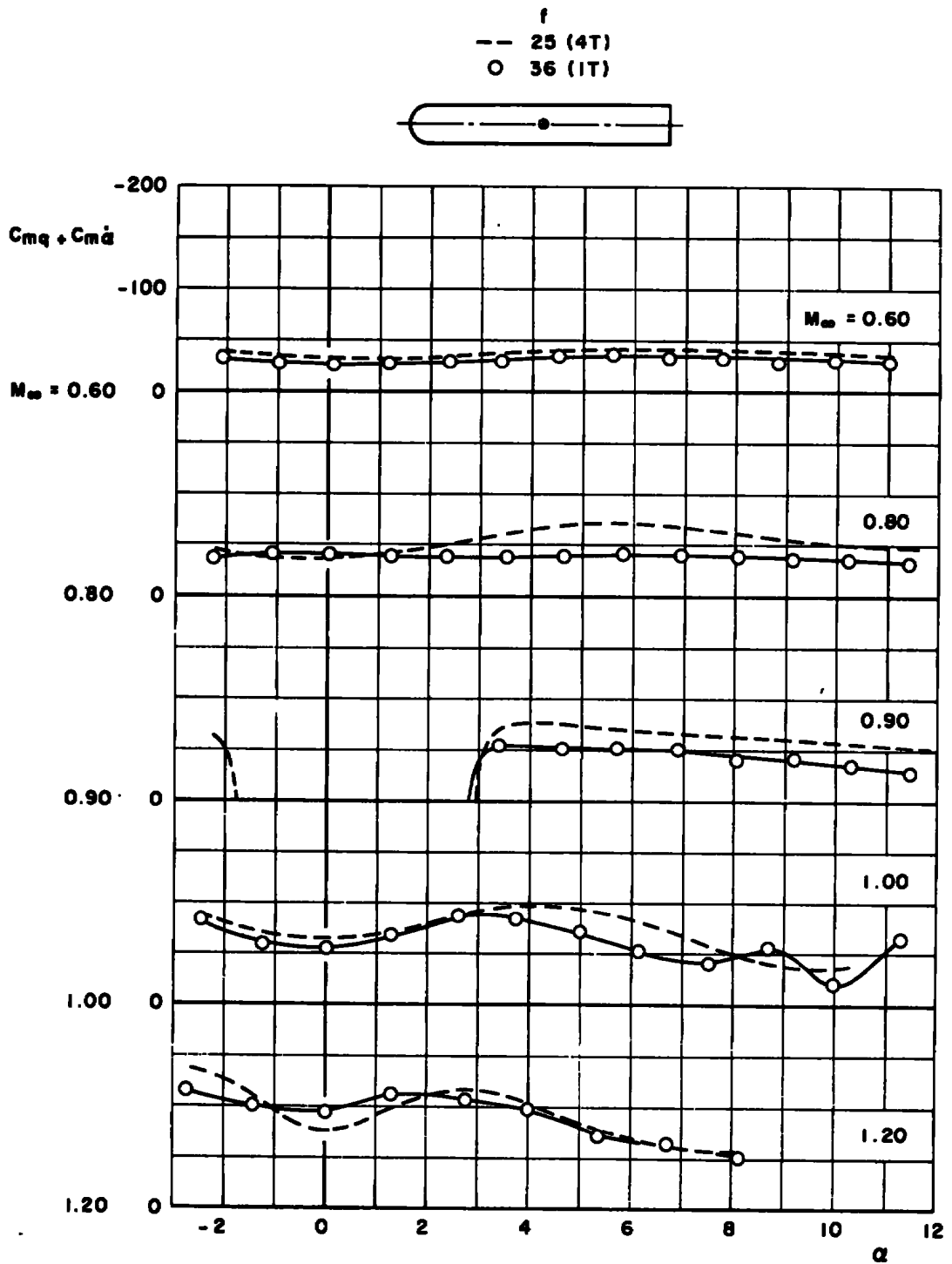


Figure 33. Effects of oscillation frequency on the pitch-damping characteristics of the full-span hemisphere-cylinder model.

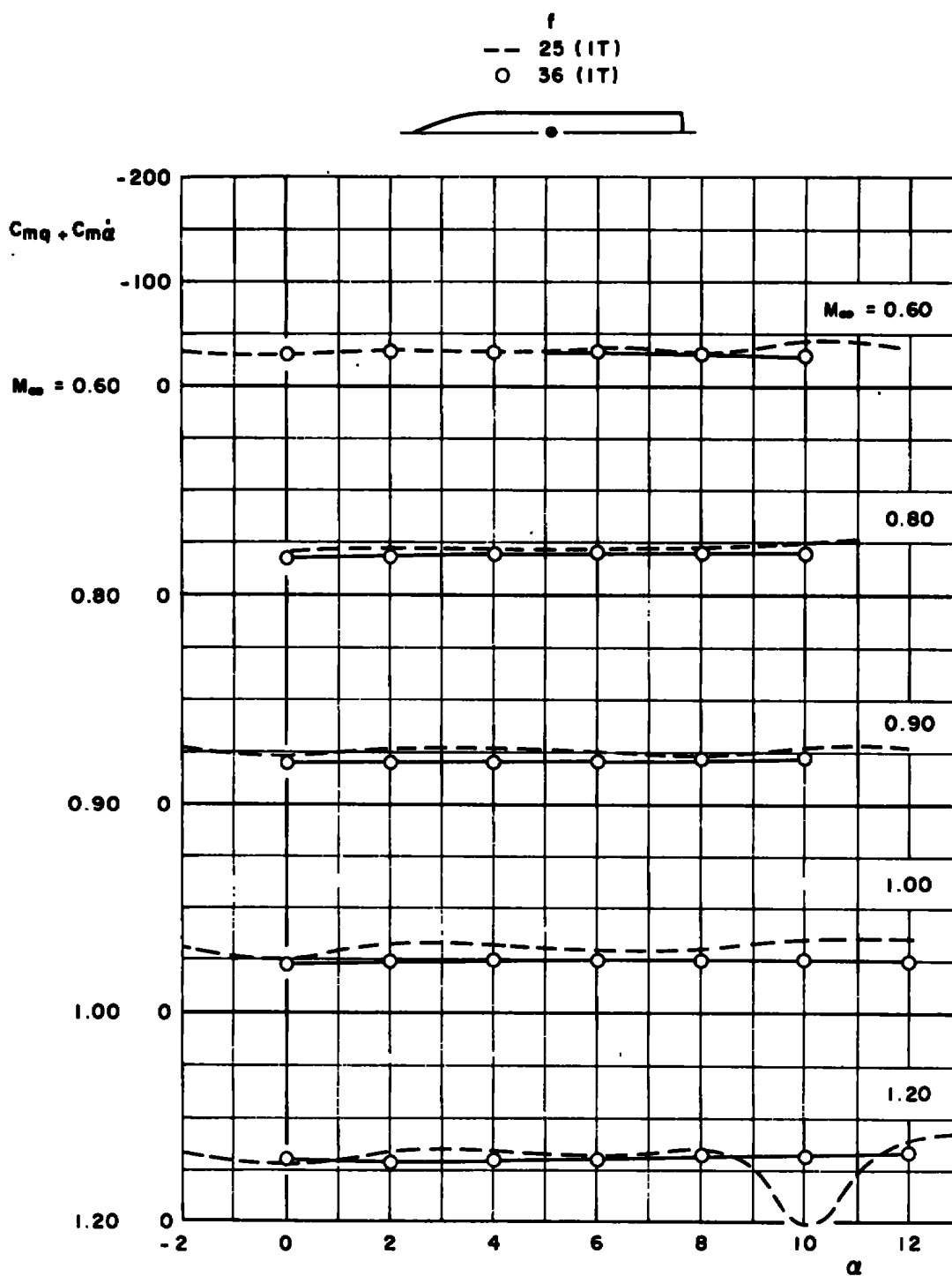


Figure 34. Effects of oscillation frequency on the pitch-damping characteristics of the half-span ogive-cylinder model.

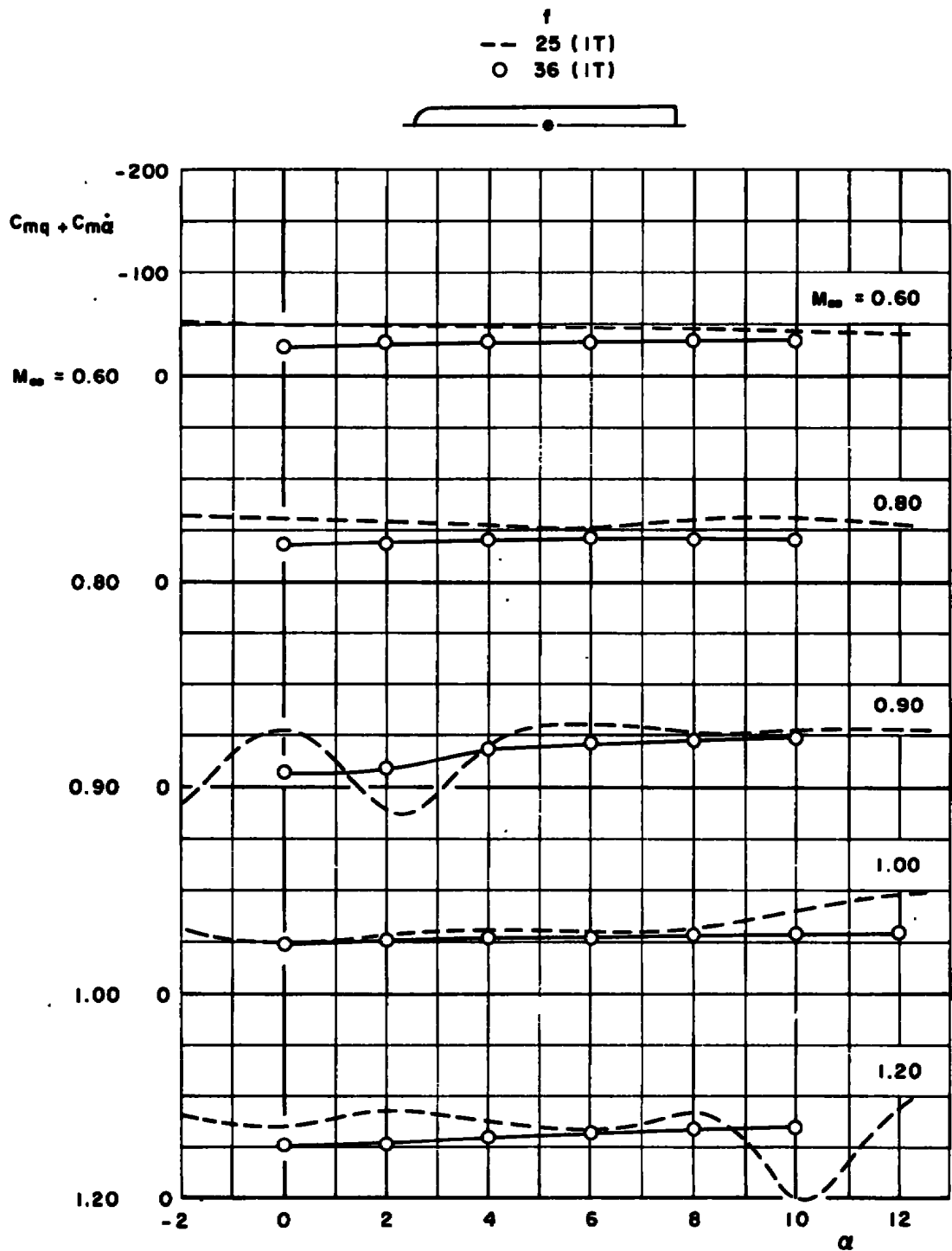


Figure 35. Effects of oscillation frequency on the pitch-damping characteristics of the half-span hemisphere-cylinder model.

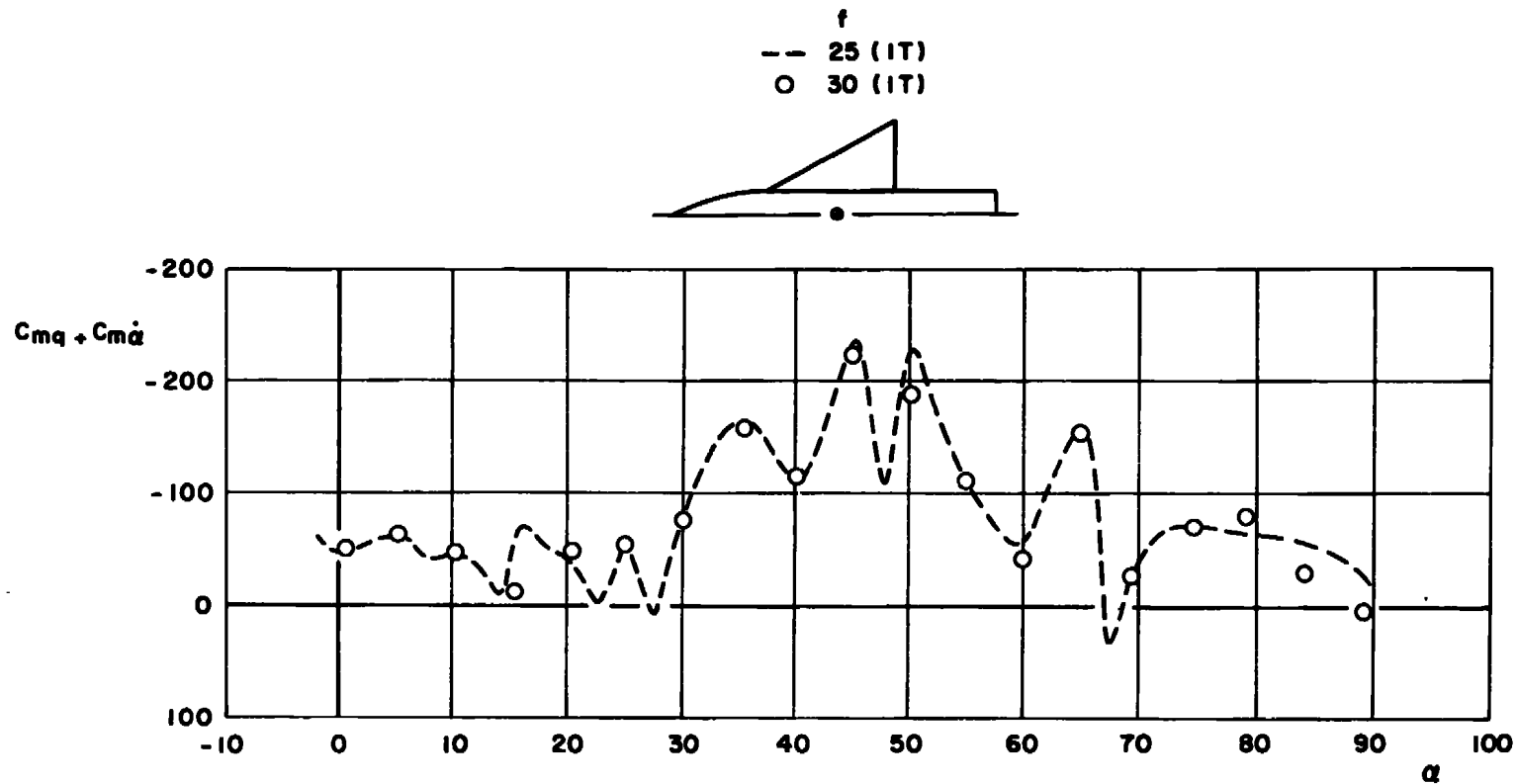


Figure 36. Effects of oscillation frequency on the pitch-damping characteristics of the half-span wing-body model, $M_\infty = 1.0$.

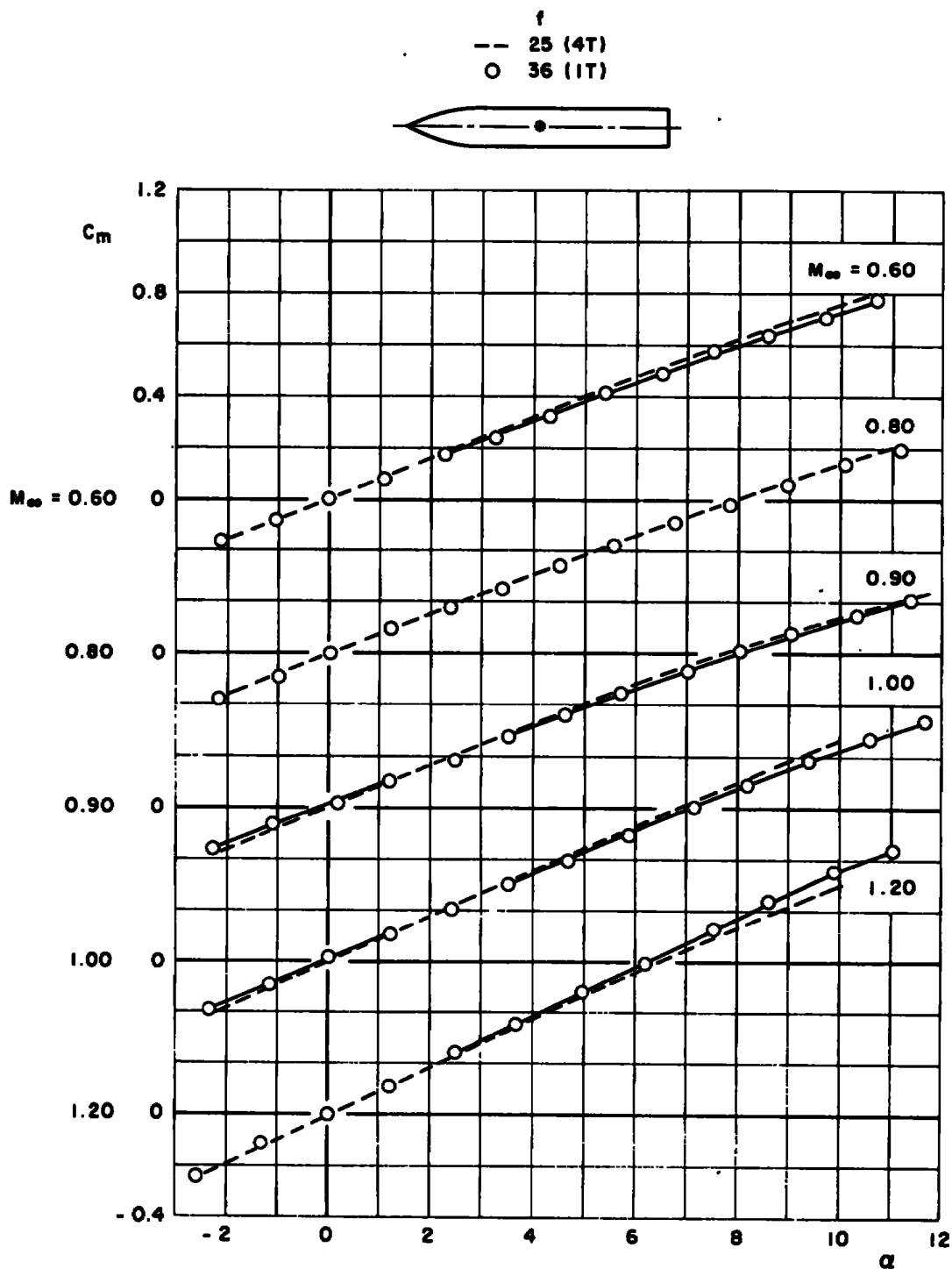


Figure 37. Comparison of static pitching-moment coefficients between Tunnels 1T and 4T for the ogive-cylinder model.

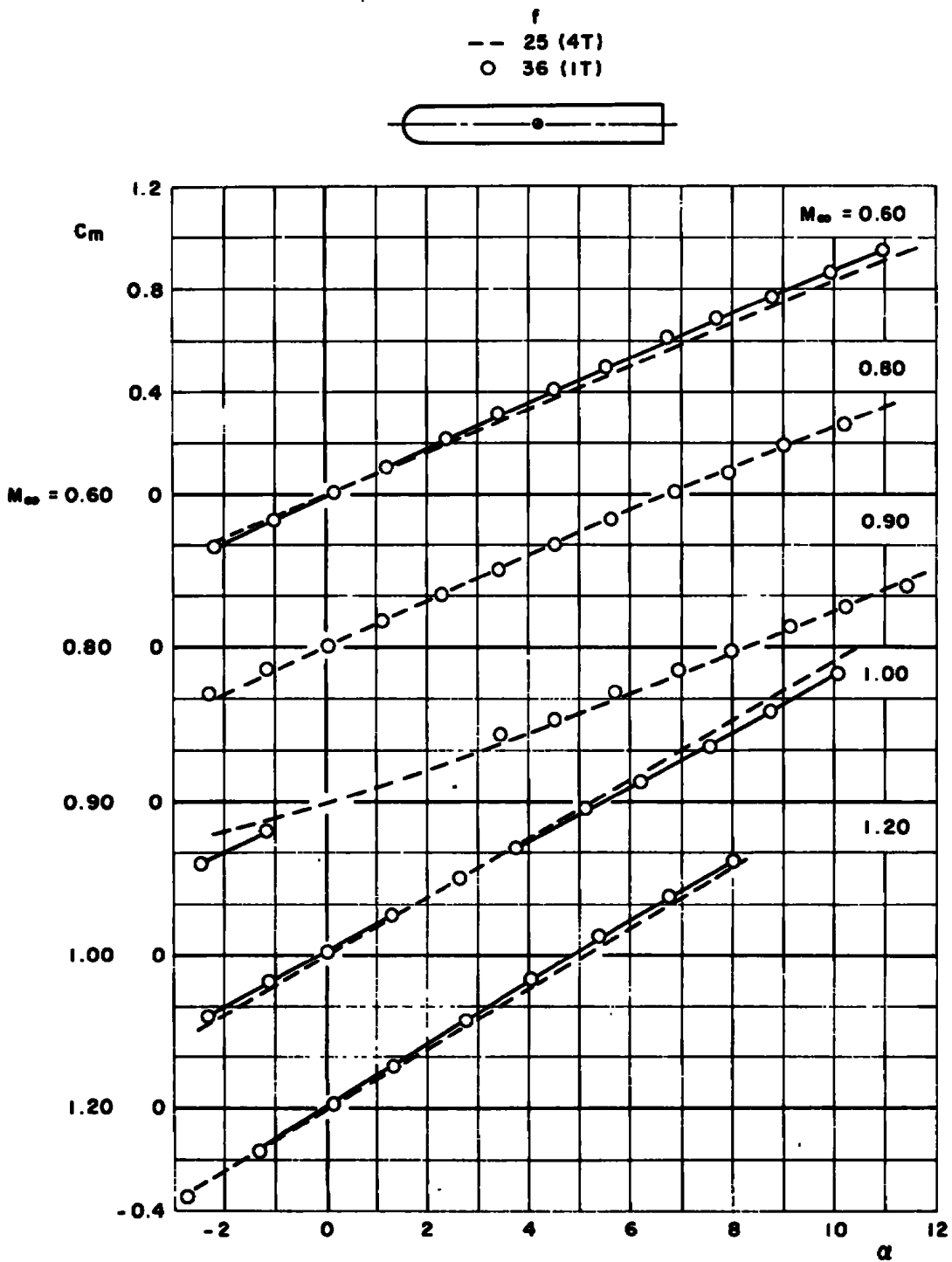
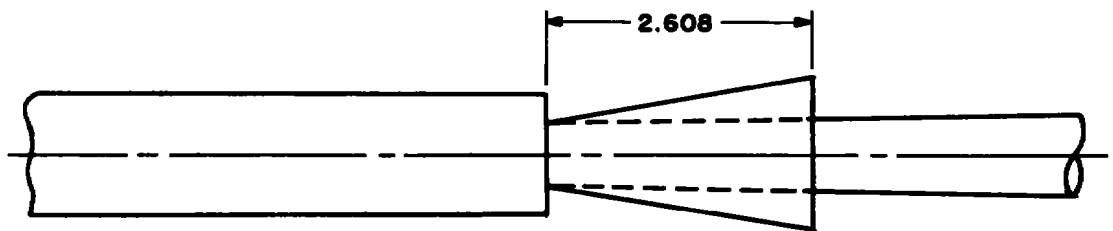
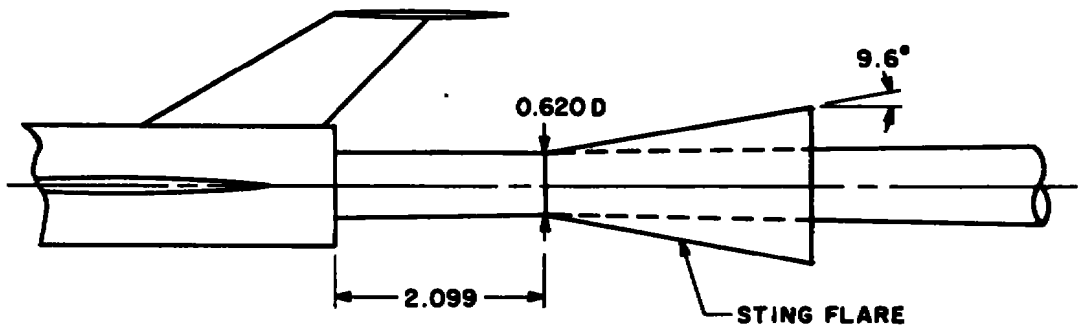


Figure 38. Comparison of static pitching-moment coefficients between Tunnels 1T and 4T for the hemisphere-cylinder model.

**HEMISPHERE-CYLINDER MODEL****AIRCRAFT MODEL****Figure 39. Details of the sting flare.**

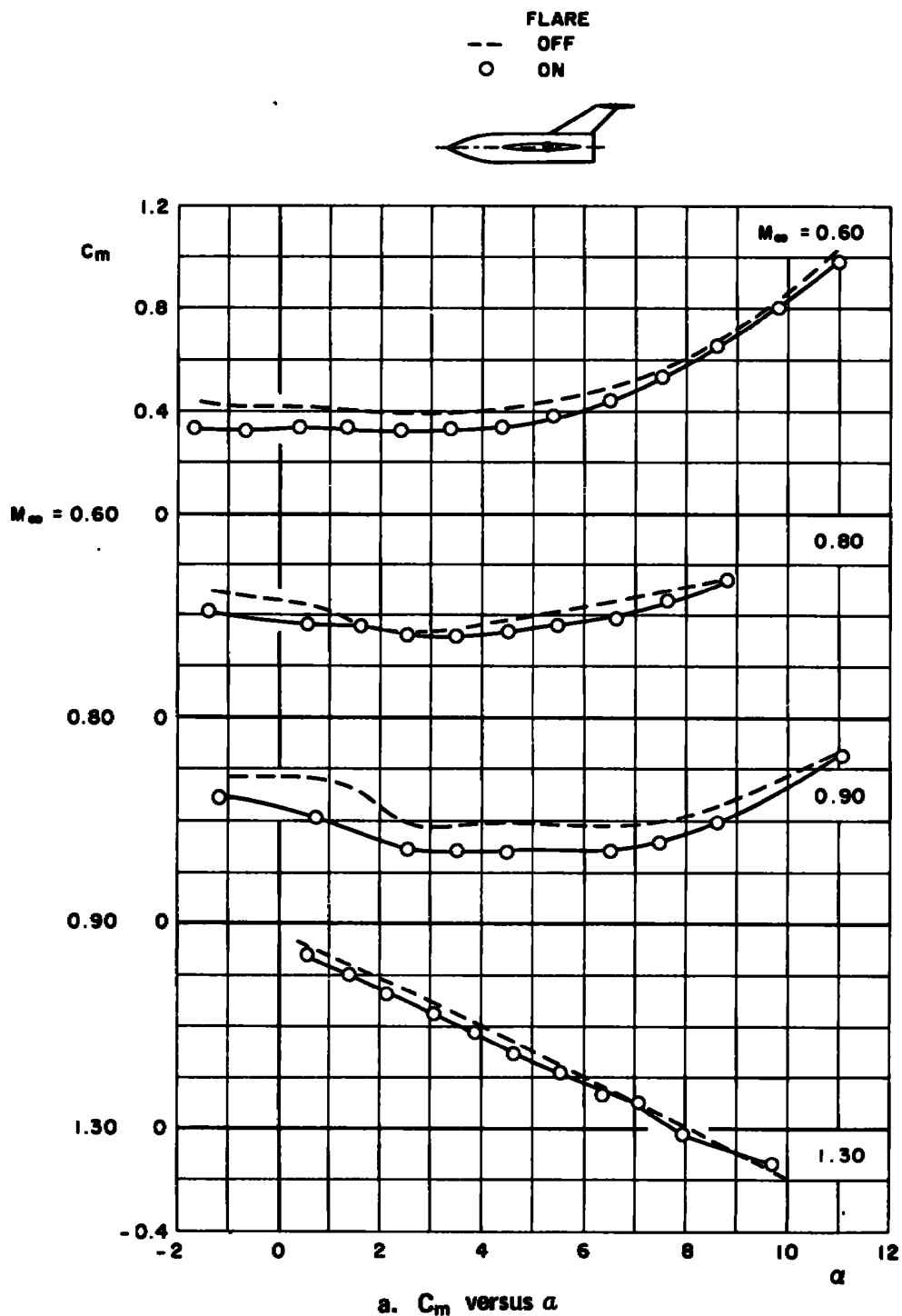
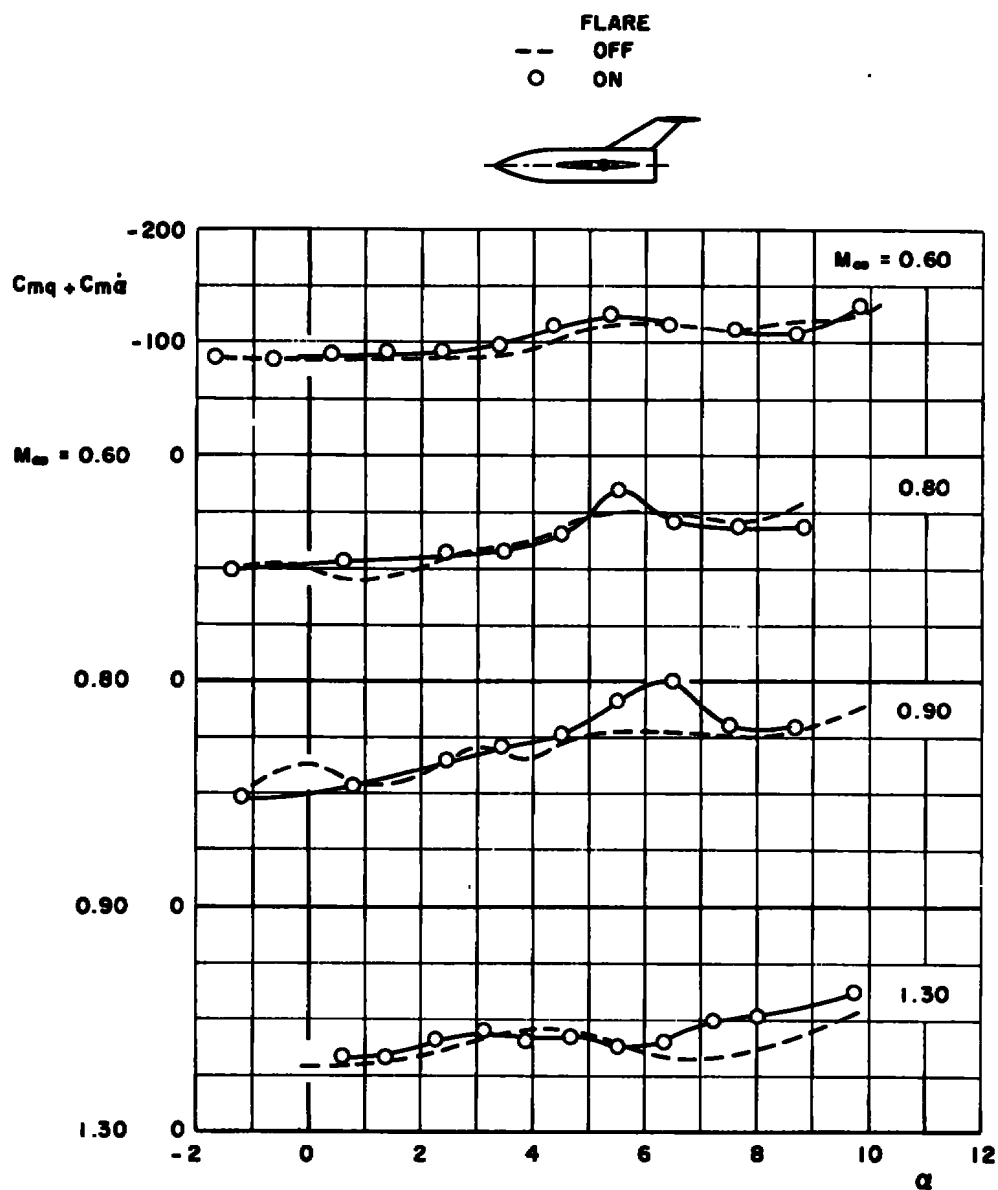


Figure 40. Effects of sting flare on pitching-moment characteristics of the aircraft model.



b. $C_{mq} + C_m \dot{\alpha}$ versus α
 Figure 40. Concluded.

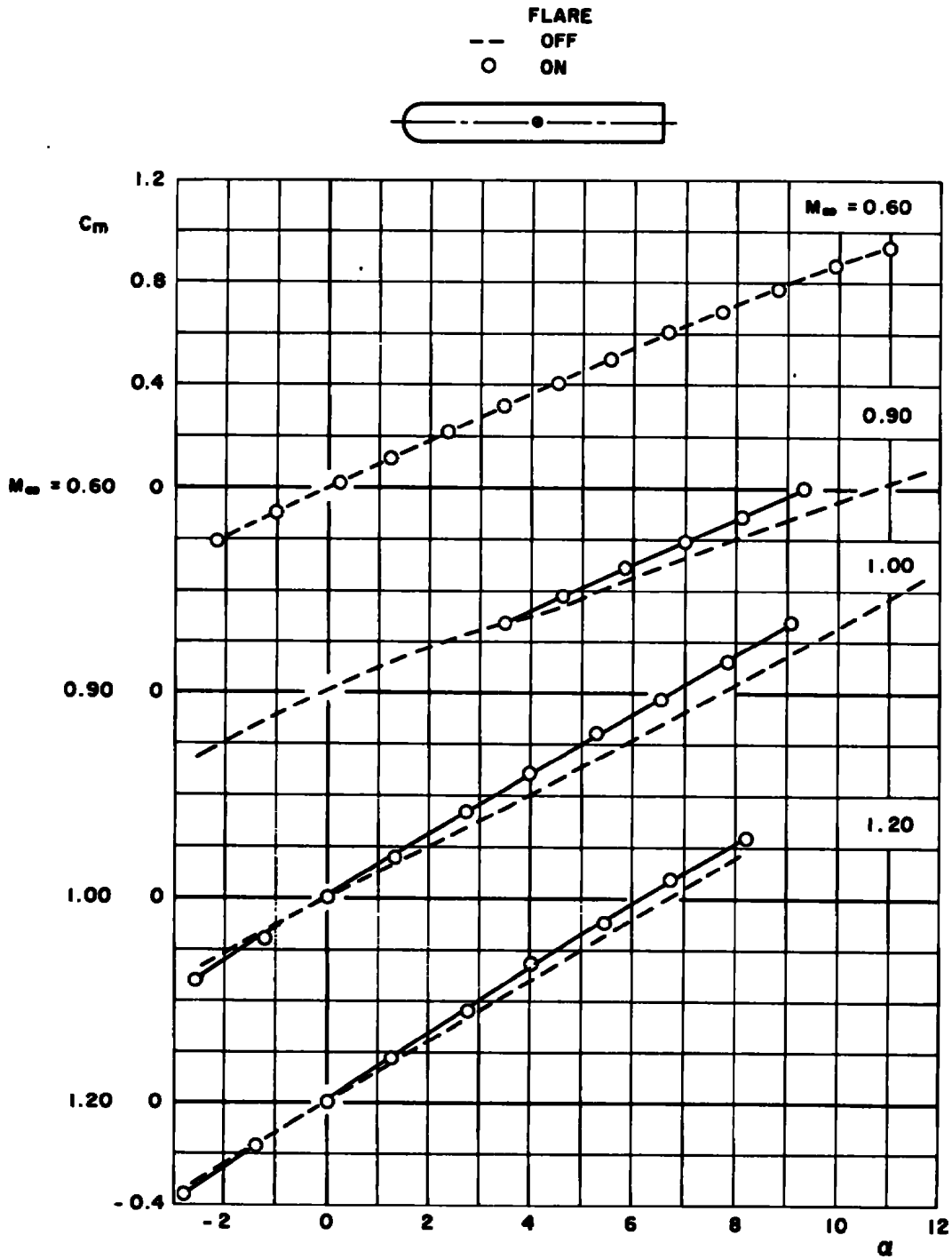
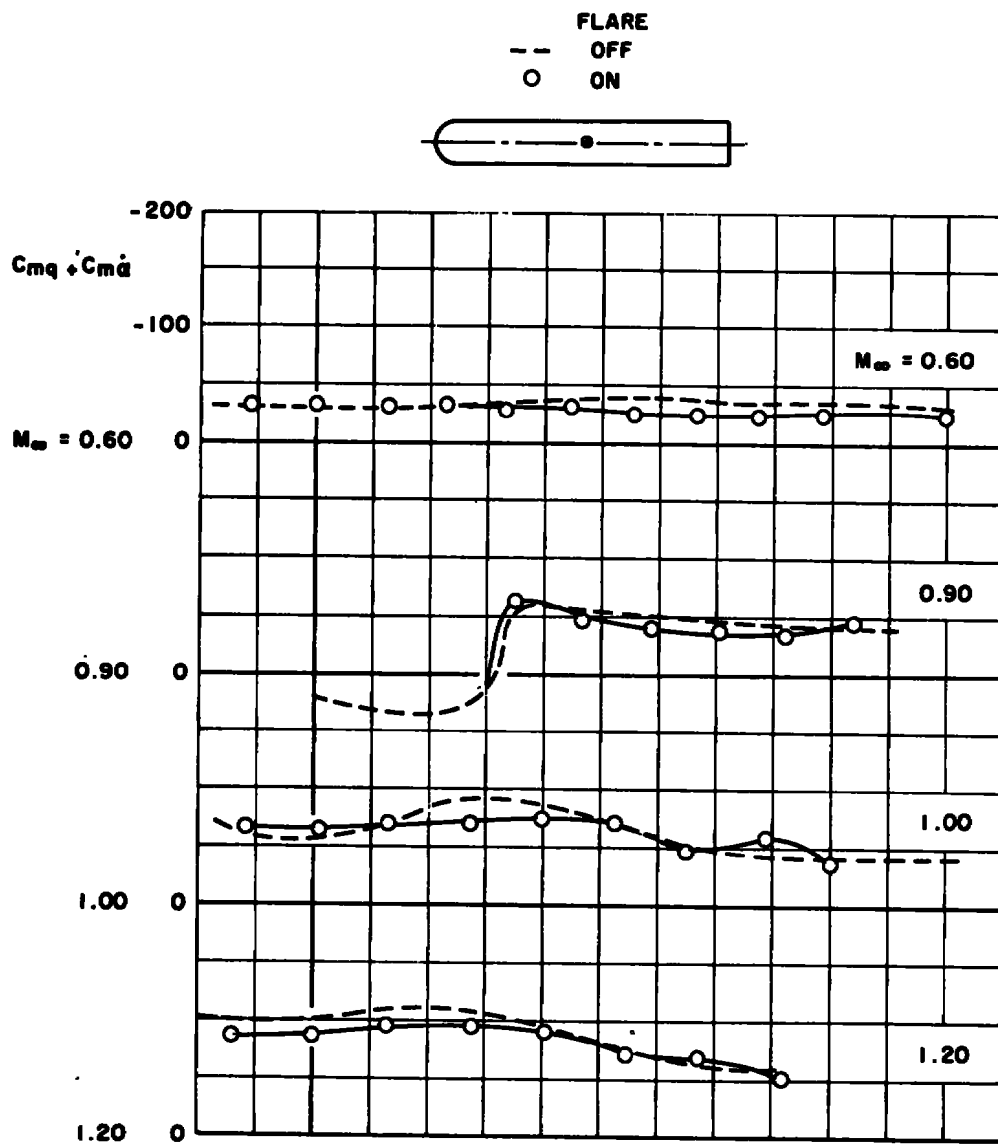


Figure 41. Effects of sting flare on pitching-moment characteristics of the hemisphere-cylinder model.



b. $C_{mq} + C_{m\dot{\alpha}}$ versus α
 Figure 41. Concluded.

Table 1. Test Phases

Test Phase	Model	M_∞	α , deg	θ , deg	Radians/sec
Pressure	Full	0.6 to 1.2	0	---	---
Pressure	Half	0.6 to 1.2	0	---	---
Low Alpha	Full	0.6 to 1.3	-2 to 10	± 3	251
Low Alpha	Half	0.6 to 1.3	0 to 12	± 4	251
High Alpha*	Full	0.6 to 1.2	-2 to 75	± 3	157
High Alpha	Half	0.6 to 1.2	-2 to 90	± 4	157

*Tunnel 4T

Table 2. Test Conditions

Tunnel	M_∞	Q_∞ , psf	V_∞ , ft/sec	T_o , °F
1T	0.6	575	705	150
4T	0.6	238, 485	670	90
1T	0.8	830	913	150
4T	0.8	355, 725	870	95
1T	0.9	945	1,010	150
4T	0.9	400, 828	970	100
1T	1.0	1,045	1,110	150
4T	1.0	442, 912	1,060	105
1T	1.2	1,190	1,280	150
4T	1.2	509, 1,022	1,230	105
1T	1.3	1,220	1,344	135

NOMENCLATURE

C_m	Pitching-moment coefficient, measured pitching moment/ $q_\infty Sd$
C_{mq}	$\left. \begin{array}{l} \partial C_m / \partial (qd/2V_\infty) \\ \partial C_m / \partial (\dot{\alpha}d/2V_\infty) \end{array} \right\} \text{Damping-in-pitch derivatives, per radian}$
$C_{m\dot{\alpha}}$	
C_Q	Suction-flow coefficient, $\sigma Q/S_T V_\infty$
C_{yR}	Cycles to damp to given amplitude ratio R, cycles
d	Model body diameter (reference length), 0.1 ft
f	Model oscillation frequency, Hz
h	Average height of reflection-plane surface above tunnel wall, in. (Fig. 13a)
I_y	Mass moment of inertia about pitch axis, ft-lb-sec ²
ℓ	Length of model body, ft (Fig. 7)
M	Moment, ft-lb
M_∞	Free-stream Mach number
M_θ	$\partial M / \partial \theta$
$M_{\dot{\theta}}$	$\partial M / \partial \dot{\theta}$
p	Static pressure, psfa
p_∞	Free-stream static pressure, psfa

Q	Total suction quantity through reflection plane, ft^3/sec
q	Pitching velocity, radians/sec
q_∞	Free-stream dynamic pressure, psf
R	Oscillation amplitude ratio
Re	Reynolds number
S	Model cross-sectional area (reference area), 0.007854 ft^2
S_T	Tunnel cross-sectional area, ft^2
T_o	Free-stream total temperature, $^\circ\text{F}$
t	Time, sec
V_∞	Free-stream velocity, ft/sec
X	Distance along reflection-plane surface from leading edge, ft
α	Model angle of attack relative to tunnel centerline, deg
$\dot{\alpha}$	Time rate of change of angle of attack, radians/sec
θ	Oscillation amplitude, deg
ρ_s	Density behind reflection plane, slug/ft^3
ρ_∞	Free-stream density, slug/ft^3
σ	Density ratio, ρ_s/ρ_∞

ψ	Reflection-plane yaw angle, positive yawed into free stream, deg
ω	Angular frequency, radians/sec
$\omega d/2V_{\infty}$	Reduced frequency parameter

SUBSCRIPTS

a	Aerodynamic contribution
t	Tare contribution (wind off)
w	Wind on
1,2	Values corresponding to beginning and end of interval t_1 to t_2